



US 20150088024A1

(19) **United States**  
(12) **Patent Application Publication**  
**Sackellares et al.**

(10) **Pub. No.: US 2015/0088024 A1**  
(43) **Pub. Date: Mar. 26, 2015**

(54) **METHODS AND SYSTEMS FOR BRAIN FUNCTION ANALYSIS**

**Publication Classification**

(71) Applicant: **University of Florida Research Foundation, Inc.**, Gainesville, FL (US)

(51) **Int. Cl.**  
*A61B 5/00* (2006.01)  
*A61B 5/04* (2006.01)  
*A61B 5/0478* (2006.01)

(72) Inventors: **James Chris Sackellares**, Gainesville, FL (US); **Scott T. Bearden**, Waldo, FL (US); **Panagote M. Pardalos**, Gainesville, FL (US); **Jui-Hong Chien**, Baltimore, MD (US)

(52) **U.S. Cl.**  
CPC ..... *A61B 5/7214* (2013.01); *A61B 5/0478* (2013.01); *A61B 5/04012* (2013.01); *A61B 5/4094* (2013.01); *A61B 5/742* (2013.01); *A61B 5/7475* (2013.01)  
USPC ..... **600/544**

(73) Assignee: **University of Florida Research Foundation, Inc.**, Gainesville, FL (US)

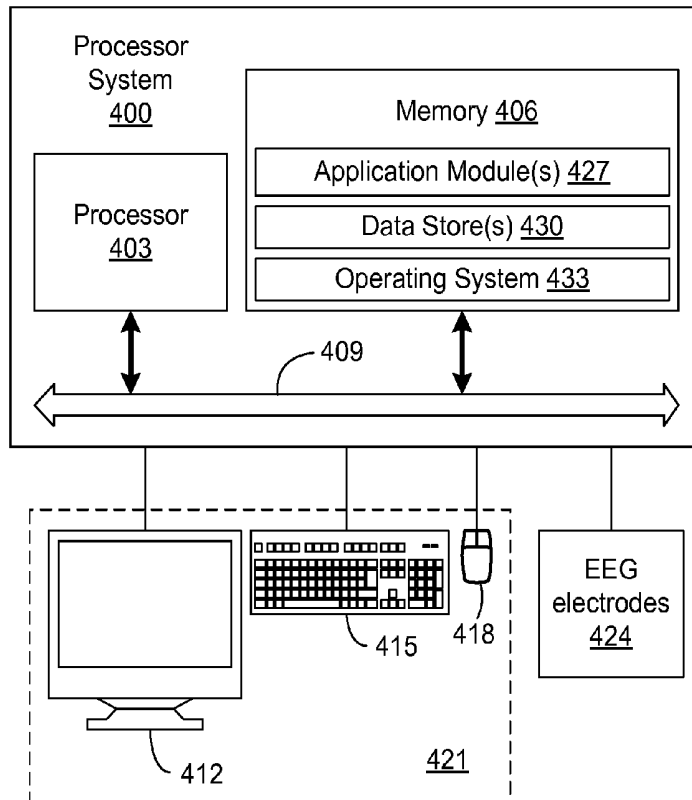
(57) **ABSTRACT**

Various methods and systems are provided for cerebral diagnosis. In one example, among others, a method includes obtaining EEG signals from sensors positioned on a subject; conditioning data from the EEG signals to remove artifacts; generating a cerebral network model based at least in part upon the conditioned data; determining network features based upon the cerebral network model; and determining a cerebral condition of the subject based at least in part upon the network features. In another example, a method includes determining a recording condition of a positioned EEG sensor and providing an indication of an unacceptable recording condition of the EEG sensor. In another example, a system includes an EEG recording module to acquire signals; a signal conditioning module to condition signal data; a signal analysis module to determine signal features and cerebral network features; and a condition classification module to determine a cerebral condition of the subject.

(21) Appl. No.: **14/386,643**  
(22) PCT Filed: **Mar. 6, 2013**  
(86) PCT No.: **PCT/US2013/029293**  
§ 371 (c)(1),  
(2) Date: **Sep. 19, 2014**

**Related U.S. Application Data**

(60) Provisional application No. 61/612,647, filed on Mar. 19, 2012.



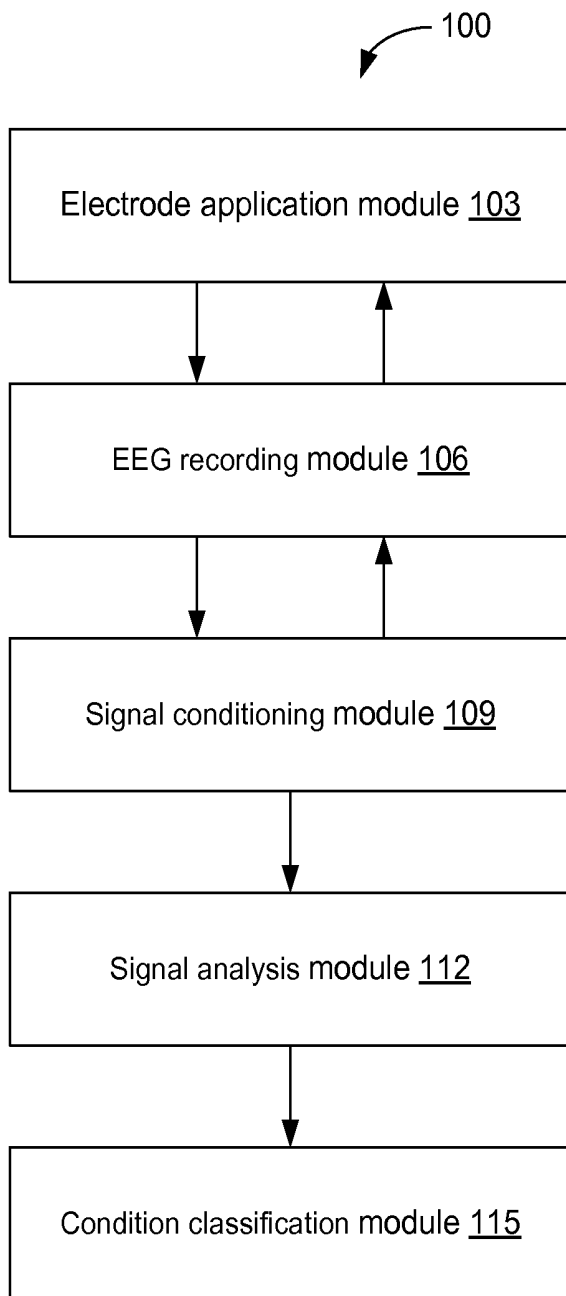


**FIG. 1**

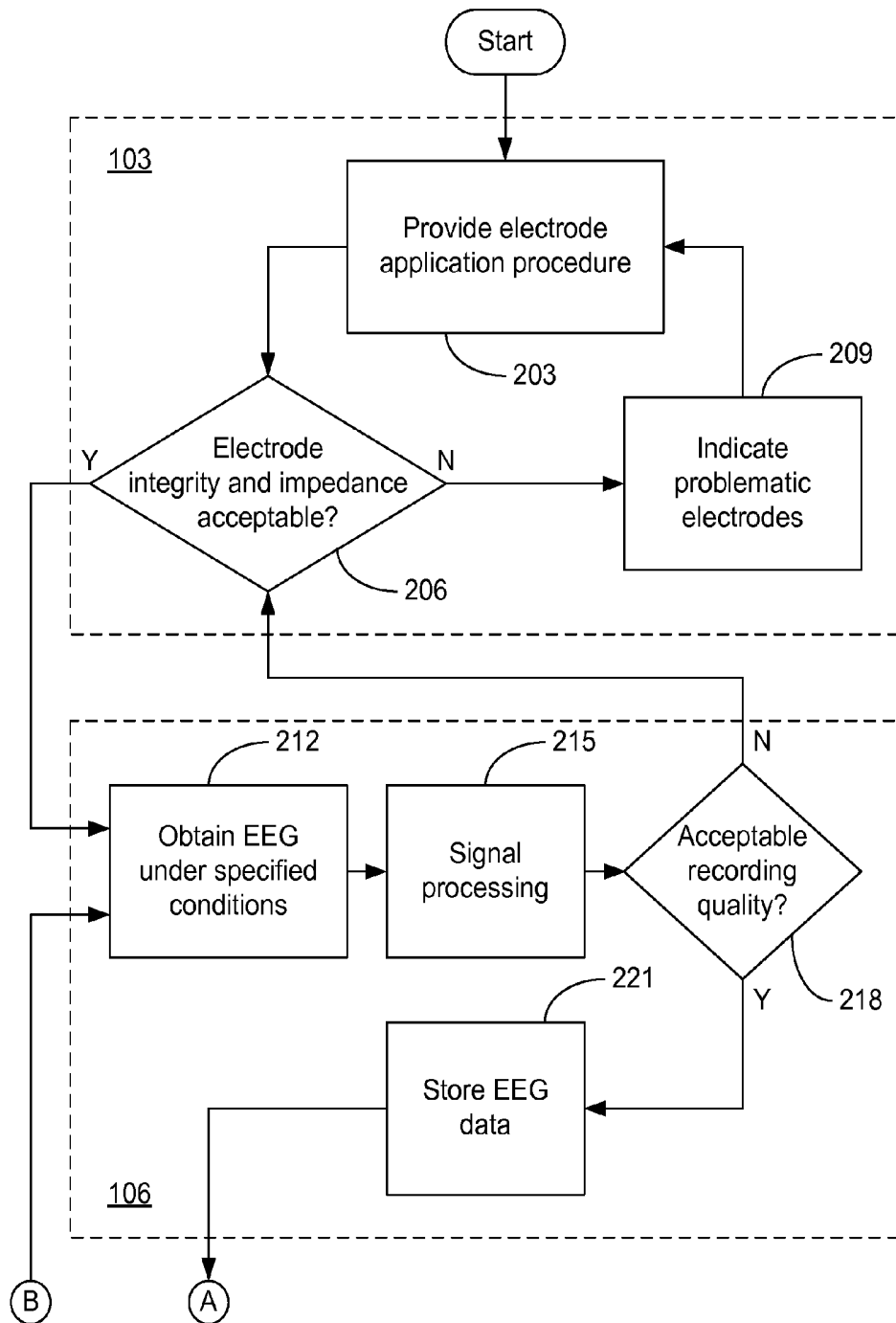


**FIG. 2A**

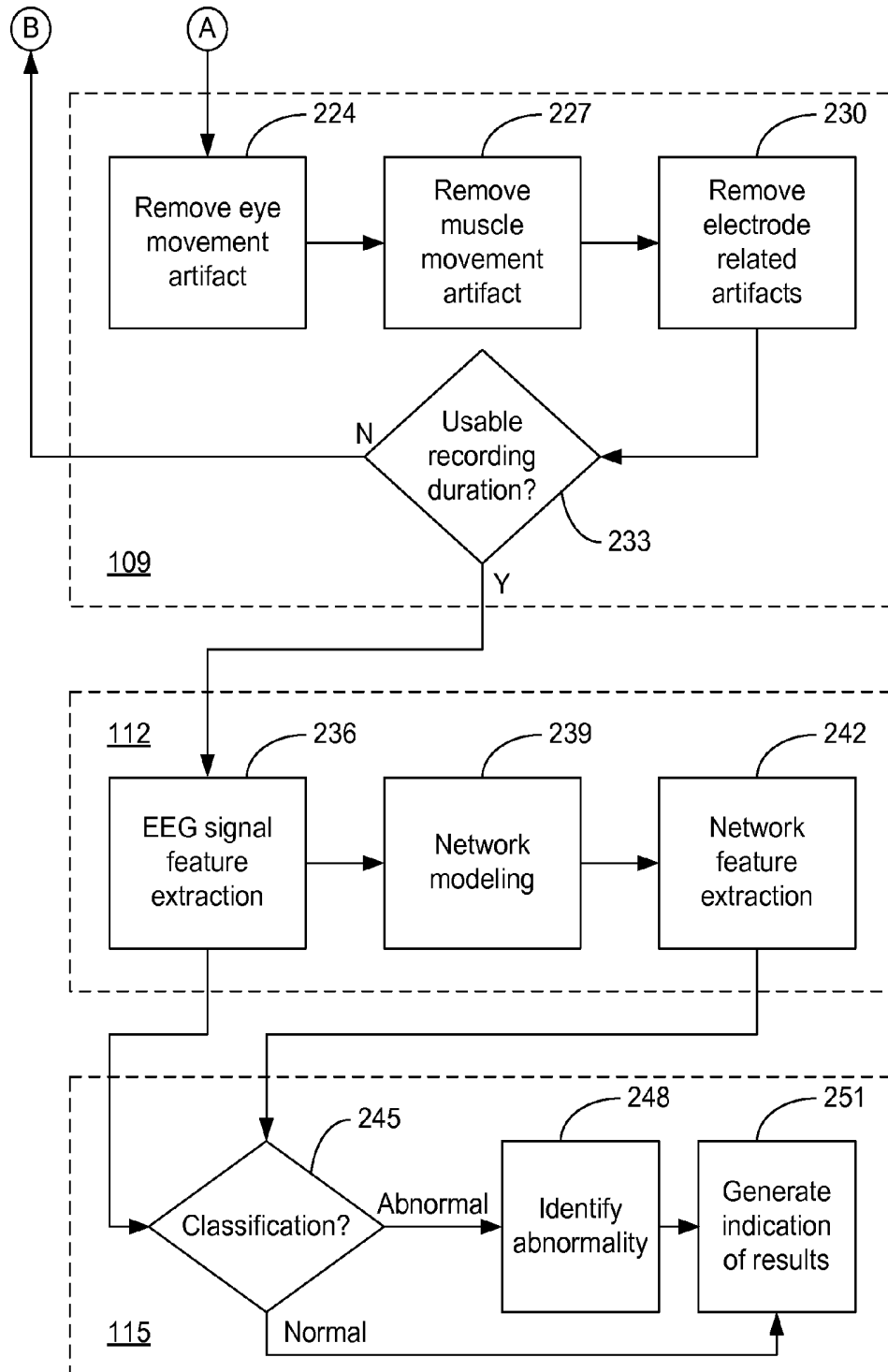


**FIG. 2B**

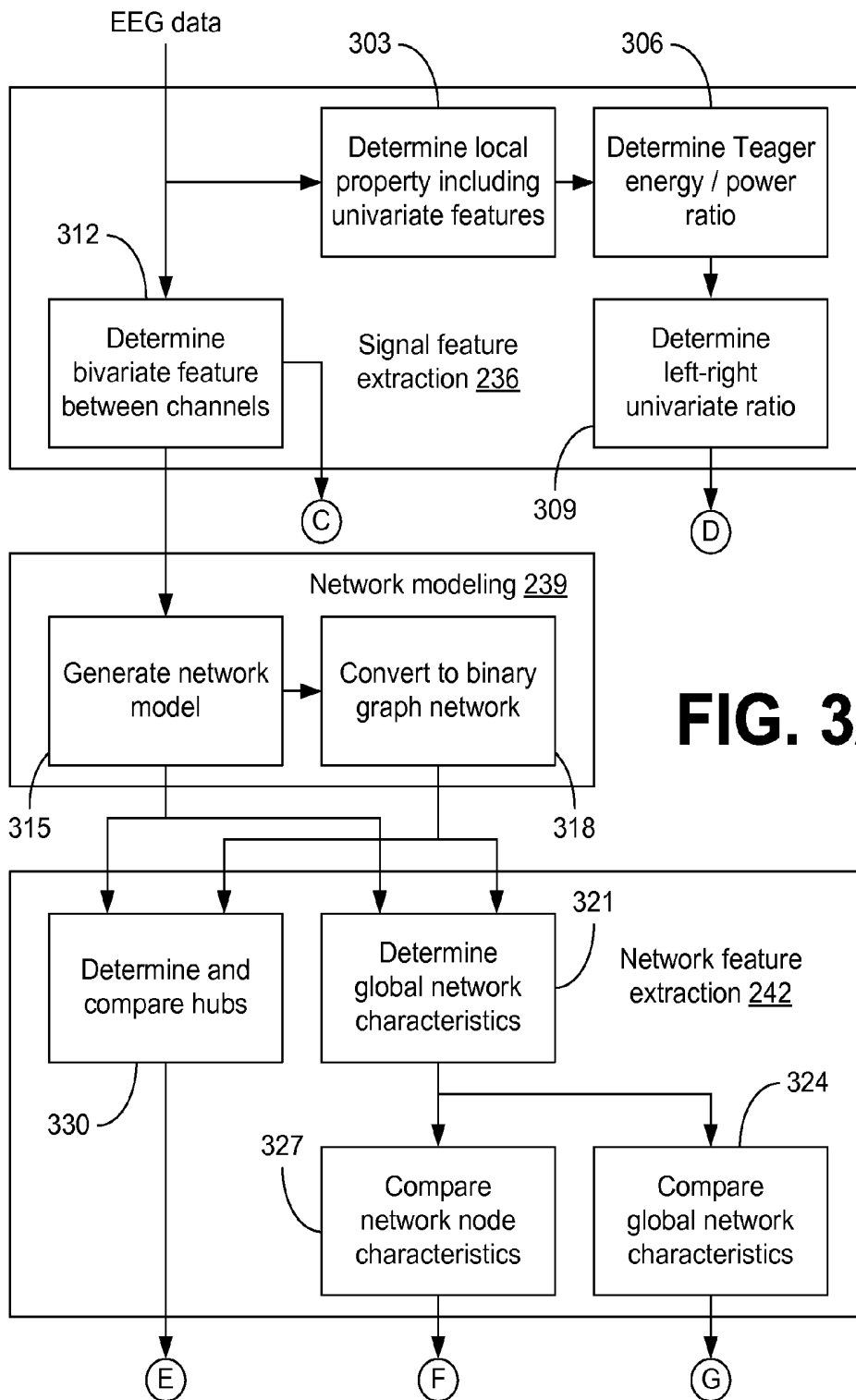


**FIG. 3A**

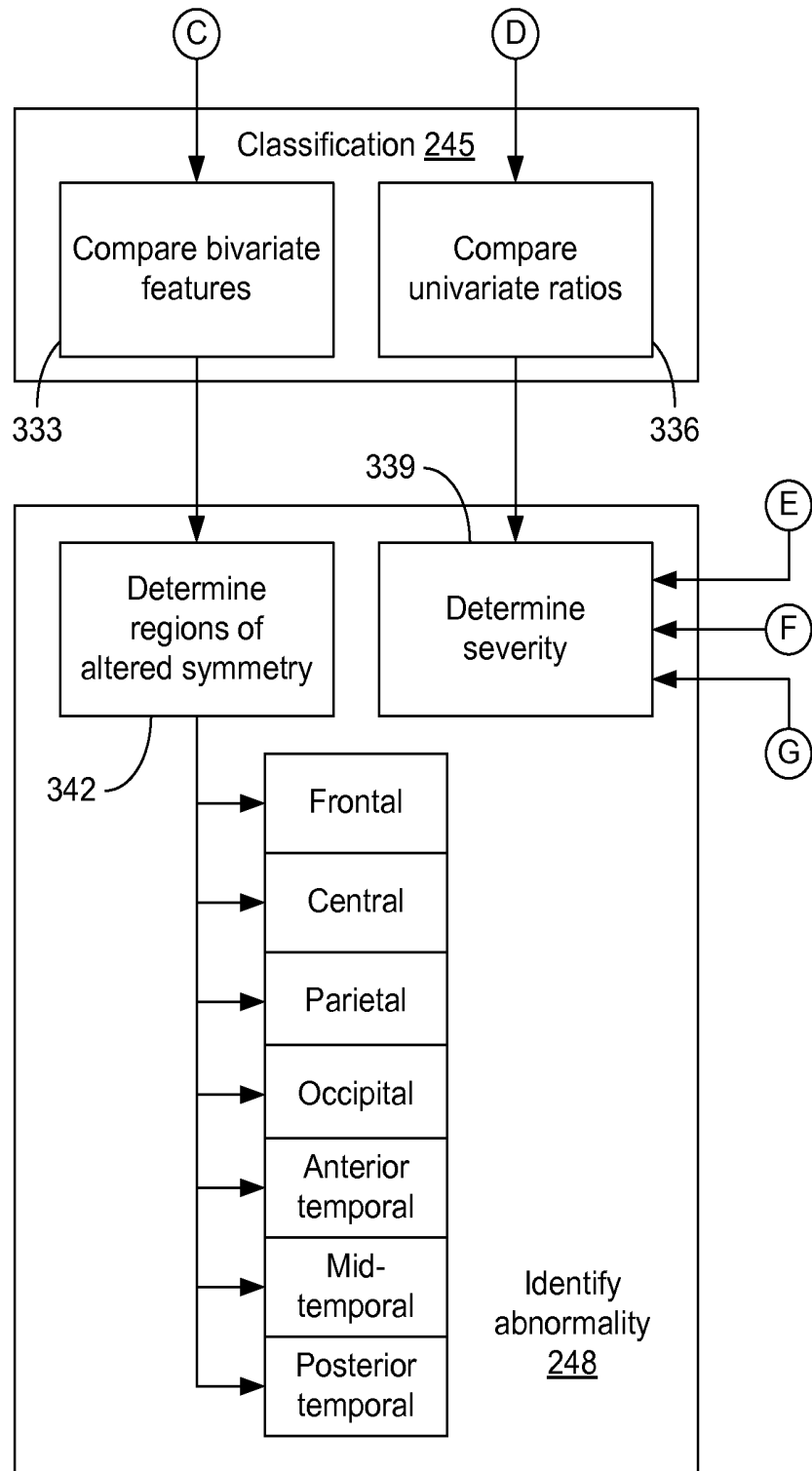


**FIG. 3B**

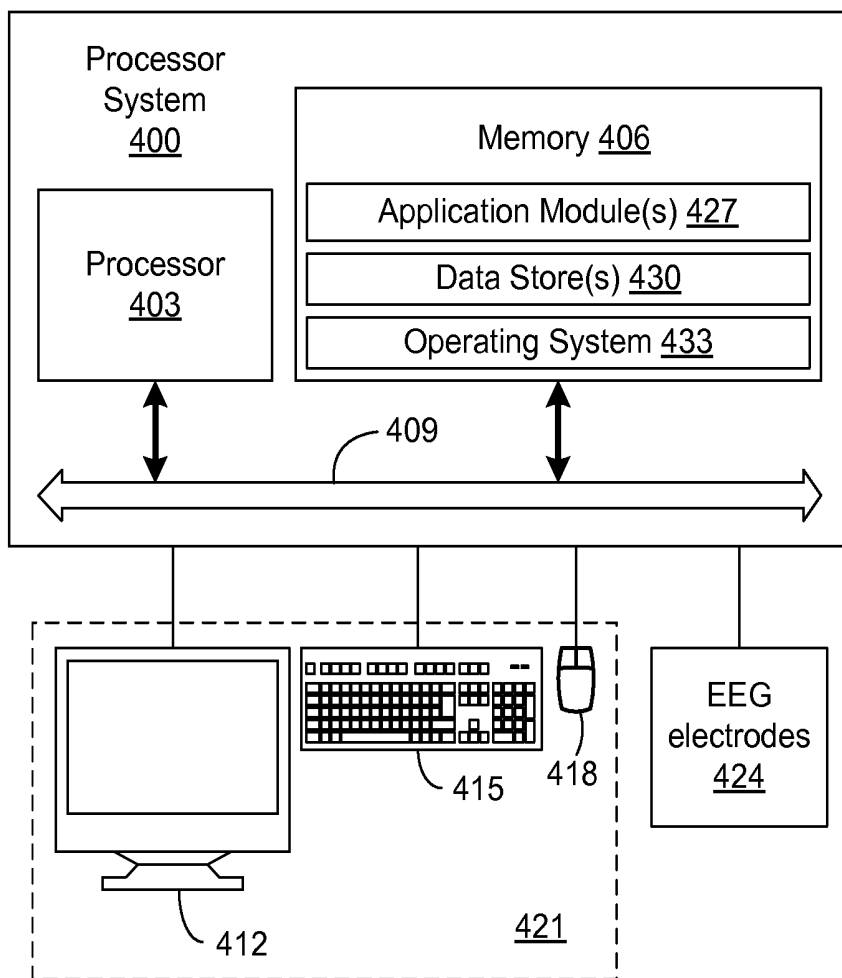


**FIG. 4**

## METHODS AND SYSTEMS FOR BRAIN FUNCTION ANALYSIS

### CROSS REFERENCE TO RELATED APPLICATIONS

[0001] This application claims priority to co-pending U.S. provisional application entitled "Methods and Systems for Cerebral Diagnosis" having Ser. No. 61/612,647, filed Mar. 19, 2012, the entirety of which is hereby incorporated by reference.

### BACKGROUND

[0002] The human brain is a very delicate organ that makes possible complex behavioral decision making. Information processing within the human brain is so sophisticated and complex that it cannot be accessed entirely even with the advanced technology available today. Once a brain is damaged, it is often very hard to achieve full recovery. The importance of accurate, timely diagnoses of brain abnormality is crucial in many clinical settings including the emergency room (ER) or intensive care unit (ICU). However, most mental and neurological states are evaluated mainly through interviews and subjective exams based on the subjects' temporary performance at that time. There is no objective quantitative test for evaluating baseline brain function. Imaging technologies such as standard magnetic resonance imaging (MRI) show only structure within the brain without providing an indication of dynamic brain function. EEG is the most effective method for evaluating brain function, but interpretation requires interpretation of multichannel graphs based on visual analysis by highly trained experts.

### BRIEF DESCRIPTION OF THE DRAWINGS

[0003] Many aspects of the present disclosure can be better understood with reference to the following drawings. The components in the drawings are not necessarily to scale, emphasis instead being placed upon clearly illustrating the principles of the present disclosure. Moreover, in the drawings, like reference numerals designate corresponding parts throughout the several views.

[0004] FIG. 1 is a block diagram illustrating an example of a system for evaluating a condition of a brain in accordance with various embodiments of the present disclosure.

[0005] FIGS. 2A and 2B are a flowchart illustrating an example of functionality of the system of FIG. 1 in accordance with various embodiments of the present disclosure.

[0006] FIGS. 3A and 3B are a flowchart illustrating examples of feature extraction, network modeling, and classification of the flowchart of FIG. 2B in accordance with various embodiments of the present disclosure.

[0007] FIG. 4 is a graphical representation of an example of a processor system suitable for implementing the system of FIG. 1 in accordance with various embodiments of the present disclosure.

### DETAILED DESCRIPTION

[0008] Disclosed herein are various embodiments of methods and systems related to diagnosis of cerebral conditions which cause disturbances in brain function. Reference will now be made in detail to the description of the embodiments as illustrated in the drawings, wherein like reference numbers indicate like parts throughout the several views.

[0009] Electroencephalography is a technology for measuring the voltage and frequency of electrical activity from neurons in the cerebral cortex. Electroencephalogram (EEG) electrodes can record brainwaves using electrodes attached to the scalp or, through electrodes placed on the surface of the brain (subdural electrodes) or within brain tissue (depth electrodes) using surgical procedures. A scalp EEG is a non-invasive procedure which provides useful information about brain state and function. This methodology is used in many fields of neuroscience (e.g., psychology, epilepsy, brain machine interface, and sleep research) for recording and analyzing brain state and function. It is used widely as a diagnostic tool in clinical neurology to evaluate and monitor brain function and to identify disturbances in the function of the brain caused by a variety of insults to the brain, such as concussion, traumatic injury, stroke, tumor, encephalopathies due to toxins or metabolic disturbances and seizures. Many disturbances of brain function can be identified by analysis of brief multichannel EEG recordings using electrodes placed in specific locations on the scalp, based of reference anatomical landmarks. The most widely accepted system of electrode placement is the International 10/20 System of electrode placement. By analyzing the multi-channel EEG data of a short period of time, ongoing background activity can be assessed. Standard routine EEG recordings are approximately 20 minutes in duration. However, background EEG can be assessed with only a few seconds of EEG recording, if the state of the subject is known (e.g., alert, drowsy or light sleep states). A normal brain generates signals with characteristic frequencies, waveforms and spatial organization. Normal brain electrical activity is remarkably symmetrical over the two cerebral hemispheres. In clinical practice, the EEG is analyzed visually to detect diffuse bilaterally disturbances in ongoing background activity as well as focal or lateralized disturbances. This information provides useful diagnostic insight. The EEG is useful for evaluation of chronic conditions, such as dementia. However, its most important use is in the evaluation of acute or subacute conditions presenting as altered mental status or impaired sensorium, such as stupor or coma.

[0010] Analysis and interpretation of EEG recordings is performed by experts (usually neurologists with training in the interpretation of EEG recordings) based on visual inspection of multichannel recordings displayed as multichannel graphs of signal voltage over time. The spatial temporal patterns of brain electrical activity can be analyzed through quantitative analysis of the spatial and temporal properties of this activity, generating a mathematical model of the activity, analyzing the properties of the model, and comparing those properties to a standard of norms based on the properties of normal individuals of similar age. A useful mathematical model for analyzing brain state and function is a network model, based on graph theory. Mathematical analysis of local and global properties allow identification of normal physiological states and allow identification of focal, lateralized or diffuse disturbances in physiological function and states. While brief EEG recordings provide useful diagnostic information regarding function and state at the time of recording, analysis of long-term recording is useful for monitoring brain conditions such as level of consciousness, identifying abnormal transients in the signal, such as interictal epileptiform discharges, seizures, acute cerebral ischemia, hypoglycemia or anoxia. Analyzing the spatial-temporal dynamics of long-term EEG recording data can be achieved through use of

quantitative dynamical network models. This approach can provide diagnostic information pertaining to the physiological states of the brain, and can be used to identify transient pathological conditions. The above described approach to network analysis of brain electrical activity can be achieved through computer-based algorithms designed to identify artifact, condition the signal, generate quantitative measures of signal properties from each of multiple EEG channels derived from multiple electrodes placed in standard locations on the scalp, generating a network model, calculating local and global properties of the network and comparing to standard network norms derived from normal subjects. These network properties can be monitored over time and compared with the patient or subject's baseline to detect significant changes in state or development of transient pathological conditions. The algorithm can provide detailed quantitative output or can summarize the results and categorize them as normal or abnormal. Abnormalities can be categorized as to focal, lateralized or diffuse, and the anatomical location focal and lateralized abnormalities can be reported. This output can be written as a report or depicted as a graph. The algorithm can be trained and compared to the interpretation of expert electroencephalographers to optimize the sensitivity and specificity of the algorithm. An appendix, which is hereby incorporated by reference in its entirety, provides additional information about EEG analysis of brain dynamical behavior.

**[0011]** This disclosure presents systems and methods for reliably evaluating a recorded EEG in real time by algorithms and providing an immediate indication of the cerebral condition. The acquired EEG data may be evaluated in real time and/or may be stored for subsequent evaluation. The system allows EEG data to be recorded and evaluated when no EEG technical personnel or neurological interpreters are readily available, allowing its use as a screening tool to assist physicians when such personnel are not available. The original EEG data may also be stored for subsequent visual analysis and/or may be transmitted to remote sites for review and interpretation by experts.

**[0012]** EEG data can be recorded with small, portable, inexpensive instruments that do not require special shielded facilities or the subject remaining motionless for long periods of time. Thus, an EEG can be utilized in noisy point-of-care environments, such as Emergency rooms and Intensive Care Units and with subjects who may be uncooperative. Portable EEG units can also be utilized in emergency vehicles and in the field. Referring to FIG. 1, shown is a block diagram illustrating an example of a system **100** for evaluating a condition of a brain. In the embodiment of FIG. 1, the system **100** includes an electrode application module **103**, an EEG recording module **106**, a signal conditioning module **109**, a signal analysis module **112**, and a condition classification module **115**. The system **100** may contain an interactive display which may provide, e.g., step-by-step instructions on electrode placement, establishing connections, preparing the subject and initiating the recording, etc. The system **100** allows for rapid acquisition and analysis of EEG signals, measurement of the spatial-temporal characteristics of the signal, analysis of local, regional, and diffuse signal characteristics, characterization of network features of EEG signals, determination of whether or not these EEG characteristics are normal or abnormal, and classification of abnormal EEG recordings to determine whether the abnormalities are local, lateralized, multifocal or diffuse. The results may be displayed as in a text and/or graphical format that may be avail-

able for immediate use by emergency room personnel, intensive care personnel, and emergency medical technicians.

**[0013]** Referring to FIGS. 2A-2B, shown is a flowchart illustrating various functions that may be implemented by modules of the system **100**. As shown in FIG. 2A, after operation of the system has been initiated (e.g., by turning on the device), an electrode application procedure may be provided in box **203** by the electrode application module **103** for rendering on the system display. The EEG provides direct information about brain functions through analysis of brain electrical activity. Depending on the location and the type of the electrodes, EEG signals can reveal different levels of neuronal activity. Numerous scalp EEG electrodes may be applied to a subject to obtain EEG data containing information from brain activity in both temporal and spatial domains. The EEG electrodes can include individual electrodes and/or an array of electrodes that are positioned on the scalp. The location of electrode placement on the scalp can follow, e.g., a 10-20 system or other appropriate system as can be appreciated. In the 10-20 system, distinct landmarks of the subject's head are first identified and then electrodes are placed at 10% or 20% distance intervals along the landmarks. In some implementations, intracranial electrodes may be utilized. The recording integrity and impedance of the electrodes are checked in box **206** to determine if there is a problem with the placement and/or operation of the EEG electrodes. If there is a problem, the problematic electrodes may be indicated in box **209** on the system display and the appropriate application or correction procedure(s) may be provided in box **203**. Guiding the operator through simple set-up and operating procedures to obtain a technically adequate EEG recording reduces evaluation errors.

**[0014]** If the electrode integrity and impedance is acceptable in box **206**, then an EEG is obtained under specified conditions in box **212** by the EEG recording module **106**. For example, EEGs may be obtained with the subject's eyes open and closed or other specified conditions of the subject. Instructions may be rendered for display on the system display to prompt the specified condition (or action) in the monitored subject. For example, during a routine EEG examination, a subject is usually asked to relax and open eyes for a period of time and then close eyes for another period of time. The acquired EEG signals are then processed in box **215**. For example, amplification and filtering may be applied to enhance the signal-to-noise ratio (SNR) of the EEG signals. Analog EEG signals from the electrodes may also be digitized for communication and storage of the information. In box **218**, acceptability of the recording quality of the EEG data is confirmed. For example, all channels of the processed EEG signal may be analyzed for the presence of excessive artifacts that may contaminate the EEG data. Criteria for acceptable signal quality may be predefined to ensure acceptable electrode contact, electrode impedance, and minimal contamination by common artifacts.

**[0015]** If the EEG data is not acceptable, then the system can return to box **206** to recheck electrode integrity and impedance. Common technical problems that degrade the recording (e.g., excess muscle or movement artifacts) may also be determined in box **218**. Instructions may be provided through the system display to guide the operator in methods to eliminate or attenuate those artifacts before repeating the acquisition of EEG signals in box **212**. Subsequent recorded EEG data may be re-evaluated and the operator notified of persistent problems, at which time the operator may attempt

to obtain further EEG signals or may abort the procedure. If the EEG data is acceptable, the digitized data can be stored in a data store or other memory in box 221. The stored EEG data may be transmitted through a wireless or wired network connection (e.g., cellular, Bluetooth, Ethernet, etc.) for remote evaluation, analysis, and/or confirmation.

**[0016]** The acceptable EEG data is further processed and/or filtered by the signal conditioning module 109 to remove common recording artifacts as illustrated in FIG. 2B. For example, eye movement artifacts may be detected and removed in box 224, electromyogram (muscle movement) artifacts may be detected and removed in box 227, and electrode related artifacts such as, e.g., electromagnetic interference from nearby instruments may be detected and removed in box 230. Other artifacts such as, e.g., 60 Hz line signals and signals produced by mechanical ventilators and other instruments may also be detected and removed from the EEG data by the signal conditioning module 109. For example, epochs of data may be examined sequentially for the presence of an artifact. If a segment contains an excessive artifact, it may then be excluded from subsequent analysis. After the signal conditioning module 109 identifies and discards the artifact-contaminated segments, the remaining EEG data is evaluated in box 233 to ensure that a useable signal of sufficient duration has been acquired and is available for analysis. An initial interpretation may be generated based upon a brief EEG recording (e.g., 2 to 5 minutes). If the available data is not long enough for reliable analysis, the system 100 will inform the operator and return to box 212 to obtain additional EEG data. If the available EEG data is long enough for analysis or evaluation, the EEG data is processed by the signal analysis module 112 to extract features in box 236.

**[0017]** The system 100 may also provide an option to continue recording to obtain a complete routine EEG (typically around 20-30 minutes of recording) or for continued monitoring the EEG for changes in brain function, such as intermittent seizures, diffuse or focal ischemia, and changes in alertness or level of consciousness. In other implementations, the system 100 may be placed in a monitoring mode in which epochs of the EEG are analyzed as they are acquired to detect transient abnormalities or state changes in the subject. In the monitoring mode, a continuous or intermittent analysis may be provided graphically and/or a summary report may be provided intermittently at specified intervals. For example, the interval between reports can be a default interval (e.g., every 10 minutes) or can be an interval that is selected by the operator.

**[0018]** The extracted features of the multichannel EEG data from box 236 may be used to provide a quantitative description of the spatiotemporal characteristics of the signals, including local and regional characteristics, inter-hemispheric asymmetries, and local and global network connectivity characteristics. The extracted features may be, e.g., linear, non-linear, univariate, or bivariate statistics. The extracted features from box 236 may be provided as inputs for network modeling in box 239 and for classification of the cerebral condition in box 245 of the condition classification module 115. For example, if the feature is univariate, such as entropy, each EEG channel will have a feature time series. The network modeling in box 239 is implemented based upon the degree of association between these univariate features between channels. If the feature is bivariate (or a relationship between two channels), the network modeling in box 239 may be directly implemented through the values of bivariate

features. After the network model has been constructed in box 239, network features may be extracted in box 242 from the network model and provided to the condition classification module 115 for classification in box 245. Classification of the cerebral condition can be more precise by including the extracted network features in the evaluation.

**[0019]** Classification of the cerebral condition in box 245 may be based, at least in part, upon comparison of extracted features from boxes 236 and 242 by comparison with established norms to determine if they indicate a normal condition within normal limits or an abnormal condition. In addition being able to utilize correlations between specific EEG findings and pathologies, the condition classification module 115 analyzes EEG signals through a network perspective. The functional network reflects the connectedness among brain regions in terms of neuron activity. The brain functional network may be represented as a graph by defining vertices and edges in the EEG data. If the EEG channels are designated as the vertices of a graph, an edge between two vertices signifies a functional connection between two EEG channels. A larger correlation between two EEG channels indicates the presence of an edge between the channels. Edges may also be values quantifying how well the two vertices correlate in weighted graphs. Applying graph theoretical analysis to EEG data can reveal topological characteristics of the neural network and brain functional network features.

**[0020]** If the cerebral condition is determined to be abnormal, then the location of abnormal features (e.g., local or focal, lateralized, or diffuse bilateral) and/or the severity of the abnormality (e.g., mild, moderate, or severe) may be identified in box 248. For example, the condition may be identified as abnormal diffuse bilateral, abnormal left hemisphere, or abnormal right hemisphere with slowing, seizures, and/or amplitude disturbance. An indication of the classification results may then be generated in box 251 for rendering on the system display. For example, a graphic display of the original EEG signal, local signal properties, inter-hemispheric asymmetries, local network features, and/or global network features may be generated. A warning may be generated when an abnormal condition has been indicated.

**[0021]** A summary (or report) of findings may be provided in several forms which may be selected by the user. For example, a default condition may provide a report labeled as normal or indicating the determined abnormal category classification (e.g., mildly abnormal, left hemisphere). In addition, a visual display of the anatomical location of the abnormalities may be provided graphically, using a color bar, grey scale or other graphic display to indicate the severity of the abnormalities. Other graphical displays which provide maps of one or more individual signal property may also be viewed. The results of the classifications may also be stored in box 251 for later access or retrieval to further evaluation, interpretations, and validation.

**[0022]** Referring to FIGS. 3A and 3B, shown are a flowchart illustrating examples of feature extraction, network modeling, and classification of the flowchart of FIG. 2B. In FIG. 3A, EEG data is received for EEG signal feature extraction in box 236. In box 303, local properties may be determined from the EEG data including the univariate feature. Kaiser-Teager energy and power in the EEG may be computed for each electrode site and referenced to a common reference electrode (e.g., average, Pz, other). Other implementations may use bipolar pairs and calculate for each pair:

Fp1-F3, F3-C3, C3-P3, P3-O1 and analogous for right side, Fp1-F7, F7-T3, T3-T5, T5, O1 and analogous for right side.

**[0023]** Local energy and power properties may be determined for each channel for comparison to predetermined normative values for each channel. Abnormality of Teager energy and abnormalities for power would be expected to be either higher or lower than the normative values. Abnormalities in the Teager energy to Power ration would be expected to be lower than norms. Norms may be derived from EEG recordings obtained from a normal test group, with appropriate age matching, or may be based upon baseline recordings obtained in the same subject (in which case, a change from baseline would be detected).

**[0024]** For each EEG channel, the follow local property values may be computed in box 303:

**[0025]** Kaiser-Teager energy (KTE). KTE may be calculated for each electrode channel. This value can be obtained for the entire recorded frequency range as well as for each of the standard EEG frequency bands (delta: 0-4 Hz, theta: 4-8 Hz, alpha: 8-13 Hz, and beta: 13-30 Hz). The value for each channel may be compared to normal values. If the values are outside of the normal range, the degree of abnormality (e.g., based on standard deviations (s.d.) from the mean) for each electrode channel can be determined. The location (left cerebral hemisphere, right cerebral hemisphere or bilateral) and degree of abnormality (1 s.d. $\geq$ x<2 s.d., 2 s.d. $\leq$ x<3 s.d, or x $\geq$ 3 s.d.) can be stored and used in the final evaluation and report.

**[0026]** Power. Standard power for the entire frequency range (0 to 30 Hz) and for each of the standard EEG frequency bands (delta, theta, alpha and beta) may be computed for each electrode channel and compared to normal values for each respective channel. If the values are outside of the normal range, the degree of abnormality (based on standard deviations from the mean) for each electrode channel can be determined. The location (left cerebral hemisphere, right cerebral hemisphere or bilateral) and degree of abnormality (1 s.d. $\geq$ x<2 s.d., 2 s.d. $\leq$ x<3 s.d, or x $\geq$ 3 s.d.) can be stored and used in the final evaluation and report.

**[0027]** Pattern match regularity statistic (PMRS). One or more measures of signal regularity or signal such as the PMRS may be generated for the entire recorded frequency range as well as for each standard EEG frequency band for each electrode channel and compared to normal values. If the values are outside of the normal range, the degree of abnormality (based on standard deviations from the mean) for each electrode channel can be determined. The location (left cerebral hemisphere, right cerebral hemisphere or bilateral) and degree of abnormality (1 s.d. $\geq$ x<2 s.d., 2 s.d. $\leq$ x<3 s.d, or x $\geq$ 3 s.d.) can be stored and used in the final evaluation and report.

**[0028]** Approximate entropy. One or more measures of signal entropy, such as approximate entropy, may be measured for the entire recorded EEG frequency range as well as for each of the standard EEG frequency bands for each electrode channel and compared to normal values. If the values are outside of the normal range, the degree of abnormality (based on standard deviations from the mean) for each electrode channel can be determined. The location (left cerebral hemisphere, right cerebral hemisphere or bilateral) and degree of abnormality (1 s.d. $\geq$ x<2 s.d., 2 s.d. $\leq$ x<3 s.d, or x $\geq$ 3 s.d.) can be stored and used in the final evaluation and report.

mality (1 s.d. $\geq$ x<2 s.d., 2 s.d. $\leq$ x<3 s.d, or x $\geq$ 3 s.d.) can be stored and used in the final evaluation and report.

**[0029]** Teager energy/power ratios are generated for each channel for entire frequency range between 1 and 30 Hz in box 306. For each EEG channel, the KTE to power ratio may be calculated for the entire recorded frequency range as well as for the standard EEG frequency bands is calculated for each channel and compared to normal values. If the values are outside of the normal range, the degree of abnormality (based on standard deviations from the mean) for each electrode channel can be determined. The location (left cerebral hemisphere, right cerebral hemisphere or bilateral) and degree of abnormality (1 s.d. $\geq$ x<2 s.d., 2 s.d. $\leq$ x<3 s.d, or x $\geq$ 3 s.d.) can be stored and used in the final evaluation and report.

**[0030]** Left-right univariate ratios may then be determined in box 309. Inter-hemispheric symmetry computation may be based upon univariate features. Each of the quantitated measures of signal properties, such as those described above, will be examined for inter-hemispheric symmetry by calculating the ration of the value obtained for each of the electrode channels recorded from the left cerebral hemisphere to the same value obtained for the homologous electrode channel in the right hemisphere.

**[0031]** In box 312, bivariate features between all channels may also be determined from the EEG data. Inter-hemispheric symmetry computations may be based upon bivariate features. Bivariate measures can be used to evaluate the relationship of signals obtained from each electrode channel from the left cerebral hemisphere to that of the homologous electrodes from the right cerebral hemisphere. These measures include mutual information, linear or nonlinear correlation, coherence, phase locking index and phase lag index. The analysis can be made for the entire range of recorded frequencies as well as for each standard EEG frequency band.

**[0032]** A network model may then be generated in box 315 based upon the bivariate feature values from box 312. A network model can be generated as a weighted graph, based on one or more of the bivariate measures relating signal properties between each pair of electrodes, such that a measure is generated for each electrode site (node) and all other electrodes in the recording. The weighted graph can be converted to a binary graph depicting the node pairs with the strongest association, as defined by one or more bivariate measure, using a threshold in box 318. For example, a threshold of 0.75 may be used, such that the resultant binary graph includes 25% of the total electrode pairs; in the case of a full set of electrodes, excluding midline electrodes, as defined by the International 10-20 System of electrode placement, the total number of pairs is 171 and 43 pairs would be selected for the binary network graph.

**[0033]** In box 321, global network characteristics of the binary and/or weighted network graphs may be determined. These characteristics include, e.g., clustering coefficient and minimum path length. These global characteristic values are compared to norms in box 324 to determine whether or not they are within the normal range. If the values are outside of the normal range, the degree of abnormality (based on standard deviations from the mean) for each electrode channel is determined. The location (left cerebral hemisphere, right cerebral hemisphere or bilateral) and degree of abnormality (1 s.d. $\geq$ x<2 s.d., 2 s.d. $\leq$ x<3 s.d, or x $\geq$ 3 s.d.) will be stored and used in the final evaluation and report.

**[0034]** In addition, characteristics for each node (or electrode) can be defined, based on the following characteristics

for each node: degree, path length to contralateral homologous electrode, and connection strength with contralateral homologous electrode. For each electrode, the degree of that node can be compared to the degree for the same electrode (node) in the normative dataset in box 327 and the location of nodes whose properties do not match those of the normative dataset can be determined.

[0035] In box 330, hubs of the binary and/or weighted network graphs may be identified using one or more criteria for defining hubs, such as degree, betweenness, closeness, and eigen vector centrality. Electrodes which exceed thresholds of the values for each respective measure can be defined as a network hub. Network hubs identified in the recording can be compared to a list of hubs obtained from a normative comparison dataset. Hubs present in the subject network which do not correspond to hubs in the normal datasets may be identified and their location determined to be lateralized to one cerebral hemisphere, localized within one cerebral, or present bilaterally. In addition, nodes in the recorded data which are not present in the normative datasets can be identified and localized. In a similar fashion, the path length between each electrode (node) and the homologous node in the contralateral hemisphere may be calculated. Values for each channel pair can be compared to those of the normal dataset and the location of those pairs which differ significantly from the normal datasets can be determined.

[0036] The cerebral condition can be classified in box 245 of FIG. 3B based upon comparison of values from boxes 309 and 312 of FIG. 3A. After signals have been analyzed and results stored, the EEG data may be classified, based on the composite results from all, or a subset, of each individual analysis: (1) local univariate signal properties, (2) inter-hemispheric symmetry computations based on local univariate signal properties, (3) inter-hemispheric symmetry based on computations of bivariate signal properties, local network properties, and global network properties. If all of these analyses are within acceptable range of normal values, the recording may be classified as normal.

[0037] In box 333, the bivariate feature of homologous pairs is compared with normal values obtained from the same electrode pairs. If the values are outside of the normal range, the degree of abnormality (based on standard deviations from the mean) for each electrode channel may be determined. The location (left cerebral hemisphere, right cerebral hemisphere or bilateral) and degree of abnormality ( $1 \text{ s.d.} \leq x < 2 \text{ s.d.}$ ,  $2 \text{ s.d.} \leq x < 3 \text{ s.d.}$ , or  $x \geq 3 \text{ s.d.}$ ) can be stored and used in the final evaluation and report. In box 336 of FIG. 3B, univariate ratios from each channel pair will be compared to normal ratios for that channel pair. If the ratios are outside of the normal range, the degree of abnormality (based on standard deviations from the mean) for each electrode channel may be determined. The location (left cerebral hemisphere, right cerebral hemisphere or bilateral) and degree of abnormality ( $1 \text{ s.d.} \leq x < 2 \text{ s.d.}$ ,  $2 \text{ s.d.} \leq x < 3 \text{ s.d.}$ , or  $x \geq 3 \text{ s.d.}$ ) can be stored and used in the final evaluation and report.

[0038] If there are abnormalities identified, the EEG data will be classified as abnormal and assigned to one of several abnormal categories in box 248 of FIG. 3B. For example, the abnormal categories may be defined as follows: (1) left hemisphere abnormality, (2) right hemisphere abnormality, (3) bilateral abnormalities. EEG data with bilateral abnormalities may be further subclassified as (3a) bilateral symmetrical abnormalities, (3b) bilateral abnormalities, left greater than right and (3b) bilateral abnormalities right greater than left. In

other implementations, the location of the abnormality may be made more precise, indicating the region(s) within the cerebral hemisphere(s) containing the abnormalities (e.g., left front-temporal abnormality). Abnormal EEG data may be further categorized as to the degree of abnormality, based upon a weighted magnitude of property deviations from normal values as well as the number of properties which deviate significantly from normal values.

[0039] In box 342, regions of altered symmetry are identified and the severity determined based upon values from box 333. In addition, the severity of the abnormality is determined in box 339 based upon values for boxes 324, 327, and 330 of FIG. 3A and box 336 of FIG. 3B. As discussed above, the degree of abnormality may be based on standard deviations from the mean the values for each electrode channel. In some cases, a weighed combination of the standard deviations may be used to indicate the degree of abnormality. The results of the abnormality identification may be stored in a data store or memory and may be used to generate an indication for the operator of the system 100.

[0040] The system 100 may be used for, but is not limited to, neurological assessment of common neurological presentations such as, e.g., acute encephalopathies, subacute encephalopathies, focal lesions, ischemic events, and chronic encephalopathies. Acute and subacute encephalopathies include such disorders as those due to traumatic brain injuries, toxic encephalopathies (e.g. drug or alcohol toxicity), metabolic disorders (e.g. hypoglycemia, hyperglycemia, ketoacidosis, renal failure, hepatic failure, hypoxia, hypercapnea), acute or subacute infections of the brain (such as meningitis, encephalitis, and brain abscess), seizures, status epilepticus, stroke, transient ischemic attacks, and autoimmune disorders affecting the central nervous system. It may also be used for detecting mild disturbances of brain function including, e.g., concussion following after head injuries. Information obtained through the system 100 may be used to refine the differential diagnosis, formulate further workup (e.g. imaging procedures) and treatment, and for purposes of triage and referral to appropriate facilities and specialists. Other potential uses include brain monitoring to evaluate level of alertness, screening of chronic cerebral disorders such as, e.g., Alzheimer's disease and other chronic dementias, and assessment of excess daytime sleepiness and sleep disorders.

[0041] One embodiment, among others, can be an altered mental status evaluator (AMSE). A unique feature of this application is its utility as a tool to assist physicians in the differential diagnosis of subjects in the hospital with acute unexplained persistent altered mental status (AMS). These subjects are commonly seen in the Emergency Room (ER), Intensive Care Unit (ICU) or hospital wards. AMSE provides reliable identification of EEG abnormalities that cause altered mental status including subclinical seizures, diffuse EEG slowing reflecting diffuse encephalopathy and focal EEG slowing reflecting focal brain dysfunction. AMSE then generates a report to assist the physician in diagnosis of subjects with altered mental status. These results can rapidly point the physician to the differential diagnostic areas that should receive the most consideration initially (but should not preclude other avenues of investigation). The physician correlates the results with their clinical examination and results of other studies to reach a final accurate diagnosis more quickly.

[0042] With reference to FIG. 4, shown is a schematic block diagram of a processor system 400 in accordance with various

embodiments of the present disclosure. The processor system 400 includes at least one processor circuit, for example, having a processor 403 and a memory 406, both of which are coupled to a local interface 409. To this end, the processor system 400 may comprise, for example, at least one computer or like device. The local interface 409 may comprise, for example, a data bus with an accompanying address/control bus or other bus structure as can be appreciated. In addition, the processor system 400 includes operator interface devices such as, e.g., a display device 412, a keyboard 415, and/or a mouse 418. In some implementations, the operator interface device may be interactive display 421 (e.g., a touch screen) that provides various functionality for operator interaction with the processor system 400. Various sensors such as, e.g., EEG electrodes 424 may also interface with the processor system 400 to allow for acquisition of EEG signals from a subject. In some embodiments, the EEG electrodes 424 may be an array of electrodes configured to be positioned about the subject's head.

[0043] Stored in the memory 406 are both data and several components that are executable by the processor 403. In particular, stored in the memory 406 and executable by the processor 403 are various application modules 427 such as, e.g., an electrode application module 103, an EEG recording module 106, a signal conditioning module 109, a signal analysis module 112, and a condition classification module 115 of FIG. 1, and/or other applications. Also stored in the memory 406 may be a data store 430 and other data. In addition, an operating system 433 may be stored in the memory 406 and executable by the processor 403.

[0044] It is understood that there may be other applications that are stored in the memory 406 and are executable by the processor 403 as can be appreciated. Where any component discussed herein is implemented in the form of software, any one of a number of programming languages may be employed such as, for example, C, C++, C#, Objective C, Java®, JavaScript®, Perl, PHP, Visual Basic®, Python®, Ruby, Delphi®, Flash®, or other programming languages.

[0045] A number of software components are stored in the memory 406 and are executable by the processor 403. In this respect, the term "executable" means a program file that is in a form that can ultimately be run by the processor 403. Examples of executable programs may be, for example, a compiled program that can be translated into machine code in a format that can be loaded into a random access portion of the memory 406 and run by the processor 403, source code that may be expressed in proper format such as object code that is capable of being loaded into a random access portion of the memory 406 and executed by the processor 403, or source code that may be interpreted by another executable program to generate instructions in a random access portion of the memory 406 to be executed by the processor 403, etc. An executable program may be stored in any portion or component of the memory 406 including, for example, random access memory (RAM), read-only memory (ROM), hard drive, solid-state drive, USB flash drive, memory card, optical disc such as compact disc (CD) or digital versatile disc (DVD), floppy disk, magnetic tape, or other memory components.

[0046] The memory 406 is defined herein as including both volatile and nonvolatile memory and data storage components. Volatile components are those that do not retain data values upon loss of power. Nonvolatile components are those that retain data upon a loss of power. Thus, the memory 406

may comprise, for example, random access memory (RAM), read-only memory (ROM), hard disk drives, solid-state drives, USB flash drives, memory cards accessed via a memory card reader, floppy disks accessed via an associated floppy disk drive, optical discs accessed via an optical disc drive, magnetic tapes accessed via an appropriate tape drive, and/or other memory components, or a combination of any two or more of these memory components. In addition, the RAM may comprise, for example, static random access memory (SRAM), dynamic random access memory (DRAM), or magnetic random access memory (MRAM) and other such devices. The ROM may comprise, for example, a programmable read-only memory (PROM), an erasable programmable read-only memory (EPROM), an electrically erasable programmable read-only memory (EEPROM), or other like memory device.

[0047] Also, the processor 403 may represent multiple processors 403 and the memory 406 may represent multiple memories 406 that operate in parallel processing circuits, respectively. In such a case, the local interface 409 may be an appropriate network that facilitates communication between any two of the multiple processors 403, between any processor 403 and any of the memories 406, or between any two of the memories 406, etc. The local interface 409 may comprise additional systems designed to coordinate this communication, including, for example, performing load balancing. The processor 403 may be of electrical or of some other available construction.

[0048] Although the electrode application module 103, the EEG recording module 106, the signal conditioning module 109, the signal analysis module 112, the condition classification module 115, and other various systems described herein may be embodied in software or code executed by general purpose hardware as discussed above, as an alternative the same may also be embodied in dedicated hardware or a combination of software/general purpose hardware and dedicated hardware. If embodied in dedicated hardware, each can be implemented as a circuit or state machine that employs any one of or a combination of a number of technologies. These technologies may include, but are not limited to, discrete logic circuits having logic gates for implementing various logic functions upon an application of one or more data signals, application specific integrated circuits having appropriate logic gates, or other components, etc. Such technologies are generally well known by those skilled in the art and, consequently, are not described in detail herein.

[0049] Although the flowcharts of FIGS. 2A-2B and 3A-3B show a specific order of execution, it is understood that the order of execution may differ from that which is depicted. For example, the order of execution of two or more blocks may be scrambled relative to the order shown. Also, two or more blocks shown in succession in FIGS. 2A-2B and 3A-3B may be executed concurrently or with partial concurrence. Further, in some embodiments, one or more of the blocks shown in FIGS. 2A-2B and 3A-3B may be skipped or omitted. In addition, any number of counters, state variables, warning semaphores, or messages might be added to the logical flow described herein, for purposes of enhanced utility, accounting, performance measurement, or providing troubleshooting aids, etc. It is understood that all such variations are within the scope of the present disclosure.

[0050] Also, any logic or application described herein, including the electrode application module 103, the EEG recording module 106, the signal conditioning module 109,

the signal analysis module **112**, the condition classification module **115**, and/or application(s), that comprises software or code can be embodied in any non-transitory computer-readable medium for use by or in connection with an instruction execution system such as, for example, a processor **403** in a computer system or other system. In this sense, the logic may comprise, for example, statements including instructions and declarations that can be fetched from the computer-readable medium and executed by the instruction execution system. In the context of the present disclosure, a “computer-readable medium” can be any medium that can contain, store, or maintain the logic or application described herein for use by or in connection with the instruction execution system. The computer-readable medium can comprise any one of many physical media such as, for example, magnetic, optical, or semiconductor media. More specific examples of a suitable computer-readable medium would include, but are not limited to, magnetic tapes, magnetic floppy diskettes, magnetic hard drives, memory cards, solid-state drives, USB flash drives, or optical discs. Also, the computer-readable medium may be a random access memory (RAM) including, for example, static random access memory (SRAM) and dynamic random access memory (DRAM), or magnetic random access memory (MRAM). In addition, the computer-readable medium may be a read-only memory (ROM), a programmable read-only memory (PROM), an erasable programmable read-only memory (EPROM), an electrically erasable programmable read-only memory (EEPROM), or other type of memory device.

**[0051]** It should be emphasized that the above-described embodiments of the present disclosure are merely possible examples of implementations set forth for a clear understanding of the principles of the disclosure. Many variations and modifications may be made to the above-described embodiment(s) without departing substantially from the spirit and principles of the disclosure. All such modifications and variations are intended to be included herein within the scope of this disclosure and protected by the following claims.

#### EEG Analysis of Brain Dynamical Behavior with Applications in Epilepsy

##### LIST OF ABBREVIATIONS

<b>[0052]</b>	AED Anti-epileptic drug
<b>[0053]</b>	ANOVA Analysis of variance
<b>[0054]</b>	AR Autoregressive
<b>[0055]</b>	ARMA Autoregressive moving average
<b>[0056]</b>	ARIMA Autoregressive integrated moving average
<b>[0057]</b>	CC Cross-correlation
<b>[0058]</b>	CPS Complex partial seizure
<b>[0059]</b>	EEG Electroencephalogram
<b>[0060]</b>	EMU Epilepsy monitoring unit
<b>[0061]</b>	EWS Evolutionary wavelet spectrum
<b>[0062]</b>	FN False negative
<b>[0063]</b>	FPR False positive rate
<b>[0064]</b>	LSW Local stationary wavelet
<b>[0065]</b>	GABA Gamma-Aminobutyric acid
<b>[0066]</b>	MSC Mean square coherence
<b>[0067]</b>	MTLE Mesial temporal lobe epilepsy
<b>[0068]</b>	PLAI Phase lag index
<b>[0069]</b>	PMRS Pattern-match regularity statistics
<b>[0070]</b>	PNES Psychogenic nonepileptic seizures
<b>[0071]</b>	STLmax Short-term maximum Lyapunov exponent
<b>[0072]</b>	SVM Support vector machine

**[0073]** TN True negative

**[0074]** TP True positive

#### Chapter 1

##### Introduction

##### Electroencephalogram

**[0075]** Electroencephalogram (EEG) is a technology measuring the voltage of activation from a set of neurons within the brain. EEG electrodes can record brainwaves from either the scalp or, through invasive procedures, deeper layers of the brain tissue. Depending on the location and the type of the electrodes, EEG signals can reveal different levels of neuronal activities. Scalp EEG is the least invasive methodology and is, therefore, widely used in many fields of neuroscience including psychology, epilepsy, brain machine interface, and sleep research. EEG has become a more popular means of recording interesting brain activity over the last few decades because improvements in computing power and storage capacity make possible sophisticated analyses of very large amounts of EEG data.

**[0076]** Like electrocardiogram (ECG), another widely used bioelectrical signal in monitoring and diagnosing heart abnormalities, numerous electrodes can be applied on one subject so that the EEG data have both temporal and spatial information of brain activity. The location of electrode placement on a scalp usually follows the 10-20 system. Distinct landmarks of a head are first identified and then electrodes are placed at 10% or 20% distance intervals along the landmarks. Through analyzing the multi-channel EEG data of a short period of time, a temporary brain network can be identified. Analyzing long-term EEG recording data can reveal the dynamics of the brain network as the subject goes through many states of mental activity or pathological manifestation.

**[0077]** The EEG data included in this disclosure contain both scalp and intracranial EEGs. All of them are continuous long-term recordings from either Allegheny General Hospital (AGH, Pittsburgh, Pa.) or the Medical University of South Carolina (MUSC, Charleston, S.C.). Depending on the study design, long-term continuous or extracted EEG recordings were analyzed. All scalp EEG data were recorded using 19 channels and intracranial EEG data used respectively different channels covering the different brain areas depending on the specific case of each epileptic patient. All recordings are from human beings who are older than 18 years old and experienced epileptic or psychological non-epileptic seizures.

##### Epilepsy

**[0078]** Epilepsy is a brain disorder, instead of a disease, characterized mostly by recurrent and unforeseen interruptions of normal brain function. It has been known from ancient times and was, at one point, attributed to divine intervention until the great Greek physician Hippocrates realized that it was a disorder of the brain. It is also the second most common disorder of the central nervous system and affects about 0.4-1% of the population.

**[0079]** The sudden interruption of brain function is termed a seizure. Many other physical or psychological sudden and severe events are also called seizures, such as a heart seizure. The meaning of a seizure, going back to its’ origin in Greek, is “to take hold”. An epileptic seizure is the manifestation of epilepsy and is due to abnormally excessive or synchronous

neuronal activity in the brain. The duration of the manifestation of an epileptic seizure is sometimes called an ictal period. Most epileptic seizures can be recorded by the electrodes of an EEG and shown in the EEG data. Through reading and analyzing the epileptic EEG data, more information is gained about the onset pattern and type of epilepsy. During the onset of an epileptic seizure (ictal period), one may observe that the synchronous and rhythmic discharges originate from one part of the brain (partial, focal or localization-related seizures) or begin simultaneously in both sides of the hemispheres (generalized seizures). Focal seizures after the onset may remain localized within one part of the brain or propagate to the other side of the hemisphere and cause a wider range of synchronous neuronal activity (secondarily generalized seizures). If a seizure is confined to a limited area of the brain, it usually causes relatively mild and transient cognitive, psychic, sensory, motor or autonomic impairment. However, generalized seizures cause altered consciousness and accompany a variety of motor symptoms from the jerking of limbs to stiff or convulsive movements of the whole body. During the ictal period of focal seizures, consciousness may be unaffected (simple partial seizures) or be impaired (complex partial seizures). Few patients with focal seizures feel unusual sensations (auras) when experiencing the beginning stage of an ictal period. Most seizures occur in a nearly unpredictable manner, stressing the patients as well as the people around them.

**[0080]** Since an epileptic seizure is characterized by excessively synchronous neuronal activity, researchers hypothesize that the dysfunction of the inhibition mechanism of neurons favors the development of seizures. Gamma-aminobutyric acid (GABA) is the most prevalent inhibitory neurotransmitter in human brains. GABAergic inhibition is one of the main control mechanisms influencing the excitability of neurons. Many compounds that increase the GABAergic inhibition are used as anti-epileptic drugs (AED). Although many studies confirm the relationship between GABAergic inhibition and the development of epilepsy, about 20-30% of epileptic patients failed to benefit from the administration of AED. These latter patients expressed poor quality of life due to both depression and neurotoxicity from AED. Although patients have different seizure onset frequencies and severities, seizure types and frequencies did not correlate with the score of quality of life. These study results suggest that the frequency or severity of seizures is not the primary cause of patient depression, but rather the sense of uncertainty regarding seizure onsets and the constant fear of unpredictable onset. The presence of correct seizure onset warnings should alleviate the degree of depression and increase quality of life by decreasing the amount of uncertainty and offering patients the ability to prepare for seizure onset.

## Chapter 2

### The Properties and Analysis of Non-Stationary Time Series

#### Foreword

**[0081]** Most phenomena happening with time can be measured and recorded as time series, such as wind speed, heart rate, stock exchange price, and EEG signals. By analyzing a time series, insight may be gained into an array of interesting and complex phenomena. A human brain is a complex system that responds simultaneously to many external inputs as well

as numerous internal processes. Analysis and quantification of the characteristics of EEG signals offer a window to observe the complex interactions amongst neurons in a brain. For example, in awake and asleep EEG signals, one can recognize that the signals usually have swiftly changing backgrounds. Therefore, EEG signals are usually regarded as non-stationary time series consisting of the many distinct background activities that occur when a subject experiences different phases of psychological events or physiological states. Analyzing and forecasting non-stationary time series have been challenging for researchers. Many possible methodologies have been developed to alleviate the difficulties of analyzing a non-stationary process. Chapter 2 introduces the basic properties and analysis of a non-stationary times series. Since the rapid growth in the power of computational machines, the ability to investigate very data rich EEG signals with sophisticated and computation-demanding techniques has been gained.

**[0082]** For an interesting time series, it is convenient to assume that there are exact mathematical models generating the time series. Understanding the underlying mechanism of these processes is very crucial in engineering and science. It is also intuitive to presume that there are rules governing the route of a time series and once those rules are understood, a forecast of how the time series may develop may be improved. However, real life phenomena are rarely that simple and usually involve many parameters, noise, and unobserved variables that can influence the time series with different time lags to a different extent. Still, with careful control of the recording environment, it is feasible to reduce many unobserved covariates and try to model the time series as a stochastic process. The more precise the time series model, the smaller the forecasting error that can be achieved.

**[0083]** To understand all the principles and rules controlling these black-box systems at once is nearly impossible. Therefore, simple non-stationary paradigms are introduced before moving to the more complicated time series. As aforementioned, a straightforward assumption is that a process possesses certain fixed properties in itself so that it evolves with principles. One of the most convenient properties in a stochastic process is stationarity. Stationarity in the strict sense means those statistics of a stochastic process do not change with time as described in Equation 2-1.

$$\int_{x_1, x_2, \dots, x_n} f(x_1, x_2, \dots, x_n) dx_1 dx_2 \dots dx_n = \int_{x_1, x_2, \dots, x_n} f(x_1 + \tau, x_2 + \tau, \dots, x_n + \tau) dx_1 dx_2 \dots dx_n \quad (2-1)$$

In Equation 2-1,  $f$  denotes the probability mass function and  $T$  denotes a time lag of any size. When a process fails to fulfill Equation 2-1, the process is considered not stationary in the strict sense.

**[0084]** Stationary processes possess relatively stable statistical properties compared to non-stationary ones; such as a fixed mean and variance. Nevertheless fixed mean and variance by themselves do not imply stationarity in the strict sense. With those fixed statistics, it is possible to begin predicting the foregoing process with more confidence. The first section of Chapter 2 focuses on some background for methods that will be introduced later. In the second section of Chapter 2, two well-known practical methods to forecast non-stationary processes are presented.

#### Properties of Time Series

##### Stationarity

**[0085]** Stationarity in the strict sense is almost impossible in real life. Even a parametric simulated process can have

stationarity only theoretically, not to mention a time series recorded from real world signals which have much more complex mechanisms. Although one can hardly have a stationary process in the strict sense, the concept of stationarity may be utilized when studying non-stationary time series because of its convenient statistical properties. A process may be claimed to have stationarity in a wide sense if it has not only a fixed mean and variance but also time-invariant autocovariance. One reason for keeping the concept of stationarity in a stochastic process is that a parametric model can hardly include all variables that affect the process, not to mention some factors that are beyond the researcher's control. To take all effects into account, a stochastic process should be modeled with several deterministic and random terms. One way to implement this is to use the concept of piecewise stationarity. Even though the whole process is non-stationary, each segment of a reasonable length may be treated as if they were stationary, after disintegrating it into segments. Based on a piecewise stationary concept in the time domain, one can make an analogue to the time and frequency domain, which is the idea of local stationary wavelet analysis which will be introduced in the non-parametric method section.

#### Local Stationarity

**[0086]** One of the crucial parameters for using the concept of piecewise stationarity is how to choose the length of a segment that is neither too short for calculating statistical estimates nor too long so that the process is no longer stationary. It should be noted that the criterion for selecting the segment length should always be dependent on the method used in order to model the non-stationary process. For example, for a quasi-stationary process, the underlying assumption is that the parametric properties might change their state between different time segments. As a result, an ideal segment should not be too long to overlap segments having different parametric values. Compared to quasi-stationary processes, parameters of a time varying autoregressive model do not suddenly change, but gradually evolve along with time. Proper selection of a method to model a process depends on some basic properties of the raw data. For instance, a seismic wave recording or an electroencephalograph recording containing a seizure shows a sudden state change. As a result, it is reasonable to use a quasi-stationary method for modeling. For other processes, such as the population of some species or the price of a stock, one might only be interested in their smooth evolution property instead of their sudden change due to special or dramatic events, so it would be reasonable to use a time-varying autoregressive model that will be introduced later. Those methods of modeling a non-stationary process are called parametric methods. In addition, one can use non-parametric methods which do not assume the existence of a model or distribution family in a process. Compared to parametric methods, non-parametric methods still involve parameter choosing to some extent but not as much as parametric methods. If one intends to observe a non-stationary process as a piecewise, quasi, or evolutionary stationary process, a very well-known and widely used non-parametric tool called time-dependent spectrum in the time-frequency analysis field can be used.

#### Parametric Methods for Analyzing Non-Stationary Time Series

**[0087]** The benefits of using a parametric method are its simplicity and lucid structure. The main feature of parametric

methods is the use of parameters as structural elements to introduce interpretation and interaction so that one can reduce ambiguity within the data itself. This, however, might be achieved at the risk of misinterpretation. Some other parametric approaches are based on specific assumptions that process outputs belong to the family or families of the distributions used in the model or can be described as the output of a stochastic process, whereas non-parametric approaches do not impose specific constraints with regards to the distribution family. One has to first carefully scrutinize the statistical properties of the observed data and the assumption for the parametric method being applied for estimation. In sum, parametric methods are beneficial only if there is a strong reason to look at the process in a particular structural way or as a member of a certain distribution family. As one can imagine, a parametric approach might not perform well on a process having a huge future random term that does not constantly fall into any distribution family and has a weak link between current and future states of the process. Time-Varying Autoregressive (AR) models, just like a stationary process, can use parametric or non-parametric means to start the analysis on a non-stationary process. One of the most commonly used models for simulating or fitting non-stationary time series is the time-varying AR model. A  $p^{\text{th}}$  order linear time-varying AR model can be written in a general form as Equation 2-2.

$$x_k = \sum_{i=1}^p \phi_{i,k} x_{k-i} + \epsilon_k \quad (2-2)$$

In Equation 2-2,  $\phi_{i,k}$  are time-varying parameters that differentiate a time-varying AR model from an AR model that has a fixed coefficient  $\phi_i$  instead of  $\phi_{i,k}$ . The main difficulty in using a parametric model for analysis lies in choosing proper values for the parameters. As Equation 2-2 shows,  $p$  and  $\phi_{i,k}$  are parameters which need to be chosen based on the training data while  $\epsilon_k$  is a zero-mean white noise process. One advantage of a parametric method is that it renders a lucid dynamic relationship between data points and gives some sense of how data evolve over time. However, the model may not be unique because of the uncertainty of parameters. One should bear in mind that models of different orders may be fit into the same datasets. In this case the time varying AR model parameter values ( $\phi_{i,k}$ ) might be significantly different especially for a complex dataset. Several methods have been proposed to find the optimal order of an AR model such as Akaike information criterion, Bayesian information criterion, and the likelihood ratio test. Once the order of the AR model is decided,  $\phi_i$  are calculated from Yule-Walker equations. Other methods exist for estimating regression coefficients, such as Burg's method, least-squares approach, modified covariance method, covariance method, parametric spectral estimation method, Prony's method, etc. However, choosing the order of a time-varying AR model is more complex than that of an AR model. A recently proposed method for time-varying AR model order uncertainty is the generalized likelihood ratio test.

**[0088]** Autoregressive Integrated Moving Average (ARIMA) Model:

**[0089]** Modeling an interesting time series as a non-stationary processes whose derivative, of proper order, is a stationary process. An autoregressive moving average model (ARMA) can be represented in Equation 2-3.

$$x_n = - \sum_{k=1}^p a_k x_{n-k} + \sum_{k=0}^q b_k u_{n-k}, \quad p, q \in Z \quad (2-3)$$

In Equation 2-3,  $\{u_n\}$  is a Gaussian white noise process. An ARIMA can exhibit not only ARMA but also non-stationarity having neither fixed mean nor fixed variance. A very important property of ARIMA is that if one takes the  $d^{th}$  derivative of the process it will result in a stationary process that can be represented by another ARMA model  $\{x_n\}$ . This relationship can be represented in Equation 2-4.

$$\Delta^d z_n \triangleq x_n = - \sum_{k=1}^p a_k x_{n-k} + \sum_{k=0}^q b_k u_{n-k}, \quad p, q, d \in Z \quad (2-4)$$

This relationship renders a powerful linkage for changing a non-stationary process into a stationary process which can be more easily analyzed. However, one should notice that the high frequency components of the process would be amplified after differentiating. Considering an ARMA (p,q), with  $q \leq p$ , it is possible that the AR part has more terms than the MA part. The realization of an ARMA state space model is given in Equation 2-5.

$$\tilde{x}_{k+1} = F_k \tilde{x}_k + \begin{bmatrix} b_{1,k} - a_{1,k} \\ b_{2,k} - a_{2,k} \\ \vdots \\ b_{p,k} - a_{p,k} \end{bmatrix} \tilde{u}_k, \quad (2-5)$$

$$z_k = [1 \ 0 \ \dots \ 0] \tilde{x}_k + u_k, \quad (2-6)$$

In Equation 2-5,  $\tilde{x}_k = \{x_k, x_{k-1}, \dots, x_{k-p+1}\}^T$  and  $\{\tilde{u}_k\}, \{u_k\}$  are both Gaussian white noise processes. Tilda indicates a vector. If the transition matrix is denoted as  $F_k$ , the noise coupling matrix as  $G_k$  and the observation matrix as  $\tilde{h} = [1, 0, \dots, 0]$ . Using Equation 2-5 and Equation 2-6, Equation 2-3 and Equation 2-4 become Equation 2-7 and Equation 2-8.

$$\tilde{x}_{k+1} = F_k \tilde{x}_k + G_k \tilde{u}_k, \quad (2-7)$$

$$z_k = \tilde{h} \tilde{x}_k + u_k \quad (2-8)$$

We can make a comparison between ARIMA and time-varying AR which has the dynamic matrix form as in Equations 2-9 and 2-10.

$$\tilde{x}_{k+1} = F_k \tilde{x}_k + \epsilon_k, \quad (2-9)$$

$$z_k = \tilde{h} \tilde{x}_k, \quad (2-10)$$

In Equation 2-9,  $\epsilon_k$  is a zero-mean innovation with time-varying variance and  $F_k$  is described in Equation 2-11.

$$F_k = \begin{bmatrix} \phi_{1,k} & \phi_{2,k} & \dots & \phi_{p-1,k} & \phi_{p,k} \\ 1 & 0 & \dots & 0 & 0 \\ 0 & 1 & \dots & 0 & 0 \\ \vdots & 0 & \ddots & \vdots & \vdots \\ 0 & 0 & \dots & 1 & 0 \end{bmatrix}. \quad (2-11)$$

## Non-Parametric Methods for Analyzing Non-Stationary Time Series

**[0090]** Non-parametric methods assume no specific distribution or fixed structure existing for a process. Some parameter settings still exist in the non-parametric methods but the parameters are mainly for the sensitivity aspects of the analysis rather than relating to whole process. As a result, non-parametric methods are less affected by the choice of assumptions or parameter value compared to a parametric method. In sum, non-parametric methods do not explain the mechanism behind a time series and are more data-driven.

### Wavelet Transforms

**[0091]** Wavelet analysis is one of the most utilized tools for time-frequency analysis. Most of the stationary processes are generated and recorded in the time domain. However, a weak stationary process can be characterized by its' frequency components. That is why Fourier transform is applied in almost every field of science and engineering. The Fourier transform represents a process formulating a superposition of frequencies.

$$X(f) = \int_{-\infty}^{\infty} x(t) e^{-2\pi j f t} dt \quad (2-12)$$

$$x(t) = \int_{-\infty}^{\infty} X(f) e^{2\pi j f t} df \quad (2-13)$$

In Equation 2-12,  $i$  denotes an imaginary unit. Although the representation through Fourier transform can clearly show those weighted components of a process in terms of frequencies, it does not include any time component. One can hardly perceive when those frequency components participate in a process. Especially for real data such as seismic waves or biomedical signals, a functional transform showing results in both the time and frequency domain can be much more informative and intuitive. A very widely used time-frequency analysis is the wavelet transform which renders a perspective with both time and frequency resolutions through imposing a mask function before the original signal.

$$X(t,f) = \int_{-\infty}^{\infty} w(t-\tau) x(\tau) e^{-2\pi j f t} d\tau, \quad (2-14)$$

In Equation 2-14,  $w(t-\tau)$  is a window function. When  $w(t-\tau)$  is a rectangular window the above equation is also called short-time Fourier transform, windowed Fourier transform, or time-dependent Fourier transform. One may observe the characteristic of the wavelet from Equation 2-14 that it has a  $t$  parameter that can characterize the signal at a certain range on the time domain. A real life signal such as seismic waves show characteristics of a short impulsive feature that can hardly be described through Fourier transform decomposing the seismic wave into a combination of sinusoidal functions ranging from negative infinity to infinity. Because of the dual property of a wavelet in both the time and frequency domain, one cannot use a wavelet for time-frequency analysis only, but also for de-noising a process that has noise with a certain unique frequency band and that occurs sporadically along the time frame.

### Local Stationary Wavelets

**[0092]** Assuming that a process  $\{X_t\}, t \in Z$  possesses stationarity, second-order statistics such as variance or autocovariance may be estimated through only a segment of observation and have confidence in the estimated statistics because its stationarity has rendered characteristic quantitative homogeneity. Having longer term observation, statistics

may be estimated better through elongating the observational period. In contrast, for a non-stationary process, assuming that the variance of a process changes slowly over time, saying that variance is a continuous and differentiable function of time, the variance could still be estimated with certain precision by gathering information around the time point of interested variance. This demand exactly fits the property of wavelet transform which preserves the local characteristics of a process to some extent on both the time and frequency domain respectively. A statistically slowly changing process can be called a local stationary process. For a covariance-stationary process,  $X_t$ , there is a Cramér representation as Equation 2-15.

$$X_t = \int_{(-\pi, \pi)} A(\omega) \exp(i\omega t) dZ(\omega), t \in Z \quad (2-15)$$

**[0093]** In Equation 2-15,  $\exp$  means exponential and  $Z(\omega)$  is a stochastic process with orthonormal increments. Non-stationary processes can be written almost the same as Equation 2-15 but  $A(\omega)$  is replaced by a function of time. Following this rationale, a non-stationary process can be represented using local stationary wavelet and non-decimated discrete wavelets  $\Psi_{j,k}(t)$ ,  $j=-1, -2, \dots, k \in Z$  where  $j$  indicates the scale and  $k$  indicates time location. To express a local stationary process, one can write it as Equation 2-16.

$$X_t = \sum_{j=-1}^{-1} \sum_{k \in Z} w_{j,k} \Psi_{j,k}(t) \xi_{j,k}, \quad (2-16)$$

In Equation 2-16,  $\xi_{j,k}$  is the mutually orthogonal zero mean random innovation. From Equation 2-15 and Equation 2-16, one should notice that  $w_{j,k}$  in Equation 2-15 corresponds to  $A(\omega)$  in Equation 2-15 and both of them indicate the amplitude of each analysis component. One should also notice that  $\Psi_{j,k}(t)$  is a replacement of the Fourier harmonics  $\exp(i\omega t)$ , in Equation 2-15. The subscript indices  $j$  and  $k$  in  $w_{j,k}$  represent scale and time location respectively just like those in  $\Psi_{j,k}(t)$ . The reason for using a non-decimated discrete wavelet is that it can be shifted to any time point and not only confined in shifts of  $2^{-j}$  compared with a discrete wavelet. Please note that non-decimated wavelets do not have orthogonalities and are an overcomplete collections of shifted vectors. An example of a discrete non-decimated wavelet is the Haar wavelet. Nason also proposed an evolutionary wavelet spectrum (EWS) to quantify how the size of  $w_{j,k}$  changes over time as in Equation 2-17.

$$S_j(z) = S_j(k/T) \approx w_{j,k}^2 \quad (2-17)$$

Please note that in EWS,  $S_j(z)$ , still has resolution on both the frequency and time domain but with a different time scale which rescales the whole observation time into  $z \in (0,1)$ . Rescaled time,  $z$ , is calculated by dividing  $k$  by the whole observation time length,  $T$ , and  $k=0, 1, \dots, T-1$ . The goal is to estimate the variance of a local stationary process. To accomplish that, one way is to put together the localized information around the time point of interest, with the concept of local stationary wavelet and EWS, let  $c(z, \tau)$  represent localized autocovariance and be defined as Equation 2-18.

$$\lim_{T \rightarrow \infty} \text{cov}(X_{[zT]-\tau}, X_{[zT]+\tau}) = c(z, \tau) = \sum_{j=-\infty}^{-1} S_j(z) \Psi_j(\tau) \quad (2-18)$$

In Equation 2-18,  $\Psi_j(\tau)$  is the autocorrelation function of  $\Psi_{j,k}(t)$  and  $[.]$  denotes the integer part of the real number.

$$\Psi_j(\tau) = \sum_{k=-\infty}^{\infty} \psi_{j,k}(0) \psi_{j,k}(\tau) \quad (2-19)$$

Once localized autocovariance is defined, localized variance at time  $z$  can be defined as described in Equation 2-20.

$$v(z) = c(z, 0) = \sum_{j=-\infty}^{-1} S_j(z) \quad (2-20)$$

Further evidence supporting that a time-frequency domain autocovariance in terms of wavelets preserves the intuitive sense of an autocovariance in the time domain can be seen through the relationship between Allan variances, which is defined as Equation 2-21, and Haar wavelet variances.

$$\bar{X}_t(\tau) = \frac{1}{\tau} \sum_{n=0}^{\tau-1} X_{t-n}, \quad (2-21)$$

It is worth noting that Allan variance involves merely localized time domain representation. However, a Haar wavelet involves both localized time and frequency domain representations. In this case, an Allan variance can be expressed as in Equation 2-22.

$$\sigma_X^2(\tau) = \frac{1}{2} E(|\bar{X}_t(\tau) - \bar{X}_{t-\tau}(\tau)|^2), \quad (2-22)$$

A Haar coefficient on the finest scale or smallest dilation,  $j=-1$ , at translation or location, can be expressed as Equation 2-23.

$$\bar{d}_{-1,k} = 1/\sqrt{2} (X_{2k+1} - X_{2k}), k=0, \dots, T/2-1 \quad (2-23)$$

Then it can see that they have the relationship as Equation 2-24.

$$\text{var}\{\hat{d}_{j,k}\} = E\hat{d}_{j,k}^2 = \tau_j \sigma_X^2(\tau_j), \quad (2-24)$$

#### Forecasting Non-Stationary Time Series

**[0094]** Based on the background mentioned above, prediction algorithms for non-stationary processes may be presented. A Kalman filter can be used for prediction on a more parametric basis. Compared to a Kalman filter, local stationary wavelets do not necessarily need to fit data with a parametric model and may concern only measurement per se. In contrast to a parametric analysis, a non-parametric analysis forsakes the idea that there is a model governing the evolution of data and that, in any case, the observation should be allowed to characterize the data by itself.

## Kalman Filter

**[0095]** The Kalman filter is a recursive filter that can estimate linear dynamic parameters given some noisy measurements. Here the word, filter, should not be taken as only a passive data processing algorithm, but think of it as an active computer program that gathers information from inputs and then optimally estimates the transition of a system. In the previous subsection introducing ARIMA, a non-stationary process can be treated as a stationary ARMA after taking appropriate orders of derivative on the ARIMA. As a result, first analyze only ARMA without loss of generality and then transform the result back to the ARIMA model. If an ARIMA fails to be differentiated properly into an ARMA, one can still implement a Kalman filter onto an ARIMA process even if the ARIMA has missing observations. Since the Gaussianity and linearity possessed in a Kalman filter are independent from the non-stationarity of a process, linearity and Gaussianity in the Kalman filter can be assumed and used to analyze a non-stationarity process.

**[0096]** According to work by McGonigal and Ionescu in 1995, a state space model should be found first before applying a Kalman filter for prediction. It was proposed that there was a simplified model based on Masanao Aoki's method that can model an ARMA state space. In Huang et al, 1995, the authors implemented a Kalman filter to predict a time-varying AR (2) process which is a non-stationary and Gaussian-Markovian process and can be described in a general form as Equation 2-25.

$$x_k = \sum_{i=1}^p \phi_{i,k} x_{k-i} + \varepsilon_k + \sigma_k, \quad (2-25)$$

**[0097]** If one compares Equation 2-25 to Equation 2-2, one should notice that the time-varying model mentioned in this section has an extra term,  $\sigma_k$ . Huang added  $\sigma_k$ , a time-varying term, to better track the moving trend in the data of wind speed which is one of the applications in his work. To describe this time-varying AR (2) model in a matrix form, first define a vector space  $\Psi(\phi_1 \phi_2 \sigma)^T$  containing parameters that need to be decided later and then represent the differences of parameters as they evolve with time using their dynamic relationship.

$$\begin{pmatrix} \Psi_k \\ \Gamma_k \end{pmatrix} = \begin{pmatrix} I & I \\ 0 & H \end{pmatrix} \begin{pmatrix} \Psi_{k-1} \\ \Gamma_{k-1} \end{pmatrix} + \begin{pmatrix} 0 \\ I \end{pmatrix} \Omega_k, \quad (2-26)$$

**[0098]** In Equation 2-26, I is the identity matrix,  $\Omega$  is a zero-mean white noise vector. If H is defined as an identity matrix,  $\Gamma_k$  is a random walk process and then  $\Psi_k$  ends up being an integrated random walk process. If H is a zero matrix, then  $\Gamma_k$  should be a white Gaussian noise process and  $\Psi_k$  ends up being a random walk process. Please note that the role of  $\Gamma_k$  is the first order difference of  $\Psi_k$  and it describes the changes between  $\Psi_k$  and  $\Psi_{k-1}$  as time moves on. A non-stationary process can be predicted, which is a time-varying AR (2) model, once the crucial step of choosing parameters in the model is done and this can be accomplished by Kalman algorithm. A general way of implementation of a Kalman filter starts with setting up the parameter model in the state space form.

$$\hat{z}_k = A\hat{z}_{k-1} + B\tilde{\varepsilon}_k, \quad (2-27)$$

$$\tilde{y}_k = C\hat{z}_k + \tilde{\eta}_k, \quad (2-28)$$

In Equation 2-28,

**[0099]**

$$\hat{X}_{t+h-1,T} = \sum_{s=0}^{t-1} b_{t-1-s,T}^{(t,h)} X_{s,T}, \quad (2-33)$$

is the state vector and  $y_k$  is the observation vector of dimension p, meaning  $\tilde{y}_k = (x_k \dots x_{k-p+1})^T$ . Given the estimation of  $z_k$  as  $\hat{z}_k$ , one can write the estimation dynamics in terms of a current estimation, a past estimation, and a dynamic transition matrix A.

$$\hat{z}_{k|k-1} = A\hat{z}_{k-1}, \quad (2-29)$$

**[0100]** Then define the covariance matrix of estimation errors  $P_k = \langle (\hat{z}_k - \tilde{z}_k)^T (\hat{z}_k - \tilde{z}_k) \rangle$ , state disturbance matrix  $R = \langle \tilde{\varepsilon}_k^T \tilde{\varepsilon}_k \rangle$ , where  $\langle \cdot \rangle$  denotes expectation, and the noise variance matrix of measurement  $Q = \langle \tilde{\eta}_k^T \tilde{\eta}_k \rangle$ . The updated state vector estimation,  $\hat{z}_k$ , can be calculated through Young's recursive algorithm

$$\hat{z}_k = \hat{z}_{k-1} + P_{k|k-1} C^T [C P_{k|k-1} C^T + R]^{-1} [y_k - C \hat{z}_{k-1}], \quad (2-30)$$

$$P_k = P_{k|k-1} - P_{k|k-1} C^T [C P_{k|k-1} C^T + R]^{-1} C P_{k|k-1}, \quad (2-31)$$

$$P_{k|k-1} = A P_{k-1} A^T + B Q B^T, \quad (2-32)$$

## Local Stationary Wavelet (LSW)

**[0101]** Given a series of t measurements, in which it is desired to use those t measurements to predict the process h step after t, an interested process can be written as  $X_{0,T} \dots X_{t-1,T}$  where  $T=t+h$  and then define a linear predictor using Equation 2-33.

$$\hat{X}_{t+h-1,T} = \sum_{s=0}^{t-1} b_{t-1-s,T}^{(t,h)} X_{s,T}, \quad (2-33)$$

The next task is to optimize  $b_{t-1-s,T}^{(t,h)}$  so that the mean square prediction error (MSPE),  $E(\hat{X}_{t+h-1,T} - X_{t+h-1,T})^2$  is minimized. To utilize the properties of LSW, approximate MSPE can be represented in a wavelet matrix form.)

$$E(\hat{X}_{t+h-1,T} - X_{t+h-1,T})^2 = \tilde{b}'_{t+h-1,T} B_{t+h-1,T} \tilde{b}_{t+h-1,T}, \quad (2-34)$$

In Equation 2-34,  $\tilde{b}'_t (\tilde{b}'_{t-1,T}^{(1)}, \dots, \tilde{b}'_{0,T}^{(1)})$  and  $B_{1,T}$  is the covariance matrix consisting of localized autocovariance whose size is  $(t+1) \times (t+1)$  and  $(m, n)$ -th element is  $c(n+m/2T, n-m)$  which is the localized autocovariance involving a wavelet form as mentioned in the background LSW section. The whole procedure of forecasting a non-stationary process with long enough observations involves two training sets. First, divide the long-term observations into two training sets and use the first one to generate the  $B_{t,T}$  matrix. Second, use the other training set to optimize  $\tilde{b}'_t$  vector such that MSPE is minimized. In practice, the first part involves selection of two more parameters. Once those parameters are selected, the model would be ready for prediction.

**[0102]** In Chapter 2, the properties of non-stationary stochastic time series and some common methods for modeling or analyzing them are introduced. Forecasting a non-stationary stochastic process can be achieved if the parametric model constructed is proper and robust or the non-parametric methods are precisely updated.

### Chapter 3

#### Signal Regularity-Based Automated Seizure Prediction Algorithm on Scalp EEG

##### Background and Significance

**[0103]** An epileptic seizure is a transient occurrence of signs and/or symptoms due to abnormal excessive and synchronous neuronal activity in the brain. The worldwide prevalence of epilepsy ranges from 0.4% to 1%. Some epileptic patients experience a prodrome or an aura, which can serve as a warning before the signs of seizure onset. Rare patients learn to abort a seizure without external intervention. However, most patients cannot predict or arrest their seizures. In industrialized countries, where antiepileptic drugs and seizure control devices are readily available, about 70% of epilepsy patients are able to gain satisfactory control of their seizures. For patients whose seizures do not respond to antiepileptic medications, less than 50% are candidates for epilepsy surgery. Therefore, approximately 15-20% of epilepsy patients have no choice but to live their lives with unforeseen and uncontrolled seizure attacks, which cause considerable stress for these patients and their care-givers and limit the range of daily activities available due to safety concerns. These lifestyle limitations decrease quality of life and may contribute to the increased prevalence of depression in patients with uncontrolled seizures. If a device could be developed that could warn an epilepsy patient of an impending seizure, it could lessen the psychological stress of epilepsy and improve patient safety.

**[0104]** Numerous studies on intracranial EEG and fMRI data in epilepsy patients suggest the existence of a preictal transition between an interictal and ictal state, and many attempts have been made to identify the most consistent patterns of preictal transitions. In the last two decades, signal processing methods in nonlinear dynamics have been popularly applied to EEG analyses because of the non-linear nature of neuronal activity and the paroxysmal character of epileptic seizures. Due to the complexity of the implement of prediction, it is not enough to just utilize features showing differences between preictal and ictal states. Decisions about issuing a warning based on features need to be made continuously as the EEG signals shift from state to state in the real life environment. Therefore, many other sophisticated engineering techniques derived from statistical learning and control theory were also employed on EEG data to facilitate seizure prediction performance. Studies utilizing a variety of engineering techniques and also the features on EEG data will be introduced. It is not surprising that most seizure prediction studies were on intracranial EEG recordings because the signals are less influenced by movement, muscle, and other normal physiologic activities. Chisci, Mavino and coworkers applied classic parametric models and machine learning techniques to accomplish seizure prediction on intracranial EEG from nine patients in the Freiburg database. The authors extracted the parameters of autoregressive models for each EEG channel as dynamic features. The feature values were

then fed into a classifier combining the support vector machine along with Kalman filter techniques. Training and testing procedures were implemented for 10 runs for each patient. Authors achieved 100% sensitivity and zero false-positive rates on data from two patients while the remaining seven patients had false-positive rates among 0.12 to 1.03 false warnings per hour. In this study, the definition of a false positive is when a classifier calls an epoch as preictal and then classifies any of the following epochs as interictal before the coming of the next seizure. In contrast, the definition of a true positive is more intuitive as any epoch classified as preictal before a seizure in a segment containing a seizure. The average time difference between warnings and seizure onsets ranged from 6 to 92 minutes among patients. Netoff, Park and Parhi reported a study that utilized a cost-sensitive support vector machine fed with the frequency power of EEG signals to achieve seizure prediction. They applied their method on 219-hour-long EEG data for nine out of the 21 patients in the Freiburg dataset. The performance was evaluated using a prediction horizon of five minutes and achieved sensitivity of 77.8% and zero false-positive rates. Mirowski, Madhavan and coworkers applied several bivariate features and classifiers on the Freiburg database to recognize preictal patterns. Cross-correlation, nonlinear interdependence, dynamical convergence, and wavelet synchrony were estimated in five-second windows. Features were then aggregated into spatio-temporal patterns to feed into classifiers. Three classifiers were used and compared. The convolutional neural network outperformed logistic regression and the support vector machine. The best result achieved by using wavelet coherence and a convolutional neural network was 71% sensitivity with zero false-positive rates for 15 out of 21 patients. For those studies mentioned above, they all applied classifiers on the Freiburg data and report promising results. It would be intriguing to see if the classifier could work as well on scalp EEG data. In research conducted by Feldwisch-Drentrup, Schelter, and colleagues, two dynamic features (mean phase coherence and dynamic similarity index) were applied on 1,456 hours of long-term continuous intracranial EEG data from eight patients. The prediction sensitivity increased (from 25% to 43.2%) when they used logical "AND" combinations to join the benefits of both features. However, the results of using individual methods and logical combination methods were all separately optimized within the same dataset. Therefore, the increase of sensitivity of combined methods is not surprising. More other Studies regarding earlier seizure prediction methodologies and development using intracranial EEG have been extensively reviewed.

**[0105]** Scalp EEG has been used to investigate normal and pathological brain function for over 80 years, when Hans Berger published his work and coined the term "Elektencephalogram" in 1929. Early attempts to predict seizures from EEG signals began in the 1970s and flourished during the 1990s. Because of the non-linear nature of neuronal function and the paroxysmal character of a seizure, non-linear signal processing methods were popularly applied to EEG for predicting seizures. By applying a non-linear similarity index, Le Van Quyen, Martinerie, and colleagues, studied preictal EEG dynamics in 26 scalp EEG recordings obtained from 23 patients with temporal lobe epilepsy. In five patients with simultaneous scalp and intracranial recordings, changes in the similarity index values was observed during preictal period in both types of EEG recordings, and 25 out of the 26 EEG segments showed changes prior to the occurrence sei-

zures (mean 7 minutes). Although this study did not evaluate the specificity of the similarity index change in long-term EEG recordings (contained only 50 minutes before seizure onsets), it rendered an encouraging result using only scalp EEG to achieve seizure prediction. Another study by Hively and Protopopescu used  $L_1$ -distance and  $\chi^2$  statistic to estimate the dissimilarity in density functions between the base-windows and the test-windows in 20 scalp EEG recordings. The result showed pre-seizure changes in all datasets with the forewarning times ranged from 10 to 13660 seconds. However, this study only examined one selected channel in each data set, and similar to, specificity of the method was not reported. In two follow-up studies by the same group, one using all available recording channels and the other using a fixed channel, showed similar results. While the results seemed promising, no validation study has been reported for this method. In the study reported by Corsini, Shoker and coworkers, 20 sets of simultaneous scalp and intracranial EEG recordings were analyzed using blind source separation and a short-term Lyapunov exponent (STLmax). This study reported changes of STLmax values before seizure onsets and noted that the scalp EEG may give better predictive power over intracranial EEG when the intracranial electrodes did not record the electrical activity in the epileptic focus. However, the practicality of this method on long-term scalp EEG recordings may be limited due to the lack of an automatic procedure to select the most relevant source component. Schad et al. investigated seizure detection and prediction in 423 hours of long-term simultaneous scalp and intracranial EEG recordings from six epileptic patients. The method used techniques based on simulated leaky integrate-and-fire neurons. The study reported that 59%/50% of the 22 seizures were predicted using scalp/invasive EEGs given a maximum number of 0.15 false predictions per hour. In the study by Bruzzo et al., a small sample of scalp EEG recordings (115 hours from 3 epileptic patients) was analyzed using permutation entropy (PE). By examining the area under the receiver operating characteristic (ROC) curve, they reported that the decrease of PE values was correlated with the occurrence of seizures. However, the authors also concluded that the dependency of PE changes on the vigilance state may restrict its possible application for seizure prediction. More recently, Zandi, Dumont, and colleagues reported a prediction method based on the positive zero-crossing interval series. The method was applied on a 21.5 hour scalp EEG dataset recorded from 4 patients with temporal lobe epilepsy. They reported a training result of 87.5% sensitivity (16 seizures) with a false prediction rate of 0.28 per hour, where the average prediction time was approximately 25 minutes. James and Gupta analyzed long-term continuous scalp EEG recordings from nine patients (5 in training set and the other 4 in test dataset). The data were processed by a sequence of techniques consisting of independent component analysis, phase locking value, neuroscale, and Gaussian mixture model. The prediction performance of this method achieved a sensitivity of 65-100% and specificity of 65-80% as the prediction horizon ranged from 35-65 minutes in the test dataset.

**[0106]** Among these studies, one of the common features used in many of the seizure warning algorithms is the change of synchronization of EEG signals recorded from different electrode sites. The concept of “synchronization” can be quantified in several different ways such as coherence, phase synchronization, or entrainment of dynamic features (denoted as “dynamic entrainment” hereafter). In this study, it

has been attempted to identify preictal transitions by detecting dynamic entrainment based on the convergence of PMRS among multiple electrode sites. PMRS is a probabilistic statistic that quantifies the regularity of a time series. It is especially useful when the moment statistics (e.g., mean, variance, etc.) or frequency cannot detect changes in a signal. By further applying a paired t-statistic (denoted as “T-index” hereafter) that quantifies the convergence of two PMRS time series over time, an automated seizure prediction algorithm may be constructed that monitors the change of T-index and issues a warning of an impending seizure when the T-index curve exhibits the pattern defined by the algorithm. The general hypothesis is that seizures are preceded by PMRS entrainment; this hypothesis was based upon findings reported previously using a different measure of signal order, STLmax. The prediction parameters and the specific EEG channels to be monitored were determined by the use of a training dataset. Algorithm performance was then assessed using an independent test dataset. The performance was further validated by comparison with that from a random warning scheme that did not use any information from the EEG signals.

## Methods

### Seizure Warning Mechanism

#### Overview

**[0107]** EEG signals were first filtered by a fifth-order Butterworth filter with a band-passing frequency between 1 to 20 Hz (the bandwidth within which most ictal epileptiform patterns occur). After the filtering process, for each channel, PMRS was calculated for each non-overlapping 5.12-second epoch. Based on the PMRS values, T-indices were then calculated for each of the selected channel groups. To increase the sensitivity of seizure warning, the proposed algorithm independently monitored four T-index curves (i.e., from four channel groups). A warning was issued when any of the monitored T-index curves met convergence criteria.

#### Pattern-Match Regularity Statistic (PMRS)

**[0108]** PMRS is a probabilistic statistic quantifying signal regularity. One of the characteristic features of EEG signals during a seizure is the rhythmic and regular discharges over a wide range of the brain. Therefore, the first step of the warning algorithm presented in this study calculated PMRS sequentially for each EEG signal analyzed. The rationale of applying this pattern match method (instead of value match) is due to its robustness over scalp signal values, which are usually more unstable than their up-and-down trends. The procedure for calculating PMRS is described below:

**[0109]** Given a time series  $U = \{u_1, u_2, \dots, u_n\}$  with standard deviation  $\hat{\sigma}_n$ , a tolerance coefficient  $e$ , and a fixed integer  $m$ , the two segments in  $U$  ( $x_i = \{u_i, u_{i+1}, \dots, u_{i+m-1}\}$ ,  $x_j = \{u_j, u_{j+1}, \dots, u_{j+m-1}\}$ ) are considered pattern-matched to each other when Equation 3-1 is fulfilled.

$$\{|u_i - u_j| \leq e \hat{\sigma}_n\} \wedge \{|u_{i+m-1} - u_{j+m-1}| \leq e \hat{\sigma}_n\} \wedge \{\text{sign}(u_{i+k} - u_{j+k-1}) = \text{sign}(u_{j+k} - u_{j+k-1}), k=1, 2, \dots, m-1\} \quad (3-1)$$

In Equation 3-1, the first two criteria require value match to some extent at both the beginning and ending points of two segments, where  $e$  was set to be 0.2 empirically. The third criterion requires pattern match between  $x_i$  and  $x_j$  within a

range of  $m$  (set as 3 in this study). To calculate PMRS, first define a conditional probability,  $p_i$ .

$$p_i = Pr\{\text{sign}(u_{i+m} - u_{i+m-1}) = \text{sign}(u_{j+m} - u_{j+m-1}) | x_i \text{ and } x_j \text{ are pattern match}\}, \quad (3-2)$$

Given  $m$ ,  $p_i$  can be estimated as  $\hat{p}_i$  as in Equation 3-3.

$$\hat{p}_i = \frac{\# \text{ of } \left\{ \begin{array}{l} [x_j^t \text{ pattern match with } x_i] \wedge \\ [\text{sign}(u_{i+m} - u_{i+m-1}) = \text{sign}(u_{j+m} - u_{j+m-1})] \end{array} \right\}}{\# \text{ of } \{x_j^t \text{ pattern match with } x_i\}}, \quad (3-3)$$

$$1 \leq j \leq n - m$$

In Equation 3-3,  $1 \leq i \leq n - m$ . Finally a PMRS can be estimated.

$$PMRS = - \frac{1}{n - m} \sum_{i=1}^{n-m} \ln(\hat{p}_i) \quad (3-4)$$

As the time series  $U$  develops into a more regular state,  $\hat{p}_i$ s become larger and PMRS decreases as a result.

#### PMRS Convergence (T-Index)

**[0110]** T-index is basically the paired t-statistic function used to quantify the degree of convergence between two PMRS time series. For two time series  $X_i$  and  $X_j$  (the PMRS value time series), their values in a calculation window  $W^t$  with a size of  $n$  data points are presented as  $L_i^t$  and  $L_j^t$  in Equation 3-5 and Equation 3-6.

$$L_i^t = \{X_i^t, X_i^{t+1}, \dots, X_i^{t+n-1}\} \quad (3-5)$$

$$L_j^t = \{X_j^t, X_j^{t+1}, \dots, X_j^{t+n-1}\} \quad (3-6)$$

Then the pair-wise differences between  $L_i^t$  and  $L_j^t$  can be expressed in Equation 3-7.

$$D_{ij}^t = L_i^t - L_j^t = \{X_i^t - X_j^t, X_i^{t+1} - X_j^{t+1}, \dots, X_i^{t+n-1} - X_j^{t+n-1}\} \\ = \{d_{ij}^t, d_{ij}^{t+1}, \dots, d_{ij}^{t+n-1}\}, \quad (3-7)$$

The T-index over the calculation window  $W^t$  between the two time series is calculated using Equation 3-8.

$$Tind_{ij}^t = \frac{|\bar{D}_{ij}^t|}{\hat{\sigma}_{D_{ij}^t} / \sqrt{n}} \quad (3-8)$$

In Equation 3-8,  $\bar{D}_{ij}^t$  and  $\hat{\sigma}_{D_{ij}^t}$  are the sample mean and the sample standard deviation of  $D_{ij}^t$ , respectively.

**[0111]** PMRS convergence is a process during which one EEG signal is influenced by or coupled with another with respect to the signal regularity. This phenomenon was used as a dynamical pattern for warning of an impending seizure. FIG. 3-1 shows the PMRS traces derived from three EEG channels (F8, T4, and T6) (upper panel) and their average T-index values (bottom panel) over a 350-minute interval containing a seizure. As shown in the PMRS plot, all PMRS values of the three channels dropped seconds after the seizure onset (indicated by a black vertical line), which was due to the extreme signal singularity during the ictal period. More importantly, the PMRS values became convergent about 60 minutes before the seizure onset, which caused the decrease of T-index values (shown in FIG. 3-1).

#### Selection of Channel Groups for Seizure Warning Monitoring

**[0112]** Channel groups were selected such that they were bilaterally symmetric along the midsagittal line. In order to avoid frequent eye movement artifact, electrodes Fp1 and Fp2 were excluded. In addition, to avoid the regular alpha rhythm pattern that might give potential false positive warnings because of the nature of the regularity statistics used in the prediction algorithm, electrodes O1 and O2 were also excluded. The frontal electrodes F3 and F4 were included in the analysis, whereas electrodes F7 and F8 were not included in order to minimize muscle artifact due to chewing.

**[0113]** The four channel groups selected in this study resemble the well-known and popular anterior-posterior bipolar (“double banana”) montage. These four channel groups were: (F7, T3, T5), (F3, C3, P3), (F4, C4, P4), and (F8, T4, T6). The main rationale for this selection was that most seizures occurring in patients with temporal lobe epilepsy start from a channel group on one side (hemisphere) of the brain, and therefore, intuitively, these channels were more likely to be entrained with each other during the preictal transition period. By monitoring four channel groups that cover both hemispheres, the algorithm was enabled to detect a PMRS convergence that preceded an impending seizure initiated from either hemisphere.

**[0114]** For each channel group  $k$ ,  $k=1-4$ , the group T-index over the calculation window  $W^t$  is denoted as:

$$GTind_k^t = \{\sum_{i=1}^2 \sum_{j=i+1}^3 Tind_{ij}^t\} / 3 \quad (3-9)$$

**[0115]** The window size for calculating one group T-index is 60 PMRS data points, with 59 points overlapping from  $t$  to  $t+1$  (i.e., sliding window). The warning algorithm only monitored the four group T-index curves instead of individual pair-wise T-indices.

#### Detection of PMRS Convergence

**[0116]** The proposed prediction algorithm, instead of attempting to detect a signal threshold crossing, was set to detect a certain pattern of T-index dynamics that gradually descends from a baseline value. Therefore, the first step to detect such a pattern was to determine an upper threshold  $U_T$  (i.e., baseline value, see an illustration in FIG. 3-2). A decrease of a group T-index from  $U_T$  was considered as a desired condition for a potential PMRS convergence, and a convergence was identified when the group T-index values fell below a lower threshold  $L_T$ . It was further defined that a period of convergence should be maintained for at least several minutes. For each group T-index, its  $U_T$  was set to be the asymptotic 95<sup>th</sup> percentile in the preceding 12 minutes, as described in equation 10. The duration of 12 minutes was decided by training across multiple patients in the training dataset.

$$U_T = \text{mean}(T_{12min}(t)) + 2 \times \text{std}(T_{12min}(t)), \quad (3-10)$$

However, if half of the following 16 T-index values (representing 81.92 seconds of data) were greater than  $U_T$ ,  $U_T$  was updated as the median of these 16 values. This operation is described in equations 11 and 12.

$$U_T = U_T \times (1 - I(A)) + \text{median}(T) \times I(A), \quad (3-11)$$

-continued

$$A = \left\{ \sum_{k=1}^{16} H[T(t+k) - U_T] > \frac{16}{2} \right\}, \quad (3-12)$$

In Equation 3-12,  $I(\cdot)$  is an indicator function,  $A$  is the criterion of updating  $U_T$ , and  $T(t)$  is the group T-index value at time  $t$ . If  $A$  is false, then  $U_T$  is kept as it is.  $H(\cdot)$  denotes the Heaviside step function.  $U_T$  is not updated with a maximum value because the existence of artifact in raw EEG recordings could affect the T-index causing an abrupt surge and therefore produce an abnormally high  $U_T$ . Once  $U_T$  is determined,  $L_T$  is equal to  $U_T$  minus  $D$ , where  $D$  is a parameter that would determine the sensitivity of the algorithm. In general, the bigger  $D$  is, the less sensitive the algorithm will be, but the less susceptible the algorithm will be to false warnings.

**[0117]** In addition to the above detection rules, the period of a descending T-index pattern from  $U_T$  to  $L_T$  should continue for more than  $t_f$  minutes to be regarded as a PMRS convergence. Therefore, the algorithm would issue a warning of an impending seizure only when any of the monitored T-index curves traveled from  $U_T$  to  $L_T$  with the traveling time longer than  $t_f$  to ensure a gradual descendent pattern.

**[0118]** Once a convergence was identified, other convergences that followed (identified within the seizure warning horizon (SWH) by the warning algorithm using the same parameter settings) were silenced due to the possibility that a convergence preceding an onset may be much longer than the  $t_f$  value and cause several convergence identifications. The work flow is depicted in FIG. 3-3 and gives an overview of the seizure warning algorithm.

#### EEG Data Characteristics

##### Subjects and EEG Recording Specifications

**[0119]** All subjects were 18 years of age or older admitted to either Allegheny General Hospital (AGH, Pittsburgh, Pa.) or the Medical University of South Carolina (MUSC, Charleston, S.C.) for inpatient seizure monitoring for diagnostic purposes or presurgical evaluation. Data collection procedure was approved by the Investigational Review Boards of AGH and MUSC, and the Western Investigational Review Board (WIRB). The EEG recordings at MUSC were obtained using XLTEK monitoring systems (Oakville, Ontario, Canada) with a sampling rate of 256 Hz and the EEG recordings at AGH used 128-channel Nicolet BMSI-6000 systems (Viasys, Madison, Wis., USA) with a 400 Hz sampling rate. The EEGs recorded at both institutions used a referential montage and the 19-electrode international 10-20 system of electrode placement. The exact locations of referential electrodes placed in the dataset were decided on-site and usually followed the recommended location of the Cz and Pz electrodes as suggested by the American Clinical Neurophysiology Society. All segments were reviewed by the collaborative clinical sites (AGH and MUSC) and all seizure events were verified by KK and JH, respectively.

##### Data Selection

**[0120]** Because a scalp EEG might be severely contaminated with artifact, typical muscle contraction, and movement artifacts include blinking, chewing, and talking, only EEG segments with a tolerable level of artifact, i.e., not present for more than 50% of the recording and not involving more than

50% of the recording channels, were included in this study. There were a total of 71 EEG recording segments from 71 patients selected for this study. All EEG segments were long-term recordings (mean=25.16 hours) containing at least one seizure. EEG segments containing more than one seizure within any two-hour interval were excluded to avoid potential overlap between preictal and postictal periods of consecutive seizures. Thus, the warning algorithm had a sufficiently long period of observation to detect the transition from interictal to ictal states. The dataset was randomly divided into complementary training (n=35) and test (n=36) sets. The total EEG recordings used in this study was 1786 hours and contained 98 seizures. The individual recording durations of each subject in the whole dataset (both training dataset and test dataset) are shown in FIG. 3-4.

#### Statistical Evaluation

##### Estimation of Performance Statistics

**[0121]** The performance of the seizure warning algorithm varies with the length of the seizure warning horizon (SWH)—the longer the SWH, the lower the sensitivity and false positive rate (FPR). In this work, SWH was defined as the time window following a seizure warning during which the patient was likely to have a seizure. It is worth noting that Winterhalder et al. defined the SWH (same as seizure prediction horizon, SPH) differently as a short intervention preparation period. The definition of SWH here is closer to the “seizure occurrence period” defined by this group. A seizure warning was considered true only when at least one seizure onset occurred within the SWH following the warning. Otherwise, the warning was considered a false positive.

**[0122]** After determining the outcome (i.e., true or false) of each warning, sensitivity was estimated by dividing the number of correct warnings by the total number of seizures in the EEG segments, i.e. the proportion of seizures correctly predicted (within SWH). FPR (per hour) was calculated by dividing the total number of false positives by the total recording hours outside the SWH before each seizure. The SWH period before each seizure was excluded because it was impossible for a false warning to occur within the SHW before each seizure.

##### Performance Statistical Validation—Comparison with a Random Seizure Warning Scheme

**[0123]** Several methods have been proposed for validating the performance of a seizure warning algorithm. Each study tested a specific statistical hypothesis. In this study, the prediction sensitivity estimates were compared with a random prediction scheme that issued random seizure warnings (in time) during the recording. Under this random scheme, the interval between two consecutive warnings followed an exponential distribution, with a condition that the length of any interval could not be smaller than the SWH. This additional condition ensured that the two compared algorithms (test algorithm and prediction scheme) were consistent in terms of the management of nearby warnings (within the SWH). Although this condition diminished some randomness from the random prediction scheme, it provided a meaningful comparison of prediction performance between the two prediction methods.

**[0124]** In order to have an unbiased comparison for sensitivity, two parameters were controlled: 1) length of the SWH, and 2) total number of warnings. For each of the test EEG segments, the total number of warnings allowed by the ran-

dom predictor was set to be the same as that issued by the test algorithm. For example, if the test algorithm issued two true positive and two false warnings in a specific segment, the random predictor would only randomly issue a total of four warnings. Under the same number of warnings allowed, the study compared overall prediction sensitivity across all test patients. A distribution of overall sensitivity by the random prediction scheme was generated from 1000 simulations, and was used to assess how significant the prediction performance by the test algorithm was over the random scheme.

**[0125]** It is worth mentioning that imposing the above conditions in the random warning algorithm compared in this study allowed for comparison with the proposed algorithm. Since this was a conditioned random process, the specific null hypothesis tested in this study was: “The overall sensitivity (or FPR) of the test algorithm is the same as that of a random prediction scheme with the same number of warnings issued by the test algorithm.”

#### Cross-Validation on Performance Comparison

**[0126]** The comparison of performance between the proposed warning algorithm and the random scheme was further implemented through cross-validation so that the comparison result is more independent from the constituents in the training dataset and test dataset. To execute the cross-validate, all 71 segments may be randomly divided into training and test datasets for 20 times to generate 20 individual trials and then repeated the training and test procedures on each trial. In each trial, the parameters ( $t_r$  and D) were selected as those causing the performance to exceed 70% sensitivity and resulting in the least FPR in the training dataset. The parameters were input to the test algorithm run on test dataset to generate the final performance results in the trial. For each trial, the final performance result of the test dataset was compared with the random seizure warning scheme mentioned above. Please note that each test segment in each trial can have a different number of warnings and even the same segment in different trial would have a different number of warnings if the parameters used in the two trials were different. Using fixing parameters for a group of epileptic patients with different seizure types and physiological backgrounds can hardly outperform that using best setting parameters for each individual patient. However, these results can offer a perspective on the robustness of using the test algorithm among several patients when the previous individual patient data is not available or sufficient for training.

#### Combining p-Values

**[0127]** In each trial, the comparison result between the test algorithm and the random scheme is quantified as a p-value, and indicates how significant the prediction performance by the test algorithm was over the random scheme. After obtaining all the p-values from the 20 cross-validation trials, the overall statistical significance of comparison between the two seizure prediction schemes was estimated by mapping the p-values to a z distribution. The z-transform method was chosen for testing combined p-values because it is not differentially sensitive to data that support or refute a common null hypothesis, whereas Fisher’s test, another widely-used method for testing combined p-values, is more sensitive to data refuting a common null hypothesis. All p-values of each trial were transformed to a z-value,  $z_p$ , in a  $N(0,1)$  distribution such that  $\Pr[N(0,1) \leq z_p] = p$ -value. The overall z-value,  $Z_{overall}$ , is carried out by calculating  $\sum z_p / \sqrt{K}$ . Lastly,  $Z_{overall}$  is transformed back to a combined p-value.

## Results

### Training Results

**[0128]** The proposed algorithm was applied on the training dataset ( $n=35$ ) to optimize settings for the parameters D and  $t_r$ . Parameter D requests the minimal decrease that a group T-index value needs to fall from  $U_T$  to be considered as a PMRS convergence, and  $t_r$  gives the constraint on the minimal time length for a group T-index curve traveling from  $U_T$  to  $L_T$ . One of the training results is presented in FIG. 3-5, which shows the receiver operating characteristic (ROC) curves (sensitivity vs. false positive rate) under different  $t_r$ , ranging from 10 to 30 minutes with 10-minute increments. Each ROC curve contains eight settings of parameter D, each representing the performance under a certain D value, ranging from 1 to 8 (in T-index units) with increments of 1. As D increased, each ROC curve first reached its peak sensitivity and then declined as D kept increasing. This was due to the constraint of  $t_r$ : when D was set to a small value,  $T_r$ , the time interval during which a group T-index curve drops from  $U_T$  to  $L_T$ , was likely to be shorter than the minimally required  $t_r$ , and therefore the drop of the group T-index curve could not be considered as a PMRS convergence. As D became bigger, the sensitivity started increasing until the D value became too large to start affecting the number of group T-index drops (i.e., sensitivity started to reduce).

**[0129]** For the training processes of all trials, the best performance was defined as when the proposed algorithm achieves sensitivity of at least 70% with the lowest possible false positive rate. The best parameter configuration was optimized within each trial according to the definition. As a result, the optimized prediction parameter values were decided for each trail after reviewing all performances using a full range of possible parameter settings. These optimized parameters were fixed for the performance evaluation in the paired test dataset within the same trail.

### Test Results

**[0130]** The test dataset consisted of 36 long-term EEG segments from 36 patients in each trial. With the parameter settings determined in the training dataset of the same trial, the test algorithm gave sensitivities among 0.6 and 0.72 (mean=0.65) while the false-positive rate was among 0.22 and 0.26 (mean=0.24).

**[0131]** The random warning scheme was designed to issue random warnings with the same number as that issued by the test algorithm for each segment in the test dataset. After the random scheme ran through all of the patients in the test dataset an overall sensitivity was calculated. The random scheme repeated 1000 times on the test dataset and thus generated 1000 overall sensitivity estimates. The overall sensitivities of all 20 trials are listed in the Table 3-1. The overall sensitivity achieved by the test algorithm was then compared with the sensitivity distribution of the random warning scheme. For example, the performance comparison in one of the trials is shown in FIG. 3-6. The combined p-value over 20 cross-validation trials showed that the proposed warning

algorithm achieved a better performance ( $p=0.015$ ) than the compared random warning scheme.

#### Discussion

##### Dataset Requirement for Performance Evaluation

**[0132]** Amongst the early seizure prediction studies, short EEG recording containing seizure onsets were often used. The claim of sensitivity can be very satisfactory especially when the result was optimized for all the data without separating them into training and test dataset. Although these studies were absolutely valuable as pioneers in the field, simply interpreting those results as successfully predicting seizures would be too optimistic. Concerns of overestimation of results soon developed and drew much attention amongst many research groups. Using interictal EEG recordings and a separate test dataset for performance evaluation was advocated to fairly estimate the false positive rate and avoid misleading conclusions. In sum, potential misleading factors that could overrate the performance should be ruled out. These concerns should not be regarded as unduly skeptical or critical of the rigor of these early study designs; rather, they represent the positive intention of expanding the previous promising results to more challenging test scenarios closer to reality. In this study, for the interictal recording requirement, 1786-hour-long EEG segments in total were included, which included 98 seizures in 71 segments. Each seizure is at least three hours away from each other. If one defines a preictal period as three hours before the onset of a seizure, the dataset contains 1492 hours of interictal period. These interictal EEG signals should be sufficient for a reasonable estimate of the false-positive rate. For the separate testing dataset requirement, the database was randomly divided into training and test dataset for 20 trials. Every EEG segment was recorded from a different patient and belongs either to the training or test dataset in a trial. This scheme of dataset treatment avoids both in-sample and patient-specific optimization.

##### Patient-Specific Optimization

**[0133]** If one has a long enough EEG recording, containing several seizures for each patient in the dataset, patient-specific training and a test scheme can be implemented, and sensitivity as well as specificity can still be fairly estimated. For many studies using classifiers to predict seizures, the classifier is usually optimized using a portion of the EEG segment of one patient and then tested on the rest of EEG segments from the same patient. Training parameters vary from method to method. As long as all parameters were fixed once after the training procedure ends, no more optimization or changing of parameter values should be allowed in the test process; otherwise, the result should not be viewed as an independent test result but a result of further in-sample optimized procedure. Although the dataset is divided into two parts, the further optimized result should not be viewed as an independent test result since some parameters have fixed before the further optimization. In a recent study by Feldwisch-Drentrup et al., they divided their dataset into two sets. They executed channel selection in the first part of the data, and optimized prediction intervention time and thresholds for two individual methods, as well as two logical combinations of two methods in the remaining part of the dataset. The

results of the four prediction methods were all in-sample optimized. In the study, the algorithm was tested using the same parameters across many patients for one trial and pre-defined a fixed prediction horizon for all patients. These test results are valid as long as the test datasets have long enough intracranial segments for estimating a false-positive rate and enough seizure onsets for estimating sensitivity. The key point is to interpret the results with the design and the hypothesis of the study combined. The study is intended to test the algorithm across patients against a random predictor issuing the same number of warnings uniformly.

##### Vigilance States as a Possible Confounding Factor

**[0134]** In addition to using interictal segments and separate test datasets for performance evaluation, there are other concerns related to study design. One possible issue is the control of other confounding factors. For example, the scalp EEG signals respond to vigilance states more obviously than intracranial EEG signals. Chewing and talking muscle artifacts on the temporal region electrodes during awake state, and prevailing alpha waves on occipital region electrodes during eyes-closed but awake state, are very dominant in the scalp EEG signals. If the interictal segments were all recorded during the awake state while seizures occurred during sleep, an algorithm detecting drowsy state can achieve a high sensitivity predicting seizures. One way to rule out of this erroneous relationship is selecting many interictal and preictal recordings under the same vigilance state for both training and test. Whether the algorithm is more sensitive to a vigilance state or an epileptic state change can be further clarified by conducting another continuous study. However, the existence of many different vigilance states in the data allows one to test the robustness of a proposed algorithm under many vigilance states. In this study, all of the EEG segments are continuous long-term EEG segments and most of them are long enough to go through several vigilance states. A seizure could happen during the sleep or awake states in a continuous recording. By including many continuous long-term segments from many different patients, seizures were scattered among several vigilance states instead of one prevailing condition.

##### Significance Test

**[0135]** The result of this study should not be interpreted to mean that the performance of the proposed algorithm outperformed any random prediction scheme. This study tested a specific null hypothesis based on the random prediction scheme designed. In fact, a comparison of performance with a completely random prediction scheme may have very little meaning, both scientifically and practically. Certain conditions should be imposed on the random scheme to prevent potential bias in the comparison, especially for the assessment of a sophisticated EEG-based prediction algorithm. Nevertheless, there are several studies that have applied different random warning schemes or surrogate data to test different hypotheses. The comparison of the proposed algorithm with other random warning schemes should be followed. Furthermore, studies on a larger sample size and the assessment of the proposed algorithm with different SWHs should be conducted in the future.

TABLE 3-1

The sensitivities, false-positive rates and p-values achieved by the proposed algorithm on training and test dataset. The sensitivities and FPRs of the training datasets presented in this table are the best performances, defined as reaching sensitivity over 70%, meanwhile, resulted in the least FPR. The sensitivities and FPRs of the test datasets resulted from applying the proposed algorithm using the best parameter configuration found using the training dataset. The p-values in the test datasets were estimated by comparing the test algorithm to the random warning scheme (1000 simulations in each trial) that issued the same number of warnings.

Trial Number	Training Dataset		Test Dataset	
	Sensitivity	FPR (times/hour)	Sensitivity	FPR (times/hour)
1	0.71	0.22	0.62	0.24
2	0.71	0.27	0.66	0.26
3	0.73	0.25	0.7	0.24
4	0.72	0.23	0.71	0.25
5	0.76	0.25	0.62	0.23
6	0.7	0.23	0.62	0.24
7	0.74	0.28	0.67	0.26
8	0.71	0.24	0.61	0.22
9	0.72	0.24	0.6	0.23
10	0.76	0.25	0.65	0.25
11	0.76	0.24	0.67	0.25
12	0.75	0.24	0.57	0.22
13	0.77	0.24	0.68	0.22
14	0.71	0.24	0.6	0.23
15	0.7	0.24	0.72	0.25
16	0.72	0.24	0.65	0.26
17	0.7	0.26	0.7	0.24
18	0.72	0.23	0.61	0.24
19	0.72	0.24	0.67	0.23
20	0.72	0.24	0.7	0.25
Average	0.73	0.24	0.65	0.24

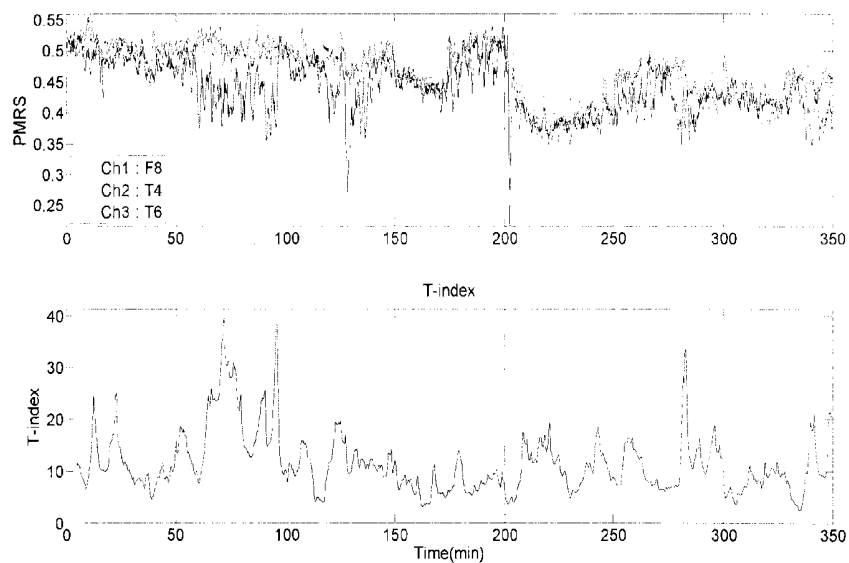


Figure 3-1. Dynamic features of three EEG electrode signals. Top: PMRS traces of F8, T4, and T6 electrodes. There is a sudden drop of PMRS values in all three channels right after the seizure onset (denoted by vertical dashed black lines in both panels at the 200-minute time point). Bottom: averaged T-index among the three channels. Approaching the time of seizure occurrence, a gradual decrease of the T-index (convergence) from approximately the 120-min point to the 160-min point can be observed. The T-index values remain small before the seizure.

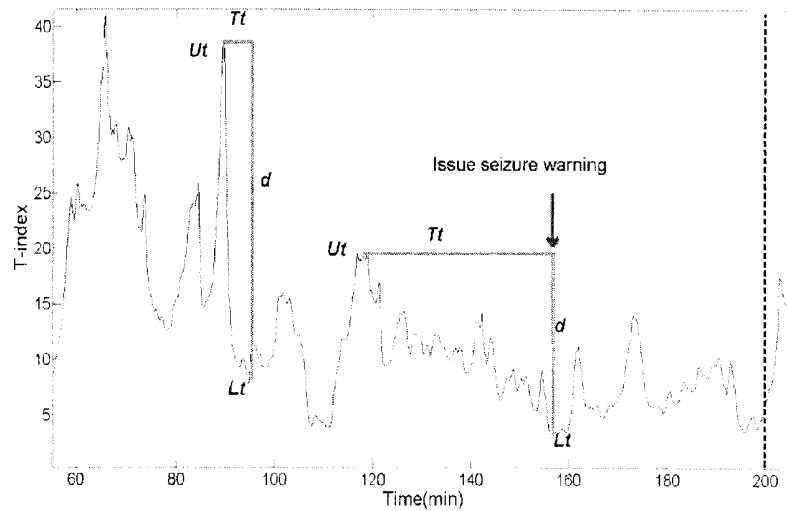


Figure 3-2. The group T-index plot with warning algorithm parameter indications. The seizure warning sensitivity relates to parameters  $t_t$  and  $D$ . As the algorithm finds both  $L_T$  and  $U_T$ , the difference of time and the group T-index between them, as indicated by  $Tt$  and  $d$  in the figure, are compared with  $t_t$  and  $D$ , respectively. Only the decrease  $d$  of a T-index curve was larger than  $D$ , and also  $Tt$  larger than  $t_t$  would trigger a seizure warning. For example, with the proper setting of  $t_t$  and  $D$ , the T-index drop at 100 min was not considered a warning event because a large  $d$  occurred during a short  $Tt$ . However, the T-index drop from the 120 min point to the 160 min point shows a gradual and persistent decrease and is considered a proper warning event. The dashed vertical line at 200 minute denoted the seizure onset time point.

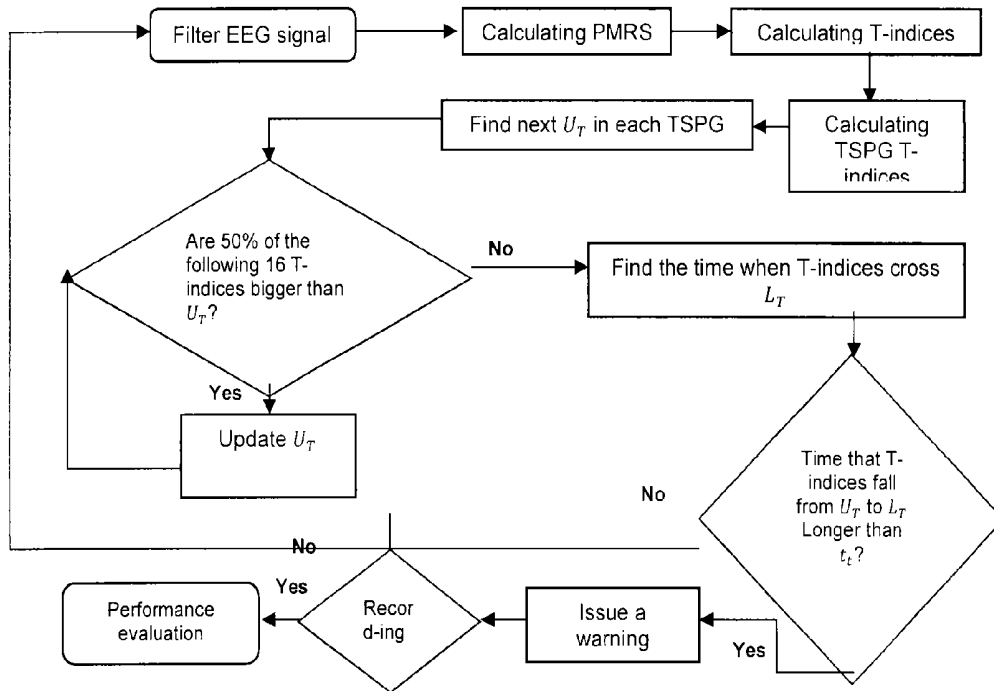


Figure 3-3. Flow chart of the seizure warning mechanism

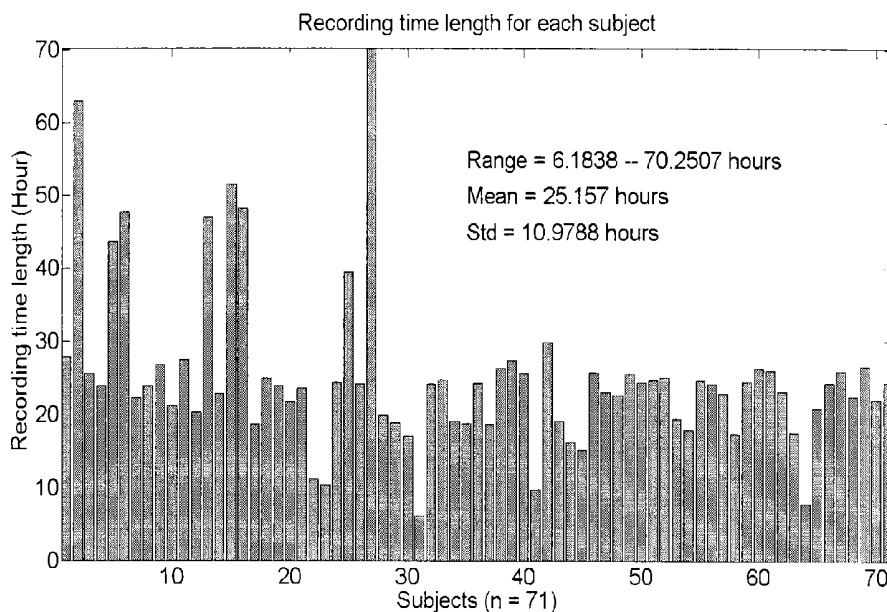


Figure 3-4. Recording duration of all 71 subjects in the dataset. The range of recording duration was between 6.18 to 70.25 hours. The mean was 25.16 hours and the standard deviation was 10.98 hours.

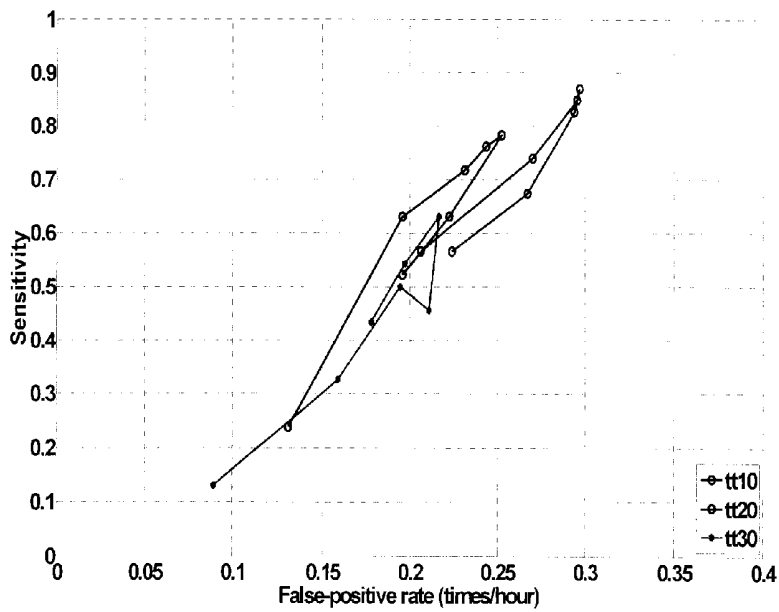


Figure 3-5. One of the training results from 20 trials. Three ROC curves are shown under different  $t_t$  values. Each point in the ROC curve corresponds to an overall result over the training dataset with a specific  $D$  value. The inset indicates the parameter  $t_t$  used in each ROC curve. For example, tt10 denotes the ROC curve using parameter  $t_t = 10$  minutes. The best parameter configuration of this training dataset was observed at the  $t_t$  value equal to 20 minutes and  $D$  equal to 3, which achieved sensitivity above 0.7 with a false positive rate of 0.232 per hour.

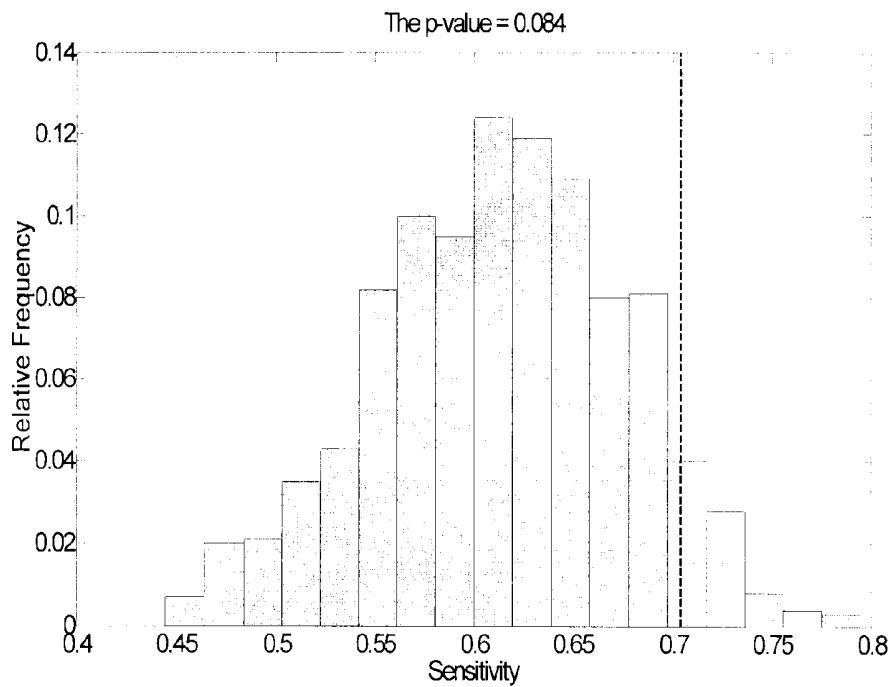


Figure 3-6. The performance comparisons of the 20<sup>th</sup> trial. The figure shows the comparisons between the performances achieved by the random scheme and that achieved by the proposed algorithm. The bar plot shows the histogram of the sensitivities achieved by the random warning scheme (generated from 1000 repetitions). The sensitivity of the proposed algorithm applied on the same test dataset is denoted by the dashed vertical line, which was better than 91.6% of the sensitivities of 1000 repetitions achieved by the random scheme.

## Chapter 4

Psychogenic Non-Epileptic Seizure and Complex  
Partial Seizure Patients Classification

## Preface

**[0136]** About 25% of the patients visiting an epilepsy monitoring unit are diagnosed as psychogenic nonepileptic seizure (PNES) patients and need to be distinguished from other patients having epileptic seizures in order to be correctly treated. Patients have PNES onsets that can be identified by monitoring the ictal pattern shown either in scalp electroencephalogram (EEG) or video. The classification using ictal symptoms requires several seizing onsets from a patient. The number or frequency of seizure onsets during a patient's stay in EMU cannot be precisely anticipated in advance. It would be convenient for EMU schedule and cost efficiency if one could identify PNES patients using only awake and interictal scalp EEG recordings. This study researched the connectivity and features of awake and relaxed interictal EEG signals. The subjects include seven patients having PNES and another seven patients having complex partial seizures (CPS) with fixed foci.

**[0137]** The hypothesis is that the inter-hemispheric connectivity and network dynamic features from the EEG of a CPS patient are different from that of a PNES patient because the repetitive focal discharges impair more around the epileptogenic zone rather than the contralateral hemisphere. Conversely, patients with PNES onsets should not have this abnormal physioelectrical consequence, and are supposed to have a sounder functional network or more similar values of features between both hemispheres.

## Small-World Network in EEG Data

**[0138]** A brain is a structurally and functionally complex network of neurons. The functional network reflects the connectedness among brain regions in terms of neuronal activity. Graph theoretical analysis is a mathematical tool to reveal topological characteristics of a network. Applying graph theoretical analysis on the EEG data reveals the brain functional network features. One of the network structures, called "small-world network" can be identified, when there is a balance between local independence and global integration in the network. The balance can be evaluated by quantifying two graph features, called the local clustering coefficient and the characteristic path length. A small world network has a relatively high cluster coefficient and a small characteristic path length. Small world networks are usually compared to a network with a lattice-like configuration or to a random network; the two extreme cases. A regular lattice network is characterized by a relatively high cluster coefficient and a long average path length. On the other hand, a random network has a relatively lower cluster coefficient and a shorter average path length. Small-world networks are efficient at information processing, cost-effective, and are relatively resilient to network damage and, as a result, can be regarded as the ideal model for a normally functioning brain network.

## Graph Theoretical Analysis on EEG Signals

## Preprocess

**[0139]** While reviewing the EEG data, one can easily observe that EEG data has one salient characteristic, the

rhythmic oscillation. Not surprisingly, therefore, frequency analysis has been broadly used to preprocess and analyze EEG signals. It is widely accepted that the different strengths of the frequency components can reveal different brain states.

**[0140]** In analyzing EEG signals, filtering is usually implemented to remove artifacts or to help focus on the frequency bands of interest. Before doing a network analysis of EEG data it is important to remove the artifacts that contribute to the multiplication of channels. Without doing this first, the shared input from the artifacts would likely result in the existence of a spurious association amongst channels having the same artifact. Therefore, applying a power line frequency notch filter on EEG data is highly recommended. Any other artifact that would affect more than one channel, such as movement of the reference electrode, should be removed; otherwise, the result of graph should be carefully inspected to rule out the spurious coupling strength amongst vertices with common artifact sources. Some montages can be used to eliminate possible common artifacts between two channels. Beside using montage, average-reference is also commonly used when dealing with EEG data.

**[0141]** In addition to using conventional fast Fourier transform-based filtering techniques to obtain EEG signals within a range of frequencies, some studies implemented wavelet transform to extract components with more specific time-frequency resolution. For example, Palva et al. (2010) used Morlet wavelets to filter EEG data into 36 frequency bands before construct the oscillatory phase synchronized network from EEG data.

## Revealing Network Structures in EEG Data

**[0142]** The brain functional network can be represented as a graph. Graph theoretical analysis is then applied after the graph has been established. To do so, first define vertices and edges in the EEG data. If the EEG channels are designated as the vertices of a graph, an edge between two vertices signifies a functional connection between two EEG channels. One would expect a larger correlation between two EEG channels when there is an edge between them. Edges can also be values quantifying how well the two vertices correlate in weighted graphs. Most of the studies using graph theoretic analysis on EEG data assume that statistical interdependencies between EEG time series reflect functional interactions between neurons in the brain regions. There are many statistical metrics computing the degree of association between time series. Some of the most commonly used metrics in EEG functional connectivity graph studies will be discussed below.

**[0143]** Phase locking value (PLI) is a statistic measuring the frequency-specific synchronization between two neuroelectric signals. This is a method focusing on the phase information of time series and is different from coherence, which gives the interrelation of both amplitude and phase between signals. The PLI is calculated by first extracting the instantaneous phase information of signals through either wavelet transform or Hilbert transform. Both methods lead to a similar result in real world EEG data. When doing the wavelet transform on a signal  $x(t)$ , a wavelet function,  $\psi(t)$ , is first chosen. Gabor and Morlet wavelet functions have both been applied on EEG data. Then the wavelet coefficient time series,  $W_x(t)$  can be computed by convolute  $x(t)$  and  $W_x(t)$ .

$$W_x(t) = \int \psi(t') x(t-t') dt' \quad (4-1)$$

Then the phase time series,  $\phi(t)$ , can be computed.

$$\phi^{X_i}(n, s) = \arctan \frac{\text{imag}(W^{X_i}(n, s))}{\text{real}(W^{X_i}(n, s))} \quad (4-2)$$

When doing the Hilbert transform, the phase information,  $\phi(t)$ , of a signal  $s(t)$  is obtained through Equation 4-3.

$$\phi(t) = \arctan \frac{\tilde{s}(t)}{s(t)} \quad (4-3)$$

$$\tilde{s}(t) = \frac{1}{\pi} p.v. \int_{-\infty}^{\infty} \frac{s(\tau)}{t - \tau} d\tau \quad (4-4)$$

In Equation 4-4, p. v. denotes the Cauchy principal value in the equation. Then the relative phase,  $\phi_{1,1}(t)$ , can be calculated as Equation 4-5.

$$\Phi_{e,f}(t) = \phi_e(t) - \phi_f(t) \quad (4-5)$$

The subscript n and m signify the relative phase relationship between channel e and f. Finally, it is possible to compute the PLI, PLV, using Equation 4-6.

$$PLV = \left| \frac{1}{N} \sum_{j=1}^N e^{i\phi_{e,f}(j\Delta t)} \right| \quad (4-6)$$

There are other computational details including windowing and unwrapping the instantaneous phase being considered. Interested readers can refer to those references mentioned above. PLI was used in a study by Dimitriadis et al. to construct the functional connectivity graphs from 30-electrode EEG data. They utilized surrogate data to generate a baseline distribution of random PLIs and then determined the functional connections (edges) if there was a significantly different ( $p < 0.001$ ) PLI for a specific pair. The surrogate data is generated by permuting the order of trials of one signal repeatedly.

**[0144]** Synchronization likelihood (SL) is a statistic measuring the non-linear similarity between time series. SL offers an extended perspective of correlation that is not limited in terms of linear relationship; while coherence, has the limitation of rendering only the linear correlation as a function of frequency. The computation of SL first requires the interested time series,  $X_{k,i}$  ( $k=1, \dots, M$  as channel number and  $i=1, \dots, N$  as time indices), to be reconstructed using the method of delays.

$$X_{k,i} = (X_{k,i}, X_{k,i+l}, X_{k,i+2l}, \dots, X_{k,i+(m-1)l}) \quad (4-7)$$

In Equation 4-7,  $l$  denotes the lag and  $m$  is the embedding dimension. A number  $H_{i,j}$  is then defined to denote the number of channels  $X_{k,i}$  and  $X_{k,j}$  that are closer than a crucial distance,  $\epsilon_{k,i}$ .

$$H_{i,j} = \sum_{k=1}^M \theta(\epsilon_{k,i} - |X_{k,i} - X_{k,j}|) \quad (4-8)$$

-continued

$$\begin{cases} \text{if } |X_{k,i} - X_{k,j}| \geq \epsilon_{k,i} : S_{k,i,j} = 0 \\ \text{if } |X_{k,i} - X_{k,j}| < \epsilon_{k,i} : S_{k,i,j} = \frac{H_{i,j} - 1}{M - 1} \end{cases} \quad (4-9)$$

$$S_{k,i} = \frac{1}{2N} \sum_{j=1}^N S_{k,i,j} \quad (4-10)$$

We can see that SL,  $S_{k,i}$ , is a measure describing how well channel  $k$  at time  $i$  is correlated to all other  $M-1$  channels. Ponten et al. used Synchronization Likelihood (SL) as the connectivity metric in their study about the relationship between epilepsy and small-world networks. The edges between vertices were determined by applying a threshold on the SL value between two time series recorded at the two vertices within an epoch. In their study, for the threshold, it was decided to keep the graph density as a constant. In other words, the threshold increases slightly until the average number of edges of each vertex in a graph is equal to a certain number.

**[0145]** Non-linear Independence Measure (NIM) estimates the strength of functional coupling of two time series embedded in their respective phase-spaces. Let  $\Gamma_{n,j}$  and  $\Lambda_{n,j}$ ,  $j=1, \dots, w$ , denote the time indices of the  $w$  nearest neighbors of two reconstructed vectors,  $X_n$  and in a phase space respectively. For each  $X_{k,i}$ , the mean squared Euclidean distance to its  $w$  neighbors can be defined as Equation 4-11.

$$R_i^{(w)}(X) = \frac{1}{w} \sum_{j=1}^w (X_{k,i} - X_{k,\Gamma_{i,j}})^2 \quad (4-11)$$

We can also define Y-conditioned mean squared Euclidean distance as Equation 4-12 but replace the nearest neighbors by the equal time partners of the closest neighbors of  $X_{k,i}$ .

$$R_i^{(w)}(X | Y) = \frac{1}{w} \sum_{j=1}^w (X_{k,i} - X_{k,\Lambda_{i,j}})^2 \quad (4-12)$$

The NIM,  $N(X|Y)$ , is computed as Equation 4-13.

$$N^{(w)}(X | Y) = \frac{1}{N} \sum_{i=1}^N \frac{R_i(X) - R_i^{(w)}(X | Y)}{R_i(X)} \quad (4-13)$$

The asymmetry of NIM ( $N(X|Y) \neq N(Y|X)$ ) is the main advantage of this nonlinear measure because it can deliver directional information between vertices. In the study done by Dimitriadis et al., they used both SL and NIM to quantify the extent of association between vertices. In their study, they found that the correlation dimension was around six from the sleeping EEG data of 10 healthy subjects. Furthermore, SL and NIM are weakly correlated and considered as revealing complementary information regarding the functional connectivity.

**[0146]** Phase lag index (PLAI) quantifies the asymmetry of the distribution of instantaneous phase differences between two time series. If the relative phase time series between

channel  $e$  and  $f$ ,  $\phi_{e,f}(t)$  have been calculated, then the PLAI can be defined as  $|\langle \text{sign}[\phi_{e,f}(t)] \rangle|$  ( $\langle \cdot \rangle$  signifies the expectation value operator). PLAI ranges from 0 to 1. PLAI values greater than 0 suggest the existence of phase locking to some extent, and values equal to 0 signify no coupling or no coupling with a phase difference centered around  $0 \pm \pi$  radians. PLAI is supposed to rule out the synchronization due to instantaneous volume conduction or a common source that is the main cause giving spurious synchronization.

#### Results of Studies Using Small-World Network Analysis to EEG Data

**[0147]** The existence of small-world structure in the cortex of a human brain has been observed through many measuring methods including fMRI, magnetoencephalography (MEG), and EEG. Many studies use graph theoretical analysis to distinguish pathological consequences or identify the state of human brains. The following paragraphs introduce summaries of some interesting studies related to small world networks in EEG data. Readers interested in more detail about the application of small world networks in EEG will find more information following the references.

**[0148]** An ageing study found out that the clustering coefficient and the value of path length were both lower in the elderly compared to the young subject group. This implies that the brains of the elderly subject group appear to be closer to random networks.

**[0149]** Small-world networks are supposed to be very efficient for data transfer. Epilepsy as a disease having excessive synchronization between neurons is assumed to have a relationship with the small-world architecture in the functional brain network. Ponten et al. conducted a study doing graph analysis on intracerebral EEG recordings from patients having drug-resistant mesial temporal lobe epilepsy and found an increase in the clustering coefficient in the lower frequency band (1-13 Hz), and an increase in the path length in the alpha and theta bands during and after a seizure compared to interictal recordings. This implies that the functional brain network changes from a more random organization to a small-world structure.

**[0150]** The efficiency of information transmission within a small-world network implies that some pathological damage to a brain may result in losing the traits of a small-world network. In an Alzheimer's disease (AD) study conducted by de Hann et al., EEG data from patients with AD were compared with control subjects. All subjects showed small-world network traits in their functional graphs in all frequency bands, but in the beta band alone, they observed significantly less small-worldness in the AD group compared to the controls.

**[0151]** Palva et al. did a study using magnetoencephalogram (MEG) and EEG to investigate the network properties when the subjects are engaged in visual working memory (VWM) tasks. The study recorded both MEG and EEG from 13 healthy subjects and applied PLV as the metric of association between brain regions. Their results implied that small-world network structures appeared dynamically during the VWM task execution within the alpha and beta band. Moreover, the small-worldness was dependent on the VWM memory load.

**[0152]** Graph theoretic analysis has also been applied to the quantitative EEG data of epilepsy patients. In a study by van Dellen, interictal electrocorticography (EcoG) of 27 patients

with pharmaco-resistant temporal lobe epilepsy (TLE) were analyzed. Because an epileptic seizure is a manifestation of overly hyper-synchronous activity between neurons, a metric measuring synchronization, PLAI, was implemented on those electrodes located on the temporal cortex and showed lower values on those patients with a longer history of TLE. In addition, the cluster coefficient and small world index were both negatively correlated with TLE duration in the broad frequency band (0.5-48 Hz). This may have resulted from the accumulative damage on the brain tissue due to intermittent excessive epileptic discharges over a long period of time. The optimal balanced small world structure had been impaired to form a more randomized one as the TLE duration continued.

**[0153]** In an interesting model undertaken by Rothkegel and Lehnertz, they observed the co-occurrence of local wave patterns and global collective firing in a two-dimensional small world network. Boersma et al. conducted a study on resting state EEG in developing young brains. They recorded resting-state eyes-closed EEG (14 channels) from 227 children when they were 5 and 7 years of age and found out that the clustering coefficient increased in the alpha band with age. Path lengths increased in all frequency bands with age. This suggests that a brain shifts from random towards more ordered, small-world like configurations during maturation. Girls showed higher mean clustering coefficients in the alpha and beta bands compared with boys.

**[0154]** Schizophrenia has been suspected as the result of a more disconnected brain network among certain crucial areas in the brain. Rubinov et al. did a study investigating the "disconnection hypothesis." They recorded resting state scalp EEG from 40 subjects with a recent first episode of schizophrenia and another 40 healthy matched controls. Nonlinear interdependences were identified from bipolar derivations of EEG data and weighted graphs were generated. Graphs of both groups showed features consistent with a small-world topology, but graphs in the schizophrenia group displayed lower clustering and shorter path lengths. This result can be interpreted as a pathological process that the small-world network transformed to a more randomized small-world network in a schizophrenia brain. This randomization may be the reason why schizophrenia evidences cognitive and behavioral disturbances. In another similar study, scalp EEG data from 20 schizophrenics and 20 controls (age and sex matched) collected when they were performing working memory tasks were analyzed using conventional coherence. After applying a threshold on the values of coherence so that the number of average edges is five in a graph, binary graphs were obtained. The results showed that schizophrenics bear a more random neuronal network organization, especially in the alpha band.

#### Inter-Hemispheric Power Asymmetry

**[0155]** The symmetric parts of a human body, such as limbs and sense organs, often have the same function and structure. The brain of a human also has symmetric shape although some functions happen on a dominant side. The EEG signals from a pair of symmetric channels usually have similar morphologies. The asymmetry of EEG signals is regarded as a pathological consequence or unusual phenomenon if the reason is not found. Many studies have used asymmetry as an index to quantify the morbidity of brain disease or abnormal states. In this study, the hypothesis is that the relative frequency powers of symmetric pairs of EEG channels are more different in CPS patients than that in PNES patients. The

powers of EEG signals in narrow frequency bands associate with different brain functions or motifs. The degree of asymmetry is quantified through the relative frequency power of several frequency bands and the T-index, a statistic measuring the degree of divergence between two groups.

## Methods

### EEG Data Characteristics

#### Subjects and EEG Recording Specifications

**[0156]** In this study, seven PNES and seven CPS patients were included. All subjects were 18 years of age or older who were admitted to the Medical University of South Carolina (MUSC, Charleston, S.C.) for inpatient seizure monitoring for diagnostic purposes or presurgical evaluation. The data collection procedure was approved by the Investigational Review Boards MUSC, and the Western Investigational Review Board (WIRB). The EEG recordings at MUSC were obtained using XLTEK monitoring systems (Oakville, Ontario, Canada) with a sampling rate of 256 Hz and the EEG recordings at AGH used 128-channel Nicolet BMSI-6000 systems (Viasys, Madison, Wis., USA) with a 400 Hz sampling rate. The EEGs recorded at both institutions used a referential montage and the 19-electrode international 10-20 system of electrode placement. The exact locations of referential electrodes placed in the dataset were decided on-site and usually followed the recommended location of the Cz and Pz electrodes as suggested by the American Clinical Neurophysiology Society.

#### Awake and Relaxed State EEG Data Selection

**[0157]** The EEG signals of each subject were reviewed to select out the awake and relaxed state sections containing the dominant alpha waves over the occipital regions and no eye-blinking events around the frontal electrodes. To classify patients using only interictal information, the awake and relaxed state EEG signals containing epileptiform discharges or other suspicious epileptic activities were also excluded. All selected awake and relaxed state sections were at least five hours before the first CPS or PNES happened. During the awake and relaxed state, the brain is supposed to be in a resting state and not actively involved in any goal-oriented events. As a result, the awake and relaxed states offer controlled background for the brain network to be compared between subjects. On the other hand, an awake and alert section of long-term continuous EEG from different patients could contain a variety of ongoing psychological activity, raising concerns of confounding if used for comparison analysis.

#### Functional Network Graph

**[0158]** Since oscillation frequency is a main characteristic of the brain and changes when the brain undergoes different psychological conditions or executes different cognitive tasks, all selected epochs were filtered to specific frequency bands including delta, theta, alpha, and beta. All signals were filtered using filters that do not distort the phase information of the filtered signals so that the instantaneous phase time series of the original and filtered signals are the same. This is crucial for this analysis because the connection strength was evaluated using phase information solely.

**[0159]** PLAI was estimated in every five-second epoch of all selected awake and relaxed state sections. A weighted graph representing the functional network can be generated after all pair-wise PLAI are calculated amongst all electrodes. The weighted graph can also be presented as a weighted adjacency matrix as in FIG. 4-3. To convert the weighted graph to a binary one, a threshold can be chosen and applied to all PLAI values such that the edges between vertices is either connected or disconnected. The choice of threshold is done by controlling the density of a graph so that the non trivial structure of the network can be revealed. It was selected to present the network in a graph with density around 0.75 so that only one quarter of the strongest connections (larger PLAI) remained in the functional network graph and the other weaker edges (smaller PLAI) are ignored. The threshold in each epoch can be different from each other and is increased slightly from a small value until the desired density of a graph is reached. The threshold changes from epoch to epoch because the brain may undergo many phases of signal processing and show different connection strength between functional regions while the structure of the information flow should persist in a small-world configuration so that the information is efficiently shared and processed among functional regions. For different subjects, it is reasonable to have individual thresholds for each epoch so that the dominant structure of the functional network can be revealed and compared across subjects.

**[0160]** A network measure is a value quantifying a characteristic of the topology of a network. Several measures have been proposed and used in analysis of network structures. For determination of the existence of a small-world configuration in a network, a clustering coefficient and minimum path length are two crucial measures to evaluate how small-world a network is. A clustering coefficient quantifies how locally entangled a network is, and a minimum path length reflects how globally integrated a network is. These two measures of a functional network graph are compared with those generated from 50 randomized graphs keeping the same number of vertices and edges. Given a clustering coefficient as  $C_p$  and a minimum path length as  $L_p$  for an epoch of selected awake and relaxed state EEG; the randomized graphs generate  $C_p$ -s and  $L_p$ -s respectively. Given  $p_i$  is the number of edges between neighbors of vertex  $i$ , and  $k_i$  is the number of neighbors of vertex  $i$ , the local clustering coefficient can be calculated as Equation 4-14. In Equation 4-15, the clustering coefficient,  $C_p$ , is the average of local clustering coefficients of every vertices in the graph as  $V$  is the number of vertices in the graph.

$$C_i = \frac{2p_i}{k_i(k_i - 1)} \quad (4-14)$$

$$C_p = \frac{1}{V} \sum_{i=1}^V C_i \quad (4-15)$$

$$L_p = \frac{1}{V(V-1)} \sum_{i,j \in V, i \neq j} m_{ij} \quad (4-16)$$

In Equation 4-16,  $m_{ij}$  is the shortest path length from vertex  $i$  to vertex  $j$ . The ratio of  $C_p / \langle C_p \rangle$  to  $L_p / \langle L_p \rangle$  is called the small-world network index,  $\lambda$ . If  $\lambda > 1$ , it suffices to claim that the investigated functional network is a small-world network because the investigated network possesses a higher

clustering coefficient or lower minimum path length comparing to 100 randomized networks possessing the same number of edges and vertices.

#### Inter-Hemispheric Power Asymmetry

**[0161]** Frequency power density,  $X(f)$ , can be estimated by applying discrete Fourier transform on the interesting time series,  $x(t)$ .

$$X(f) = \sum_{t=1}^N x(t) e^{\frac{-2\pi i}{N}(t-1)(f-1)} \quad (4-17)$$

However, discrete Fourier transform is not a consistent estimator and modification is needed to better estimate frequency power density. For each five-second epoch,  $x(t)$  was divided into eight windows that overlapped half of the neighbor windows. For each window, hamming window technique was applied to reduce the noise due to truncation of signal and power density was estimated. All power density functions from eight windows were averaged as the estimate of the power density of the epoch. Relative powers of delta (1-4 Hz), theta (4-7 Hz), alpha (8-12 Hz), beta (13-30 Hz), and gamma (30-58 Hz) band were computed from the power density function of frequency. For example, the alpha band relative power would be the ratio of the sum of powers in the alpha band to the sum of powers from 1-58 Hz. These ratios,  $rp$ , were further transformed to a variable,  $rp'$ , as described in Equation 4-18 so that  $rp'$  has a distribution close to the normal distribution

$$rp' = \log\left(\frac{rp}{1-rp}\right) \quad (4-18)$$

The relative powers in each frequency band were compared to those of the contralateral hemispheric EEG signals by the computation of the T-index. T-index is a function to compute the degree of divergence between paired-samples from two groups. In this case, the sample groups were the relative powers of a certain frequency band from an anatomically symmetric, left and right, pair. Left and right relative powers in each epoch should be paired up because they both reflected the state of the brain during the same period of time.

$$Tind_{LR} = \frac{|\bar{D}_{LR}|}{\sigma_{D_{LR}} / \sqrt{n}} \quad (4-19)$$

In Equation 4-16,  $\bar{D}_{LR}$  is the mean of the differences of relative powers,  $rp'$ , of each awake and relaxed state EEG epoch and  $\sigma_{D_{LR}}$  is the standard deviation of the differences. Due to the fact that each subject has a different length of awake and relaxed state EEG recordings, and the number of samples (degree of freedom),  $n$ , for calculating T-index should be fixed so that the comparison is meaningful, random sampling was performed for each subject so that each subject has 36 (9 random samples from 4 continuous awake and relaxed state EEG segments) epochs input to the T-index function.

## Results

### Network Measures

**[0162]** For each five-second epoch, one functional network graph was generated after the PLAIs were estimated pair by pair. For each functional network graph, the clustering coefficient, minimum path length, and small-world index was calculated from the adjacency matrix. All network measures of every epoch from a patient were averaged into one value for each network measure. As a result, every subject has one final value for each network measure. Totally, the PNES or CPS patients group has seven subjects and therefore, seven values for each network measure. The small-world index,  $\lambda$ , is larger than 1 in all frequency bands for both patient groups, supporting the existence of a small-world network structure in both groups in all frequency bands. A Student T-test was performed to test if the  $\lambda$  in CPS or PNES patient group was larger than one. The p-values showed significance in all frequency bands for both groups (see Table 4-1). Wilcoxon signed rank test was also performed and all subjects showed p-values as 0.0156. The Wilcoxon signed rank test results were the same for all frequency bands since the sample number is always seven and there were seven patients in both groups and all samples were larger than one.

**[0163]** Following this, it was tested if these network measures showed a difference between the CPS and PNES patient groups. A Mann-Whitney U test was performed to assess if the network measures were different enough between both groups and the p-values were shown in the Table 4-2. Only the minimum path length ratio ( $L_p/L_{p-s}$ ) in the delta band showed a significant p-value.

### Inter-Hemispheric Power Asymmetry

**[0164]** The inter-hemispheric power asymmetry was quantified by  $Tind_{LR}$ . In the delta, theta, and alpha bands, the means of  $Tind_{LR}$  of every pair (besides T5-T6) in the CPS group were larger than that of the PNES group. In the beta band, the means of  $Tind_{LR}$  of every pair (besides P3-P4) in the CPS group were larger than that of the PNES group. In the gamma band, the means of  $Tind_{LR}$  of every pair in the CPS group were larger than that of the PNES group. Almost every anatomically symmetric pair in the CPS patient group showed more power asymmetry than that in the PNES patient group. A Mann-Whitney U and Student's T test were performed to test if the means of divergences (T-indexes) of individually symmetric pairs were the same between the two groups and the p-values are listed in Table 4-3 and Table 4-4 respectively. The Student's T test results showed that the relative powers of delta, theta, and alpha band on the C3-C4 pair in the CPS group had significantly larger divergence than that in the PNES group.

**[0165]** Analysis of variance (ANOVA) partitions an observed variance into several components of some possible factors and provides a test of whether the means of groups are equal. It was hypothesized that the variance of the T-indexes, which quantify the inter-hemispheric asymmetry, can be partitioned into components explained by patient groups, pairs and frequency bands. Two-way ANOVA considers two factors in a linear model to explain the interesting dependent variable, and tests if the means of factor groups are the same. Amongst three factors, the main interest is to test if the patient group is a strong factor explaining the variance of the T-index. The patient groups and anatomically symmetric pairs were

first chosen as potential factors for explaining the variance of T-indexes in the two-way ANOVA for each frequency band. The results showed that patient groups were the significant factor in the T-indexes, and the T-indexes were significantly different between the two patient groups under all frequency bands except the beta band. The ANOVA p-values are presented in Table 4-5. The patient groups and frequency bands were later used as factors and did the two-way ANOVA again for each anatomically symmetric pair. The results are presented in Table 4-6 and show that the patient group was a significant factor explaining the variance of T-index for those anatomically symmetric pairs in the frontal brain area.

Discussion

[0166] The global network structure and specific symmetric pair connections were investigated in both PNES and CPS EEG recordings. The small-world network index indicates how small-world a graph is comparing to relatively random graphs having the same number of vertices and edges. In Table 4-1, the small-world index was always bigger than 1 and the Student's T-test showed significance in all frequency bands for both patient groups. The non-parametric Wilcoxon signed-rank test showed the same results of being significant in all frequency bands. Both patient groups showed small-world network structure in their functional graphs and the small-world indexes had no significant difference between two groups. Only the minimum path length in the delta band showed significant difference between the two patient groups. Minimum path lengths in the delta band of the CPS group were mostly shorter than that of the PNES group (p-value=0.037). This implied that the global integration is more efficient in CPS patients than that in PNES patients during the awake and relaxed states. This is not surprising because seizure itself is a synchronous activity amongst many brain areas. Furthermore, about half of partial seizures happen during sleep. Moreover, temporal lobe complex partial seizures were more likely to secondarily generalize during sleep than during wakefulness. My result could explain these interactions between partial seizures and sleep. Before entering the sleep state, the epileptic brain functional network showed higher global integration and could possibly facilitate the generation of seizures or the secondary generalization during sleep. This study did not include any sleep EEG data so the hypothesis should be further pursued. Other network measures did not show that significant differences could result from several reasons and the possible combination of these reasons. First, the pathological network structure may not manifest during the interictal awake and relaxed state of a patient. Second, the metric of association (PLAI) may not be sensitive enough to differentiate the pathological nuance of neuronal interaction. Third, the network structure of the brain itself may be attack-tolerant. Even though there have been some lesions due to epileptic discharge, the brain could be organized in a fashion such that tissue damage does not affect much of the existence of the small-world feature in the functional network. These hypotheses can be confirmed through further study. For example, a study comparing the interictal and preictal network structure could determine whether or not the pathological network appears during the interictal state. Applying other interdependence measures could show a different perspective of the functional network in the awake and relaxed state. It would also be intriguing to design an integration index from different interdependence measures so that

the integration index values correspond to the synchronous activities of the greatest interest.

[0167] Inter-hemispheric power asymmetry is a more specific and local measure to investigate the quality of connection between hemispheres. For CPS patients, the brain tissue around the foci could be damaged by the recurrent onsets of partial seizures. The lesion of the brain tissue should affect the ensemble neuronal activity and cause the EEG signal to deviate from the EEG signal of the anatomically symmetric channel. On the other hand, PNES patients have more similarity between EEG signals from anatomically symmetric channels due to symmetrically commensurate tissue integrity. Other than the lesion, the fixed focal hemisphere of partial seizures could result from substantially different pathological structures within the hemisphere. If both of the abovementioned causes are valid and additive, the asymmetry could exacerbate.

TABLE 4-1

Small-world network index, $\lambda$ , of functional networks of CPS and PNES patients during awake and relaxed state.					
		Delta	Theta	Alpha	Beta
CPS	Mean	1.182	1.119	1.124	1.108
	SD	0.052	0.063	0.036	0.063
	T-test p-value	8.72E-05*	0.002510*	0.000103*	0.003772*
PNES	Mean	1.150	1.162	1.112	1.129
	SD	0.054	0.049	0.038	0.037
	T-test p-value	0.000315*	0.000124*	0.000232*	9.96E-05*

\*significant result when the hypothesis was that the  $\lambda$  is equal to one.

TABLE 4-2

Mann-Whitney U test results of network measures of CPS and PNES patient groups during awake and relaxed state.					
	CPS		PNES		U test p-value
	Mean	SD	Mean	SD	
$\lambda$					
Delta(1-4 Hz)	1.182	0.052	1.150	0.054	0.259
Theta(4-7 Hz)	1.119	0.063	1.162	0.049	0.209
Alpha(8-12 Hz)	1.124	0.036	1.112	0.038	0.456
Beta(13-30 Hz)	1.108	0.063	1.129	0.037	0.383
$Lp / <Lp-s>$					
Delta(1-4 Hz)	0.997	0.015	1.004	0.003	0.037*
Theta(4-7 Hz)	1.003	0.009	1.000	0.010	0.902
Alpha(8-12 Hz)	1.004	0.009	1.003	0.003	0.805
Beta(13-30 Hz)	1.001	0.008	1.003	0.006	0.383
$Cp / <Cp-s>$					
Delta(1-4 Hz)	1.177	0.041	1.155	0.056	0.383
Theta(4-7 Hz)	1.121	0.064	1.162	0.043	0.383
Alpha(8-12 Hz)	1.128	0.035	1.115	0.040	0.535
Beta(13-30 Hz)	1.109	0.062	1.132	0.039	0.318

\*significant result.

TABLE 4-3

Mann-Whitney U test results of relative power asymmetry of CPS and PNES patient groups during awake and relaxed state.							
	F3-F4	C3-C4	P3-P4	O1-O2	F7-F8	T3-T4	T5-T6
Delta	0.209	0.017*	0.805	0.209	0.209	0.535	0.053
Theta	0.097	0.073	0.805	0.535	0.165	0.038*	0.805
Alpha	0.318	0.053	0.097	0.318	0.073	0.620	0.710
Beta	0.259	1.000	0.259	1.000	0.053	0.383	0.902
Gamma	0.535	0.710	1.000	0.710	0.128	0.535	1.000

\*significant result.

TABLE 4-4

Student's two-sample T test results of relative power asymmetry of CPS and PNES patient groups during awake and relaxed state.							
	F3-F4	C3-C4	P3-P4	O1-O2	F7-F8	T3-T4	T5-T6
Delta	0.184	0.029*	0.293	0.201	0.326	0.257	0.049*
Theta	0.415	0.047*	0.633	0.412	0.236	0.054	0.944
Alpha	0.262	0.050*	0.057	0.364	0.075	0.623	0.532
Beta	0.244	0.424	0.450	0.644	0.110	0.170	0.752
Gamma	0.222	0.405	0.568	0.529	0.147	0.394	0.476

\*significant result.

TABLE 4-5

P-values of two-way ANOVA (patient groups as factor) in each frequency band.					
Frequency bands	Delta	Theta	Alpha	Beta	Gamma
P-value	0.0036*	0.0034*	0.0019*	0.0584	0.0254*

\*significant result.

TABLE 4-6

P-values of two-way ANOVA (patient groups as factor) for each anatomically symmetric pair.							
Symmetric pair	F3-F4	C3-C4	P3-P4	O1-O2	F7-F8	T3-T4	T5-T6
P-value	0.011*	0.001*	0.109	0.070	0.002*	0.017*	0.905

\*significant result.

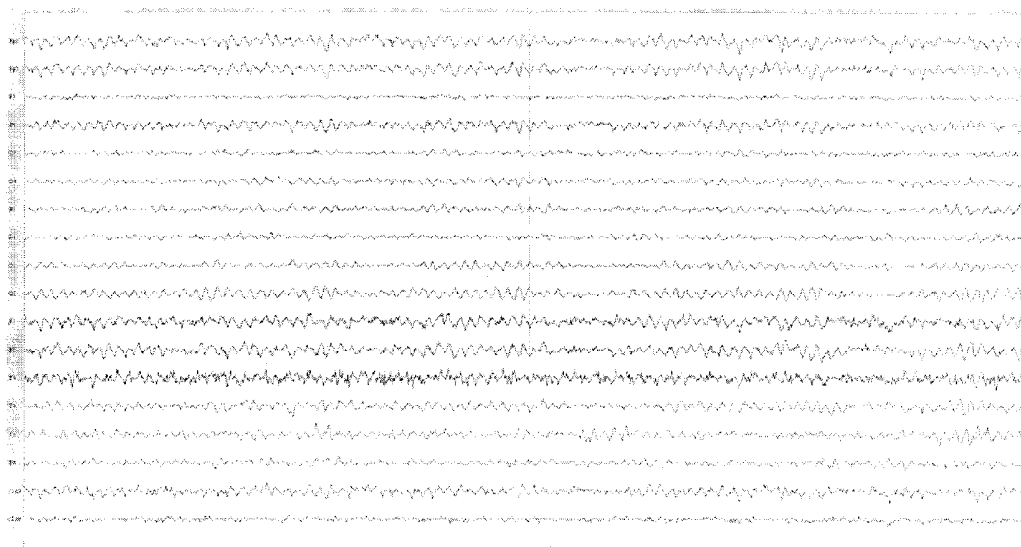


Figure 4-1. Eye-closed awake and relaxed state EEG signals of a patient having CPS.

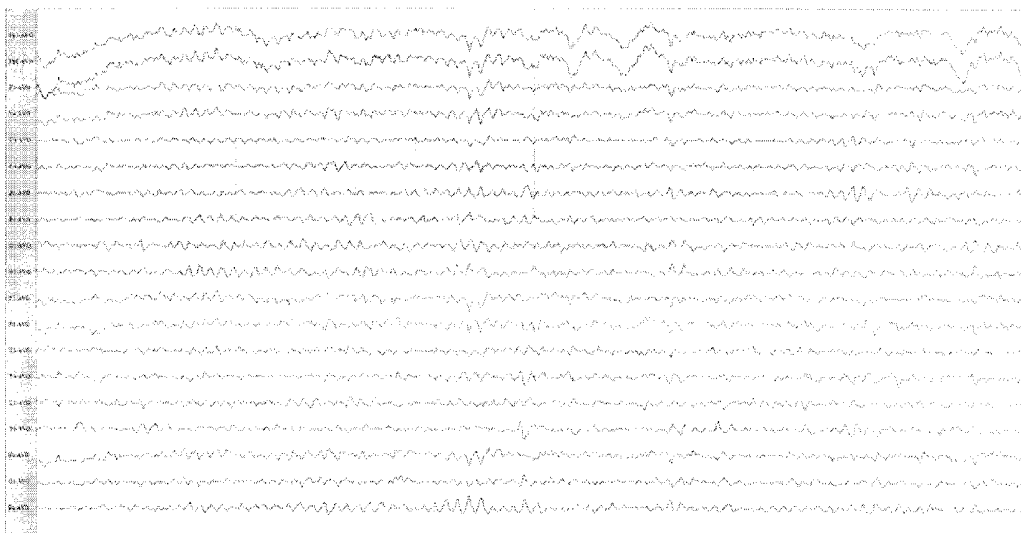


Figure 4-2. Eye-closed awake and relaxed state EEG signals of a patient having PNES.

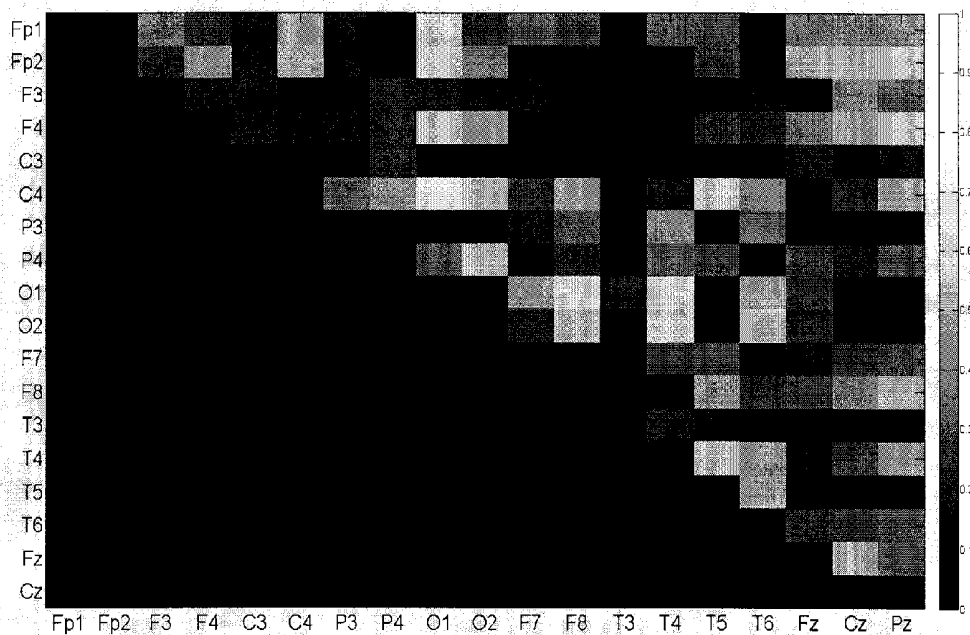


Figure 4-3. A weighted adjacency matrix. The matrix has 18 rows and 19 columns. The adjacency matrix is supposed to be a square symmetric matrix. To eliminate the redundant information, the last row is eliminated and the diagonal as well as the lower triangular part of the original adjacency matrix are forced to be zero.

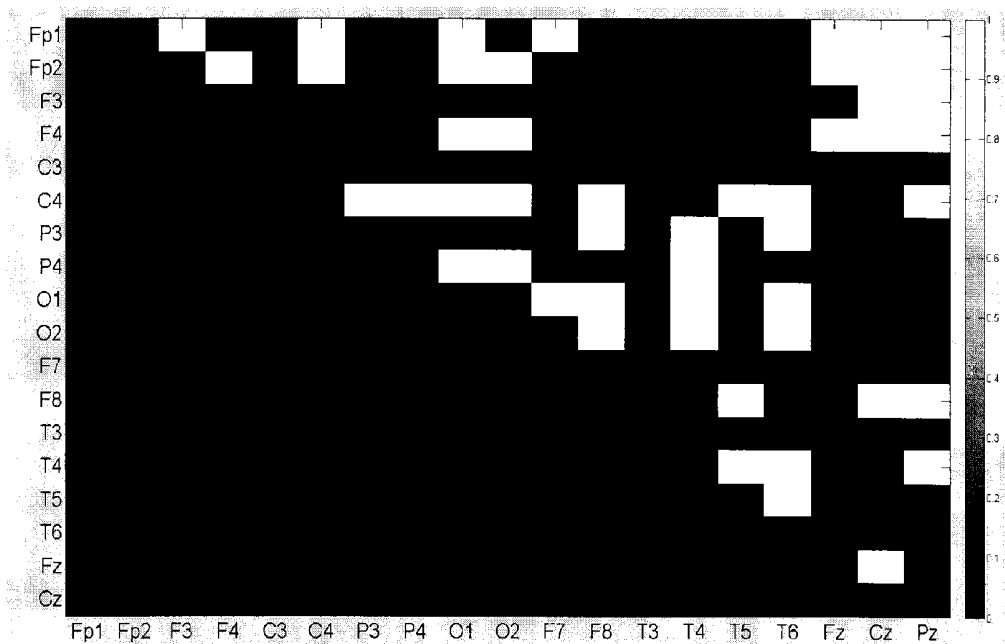


Figure 4-4. An adjacency matrix after applying a threshold on the weighted adjacency matrix in Figure 4-3. The matrix has 18 rows and 19 columns. The adjacency matrix is supposed to be a square symmetric matrix. To eliminate the redundant information, the last row is eliminated and the diagonal as well as the lower triangular part of the original adjacency matrix are forced to be zero. The threshold is applied and the entries in the matrix are either one or zero.

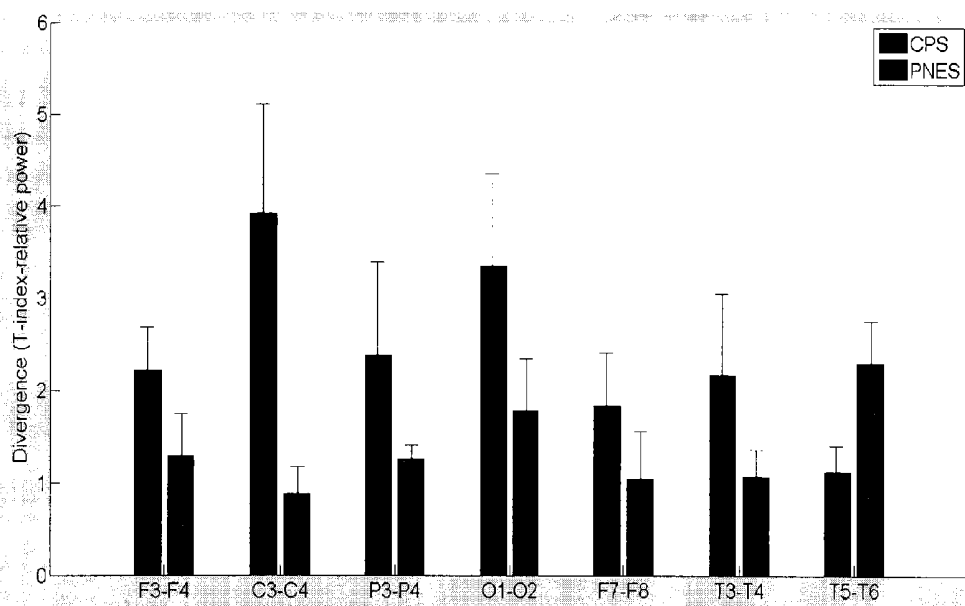


Figure 4-5.  $Tind_{LR}$  of individual anatomically symmetric pairs in the delta frequency band.

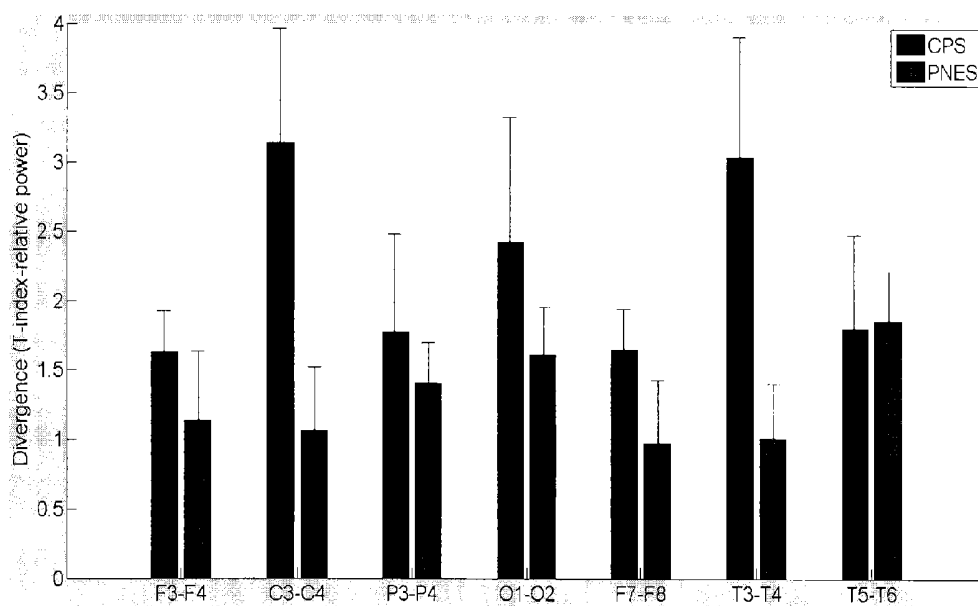


Figure 4-6.  $Tind_{LR}$  of individual anatomically symmetric pairs in the theta frequency band.

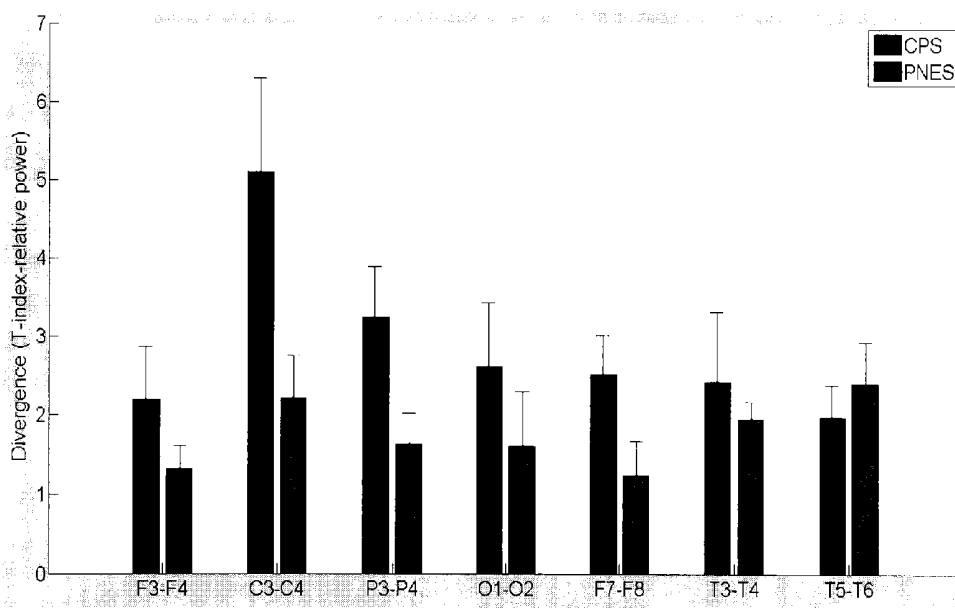


Figure 4-7.  $Tind_{LR}$  of individual anatomically symmetric pairs in the alpha frequency band.

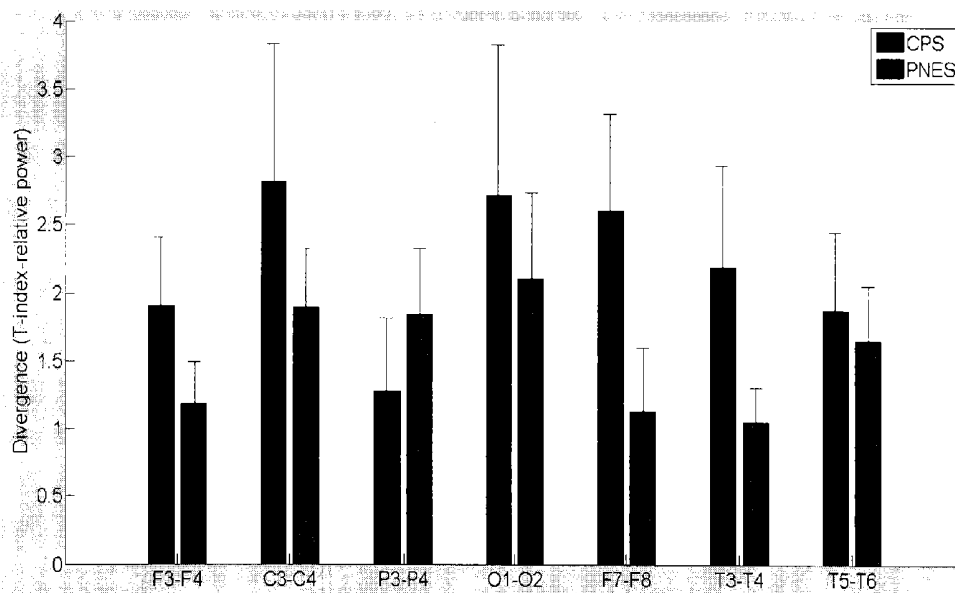


Figure 4-8.  $Tind_{LR}$  of individual anatomically symmetric pairs in the beta frequency band.

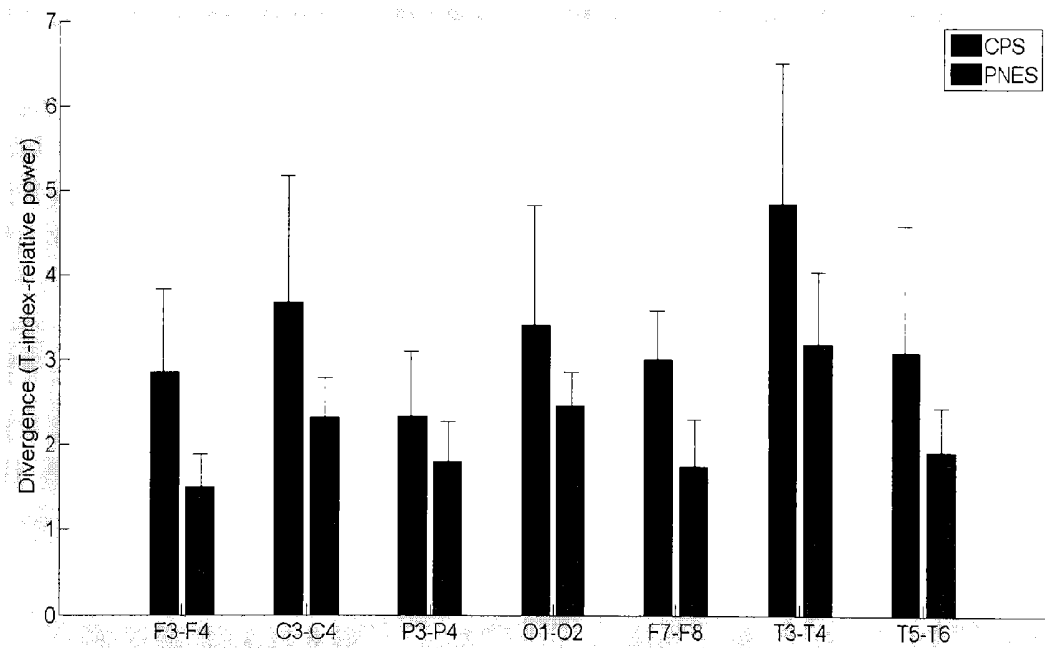


Figure 4-9.  $Tind_{LR}$  of individual anatomically symmetric pairs in the gamma frequency band.

## Chapter 5

Connectivity Transition from Interictal to Ictal States  
on Neocortical Epilepsy

## Preamble

**[0168]** Neocortical seizures originate in the neocortex—the external surface part of the cerebral hemispheres. Neocortical epilepsy differs from mesial temporal epilepsy in that it is difficult to clearly define a single area from which the seizures originate. Since seizures associated with neocortical epilepsy generally do not respond well to medication, epilepsy surgery is often one of the few options that patients with neocortical epilepsy have. However, surgery for neocortical epilepsy has a significantly lower success rate than other kinds of epilepsy. In patients with other types of epilepsy, such as mesial temporal lobe epilepsy (MTLE), surgeries can provide seizure freedom in more than 70 to 90% of cases. Possible reasons that could result in the low success rate of neocortical epilepsy are: (1) there may be multiple seizure onset zones, (2) the initiation site may vary from seizure to seizure, and (3) with currently available technologies, it is difficult to precisely identify the duration and extent of seizure onset zones. A recent study by Lee et al. in 2005 on nonlesional neocortical epilepsy showed that, based on the epileptogenic focus locations, only 47 out of 89 patients were seizure-free (Engel Class I) after the surgery, and an additional 7 experienced significant reduction in seizure frequency (Engel Class II). Therefore, developing a more reliable and effective method for identifying suitable parts and critical regions for neocortical epilepsy surgery would be a major contribution to improve the service of medicare and quality of life for those patients.

**[0169]** Many epilepsy researchers have postulated that there exists a network of anatomical regions in the cerebral cortex and its connections that initiates the transitions between normal (interictal) and seizure (ictal) states, resulting in recurrent seizures. In this case, identifying the configuration of the network and understanding the characteristics and dynamics of the network could lead to a greater understanding of neocortical epilepsy.

**[0170]** One of the most obvious hallmarks of the epileptogenic brain is the presence of interictal spikes in the EEG. However, areas that generate interictal spikes do not consistently correspond to the seizure onset zones (brain site where the seizure discharge first appears). Nevertheless, it is very likely that areas with interictal spikes and the seizure onset zones are both within the same epileptic brain network. Furthermore, there may be other critical brain regions that are related to seizure occurrences but are not exhibited through interictal spikes or ictal discharges. My research, by analyzing intracranial EEGs, seeks to explore, quantitatively, the existence and structure of a neocortical epilepsy brain network. The methods and results section indicates how to identify the nodes and edges in the network quantitatively, and how the characteristics of the brain network change from an interictal state to a seizure (ictal) state.

**[0171]** Another important diagnostic tool for neocortical epilepsy surgery is high-resolution magnetic resonance imaging (MRI). Often this offers a high predictive value for surgical outcomes. However, MRI does not work well in 29% of patients with partial epilepsy. Many patients referred to epilepsy centers for surgery have normal MRI results (no lesion) and previous studies report that surgical outcomes were poor

for patients with neocortical epilepsy with a normal MRI result. Intracranial EEG recording is also indispensable for localizing seizure onset zones. However, sampling error can lead to false or missed localization during intracranial EEG recording. This problem is particularly common in cases with extratemporal seizure origin. Nevertheless, several studies have demonstrated the usefulness of focus localization in neocortical epilepsy with quantitative analysis on intracranial EEG. For example, Andrzejak et al. in 1999 applied methods derived from nonlinear dynamics on intracranial interictal EEGs (N=8) to lateralize the primary epileptogenic area in two patients with neocortical epilepsy. They found that a nonlinear deterministic measure can contribute to an interictal localization of the primary epileptogenic area in patients with neocortical epilepsy. Based on a “focus index” measure, Roopun et al. used a few examples to demonstrate that basic dynamic changes in focal epilepsy of neocortical origin may be useful in localizing the origin of seizures. The findings of these studies and many others support the hypothesis that the dynamics of intracranial EEGs are associated with the behavior of epileptogenic focus in neocortical epilepsy. Recent observations in humans with MTLE and in the animal models for this condition helped conceptualize multifocal seizure onset (i.e. seizures that begin focally within different limbic structures with each seizure) as well as synchronized regional seizure onset (i.e. presumed simultaneous seizure initiation). These observations, together with multifocal physiological and anatomical changes in the animal models have raised the possibility of a widely distributed neural network (e.g., specific cortical and subcortical networks) in the genesis and expression of partial onset seizures. Spencer (2002) defined a network to be “a functionally and anatomically connected, bilaterally represented, set of cortical and subcortical brain structures and regions in which activity in any one part affects activity in all the others.” One central observation on which this definition is based is that vulnerability to seizure activity in any one part of the network is influenced by activity everywhere else in the network, and that the network as a whole is responsible for the clinical and electrographic phenomenon that may be associated with human seizures. She further distinguishes between the network and the “seizure onset zone”. The seizure onset zone for neocortical seizures is defined by the ictal EEG. It is the area where the seizure discharge is first seen on ECoG (subdural electrodes). It may involve one or many electrode sites. In some patients, seizures (based on clinical manifestations) can start with EEG discharges beginning in different “onset zones” and spreading along different routes as the seizure progresses.

**[0172]** Spencer (2002) suggested that the existence of an epileptic network is supported also by the responses to invasive therapy. If human epilepsy is the expression of specific, abnormally active, intrinsically defined and connected cortical/subcortical/bilateral networks, then one could theoretically alter seizure expression by intervening in any part of the specific network. Operations involving anterior temporal lobe, medial structures only, lateral structures only, or more or less extensive lateral temporal resection, can cure this disorder. Procedures with no anatomic overlap are similarly successful. This cannot be explained unless the multiple areas are all critical in the production of the intractable seizures of this disorder. Then, interruption of the network in any one of those areas would be (and apparently is) sufficient to alter the seizures. The similarly excellent response with cessation of seizures after temporal lobe resection in well-selected patients

who have bilateral independent medial temporal lobe origin of seizures is another example of the existence of a network, interference with which at any site alters the expression of the intractable seizures.

**[0173]** Based on the above observations, it may be pertinent to consider study of other kinds of phenomena in individual patients, which may define the network in better terms than has been sought in the past because of the single-minded attention to defining regions of so-called seizure onset. For example, quantitative intracranial EEG analysis, background patterns, sleep effects on interictal and ictal activity, and other types of functional assessments may contribute considerably to the understanding of the role of networks in the expression of the epilepsies. Studying broad regions of brain structures related by the presence of such networks, using quantitative EEG analyses and sophisticated approaches, may detect alterations in the behavior of the network before the more traditional “seizure discharge” is seen, and allow prediction of seizures before manifestation clinically or on traditional EEG.

#### Material

**[0174]** Intracranial EEGs provides the most convincing evidence to support the network hypothesis. Because the entire network participates in the expression of the seizure activity and can be entrained from any of its various parts, initial electrical events (at “seizure onset”) may vary in their specific location of expression and occurrence within the network. The initial area of apparent seizure involvement is not really an onset area, because “onset” could be expressed at any place in the network, and might even vary from seizure to seizure in a given patient. This locational variability may produce different morphologies of “seizure onset” when EEG recording is performed in only one part of the network. This may be the main reason for surgical failure in the neocortical epilepsy. A reliable quantitative method based on intracranial EEGs for determining the spatial distribution of the nodes of the epileptic network may lead to a better understanding of the mechanisms that lead to the generation of a seizure, and provide insights into more effective approaches to seizure control.

**[0175]** We selected one subject with neocortical epilepsy and used the intracranial EEG of the subject to construct a representative network which is capable of showing the critical region with recording electrodes as vertices in the network. The patient is a 21-year old male, with a history of intractable seizures. Continuous VEEG monitoring was performed with XLTEK monitoring systems (Oakville, Ontario, Canada) equipment with a sampling rate of 499.707 Hz. Totally, 44 electrodes were applied on the left hemisphere cortex of subject. Data were obtained, stored, and interpreted according to ACNS guidelines. During the recording, frequent interictal spikes discharges were present at the G4, G5, G9, G14, G15, IH2, and IH3 electrodes.

**[0176]** Two EEG segments were cut and used to construct a brain network from a continuous EEG recording containing one neocortical epilepsy seizure from the patient. The seizure events were identified by the recording facility based on both clinical observation and a review of the EEG. In order to avoid the potential overlapping between ictal, postictal and preictal stages, only seizures that were at least 2 hours apart from the previous or next one were used. The two segments analyzed were both 150 min long. One contained a seizure starting at 120 min and the other was seizure free. For the later, the

previous or the next seizure happened at least 5 hours away from the beginning or ending of the seizure free segment. Both segments were preprocessed with a band-pass filter (1-220 Hz) and several notch filters (60 Hz, 120 Hz, and 180 Hz) to remove the alias, power line artifacts and DC component.

#### Methods

**[0177]** This paper sought to identify the critical regions in the brain that are closely related to the development of neocortical epileptic seizure. In intracranial EEG recording, each electrode was treated (channel) as a node (vertex) in the network and cross-correlation functions were used to calculate the weighting on the edge of each pair of nodes. To convert a weighted network into a binary one, an edge stay was kept in the network if and only if the two nodes adjacent to it were sufficiently connected.

**[0178]** The brain network was constructed as follows. Both 150-minute segments were further chopped into non-overlapping calculation windows of 6 seconds to construct transient brain networks. In every calculation window, each electrode was treated as a node in the network. Pair-wire cross-correlation coefficients were calculated among all 44 nodes. A cross-correlation coefficient,  $r(d)$ , with delay  $d$ , was calculated as Equation 5-1.

$$r_{x,y}(d) = \frac{\sum_{v=1}^N [(x(v) - mx) \times (y(v-d) - my)]}{\sqrt{\sum_{v=1}^N (x(v) - mx)^2} \sqrt{\sum_{v=1}^N (y(v) - my)^2}} \quad (5-1)$$

$$mx = \frac{1}{N} \sum_{v=1}^N x(v), \quad my = \frac{1}{N} \sum_{v=1}^N y(v) \quad (5-2)$$

**[0179]** where  $x(v)$  and  $y(v)$  are EEG signal values of a pair of electrodes at time  $v$  and  $N$  is the number of sampling points in each 6-second calculation window. The cross-correlation coefficients with various delay  $d$  (range from  $-1$  to  $+1$  second) were calculated. Then, the maximum of the absolute value of the cross-correlation coefficient was obtained by selecting delay  $d$ . For each pair of nodes  $p$  and  $q$ , the weight of edge  $e_{p,q}$  is defined by this maximum value. In this way, one obtains a weighted network. To convert it to a binary network, only the edges with a weight higher than a threshold (0.9) stay in the network.

$$e_{p,q} = \max_d [r_{p,q}(d)] \quad (5-3)$$

$$E_{p,q} = H(e_{p,q} - thr) \quad (5-4)$$

**[0180]** In each six-second epoch, a graph representing the instant brain network was constructed and then the degree of electrode  $x$ ,  $D_x$ , was calculated in Equation 5-5.

$$D_x = \sum_{y=1}^{N_{nodes}} E_{p,q} \quad (5-5)$$

**[0181]** In Equation 5-5,  $N_{nodes}$  is the total number of nodes implanted under the scalp and equals 44 for this neocortical epilepsy patient. The five-minute mean occurrences of degree of node  $x$ ,  $D_{x(5-min)}$ , was calculated and then an average degree over all nodes, AveD was calculated by averaging  $D_{x(5-min)}$  over all channels as Equation 5-6.

$$AveD = \frac{1}{N_{nodes}} \times \left[ \sum_{x=1}^{N_{nodes}} D_{x(5-min)} \right] \quad (5-6)$$

#### Results and Hypothesis Testing

**[0182]** After the coupling strength between each pair of nodes was quantified as the maximum cross-correlation, the functional epileptic network was constructed. There are many features of network structures, and degree is one of the most widely-used basic properties of network analysis. Based on the degree results, the connectivity of an instant network was defined as the average degree of all nodes during a five minute period and quantified as AveD. One of the main purposes of this study was to find if there was a significant change in the instant network structures before and after a seizure onset. Therefore, one of those proper hypotheses to test this idea was that the connectivity of an epileptic brain network increases when a brain approaches a seizure onset and then decreases after the onset. The results are shown as follows and the hypothesis test will be done in the discussion section.

**[0183]** To have a better time resolution and globally spatial layout of connectivity, AveD was used to present the connectivity. After the AveD calculation, the trajectories of AveD were drawn. The slope of the average degree over all channels was estimated between the beginning and 120 minute time point (i.e., onset time) of the segment. The slope from the 0 to 120 minute time point in the seizure segment was 0.02/5 minutes ( $p=0.028$ ), and was  $-0.0036$  ( $p=0.447$ ) during the same time period of the interictal segment. The degrees of nodes in the network were averaged over 300 calculation windows that spanned over 30 minutes, and then plotted in FIG. 5-4.

#### Discussion

**[0184]** In FIG. 5-2 and FIG. 5-3, the regression slope of the segment with an onset is larger than zero, while the segment without any onset is less than zero. This suggested that the connectivity increases before an onset. Although the interictal segment had high values of AveD around the 95 minute, the regression slope was not larger than zero. Based on this observation, the following can be concluded. If the recording is done during interictal state, the connectivity should fluctuate within a range and have a regression slope around zero. If one has a preictal recording, one should more likely detect a positive regression slope within a period right before the seizure onset. The p-value provides information about how unlikely the regression slope is compared to the value of zero. The regression slope equal to zero means that the connectivity does not correlate with the time within the segment. This is also what was presumed to happen during an interictal state. Additional support for this hypothesis is the result that the p-value is equal to 0.0028 ( $<0.05$ ) in the segment preceding an onset and 0.447 ( $>0.05$ ) in the interictal segment.

**[0185]** An epileptic seizure can be interpreted as an activity during which the neurons from different region overly correlate with each other. Therefore, one should observe a decrease of connectivity after a seizure. Network connectivity in terms of AveD 30 minutes before and 30 minutes after the seizure onset were compared. The average degree before the seizure was 0.33 versus 0.09 after the seizure ( $p=0.027$ ). Applying the same comparison of average degrees in the interictal segment, the difference was not significant ( $p=0.366$ ). The results of this pilot study suggest that transitions in the brain networks may exist and are related to the underlying dynamics of seizures caused by neocortical epilepsy. An increase of connectivity can be observed before seizure onset. The onset of a seizure can cause the reset of the connectivity closer to a baseline level.

**[0186]** Prokopyev et al. (2003) conducted additional analyses on the brain and found significant changes in the network characteristic during a seizure. In this paper, a decrease of connections was observed in results after the onset (in FIG. 5-4); this is consistent with the reset phenomenon after seizure. Monto et al. in 2007 studied epileptic brain networks by quantifying the long-range temporal correlation in subdural human EEG recordings. Their observations on the spread of abnormally large LRTCs suggested that the epileptic focus is associated with significant changes in network behavior even in the cortical areas immediately surrounding the clinically determined focus. By applying synchronization and graph analysis to intracranial EEG recordings, Ponten et al. (2007) investigated the hypothesis that functional neuronal networks during temporal lobe seizures change in configuration before and during seizures. The study found that the functional brain networks change from a more random configuration during an interictal recording period to a more ordered configuration during seizures, especially during seizure spreading. The authors further suggested that the findings supported the theory that a random network (during interictal periods) even had a stronger tendency to synchronize, which could cause seizures. More recently, Zaveri et al. (2009) calculated a magnitude squared coherence on background intracranial EEG as a measure of functional connectivity to investigate the network effects within and outside the seizure onset area. The analysis demonstrated an inverse relationship between the connectivity strength and the distance from the seizure onset area (especially during the frequency band). Another similar work by Ortega et al. in 2008 showed the presence of clusters of increased synchronization in different locations on the lateral temporal cortex in patients with temporal lobe epilepsy. As yet unproven, it is possible that increased connectivity (as can be defined by coherence, synchronization clusters, or nonzero functional connectivity) helps initiate seizures. If increased brain connectivity or alteration in network topology helps initiate seizures, then network nodes and pathways could serve as targets for resective or disconnective surgery, implantable devices, and investigations of seizure anticipation. Applying classification techniques for circumscribing some communities within the network could be done after the network is constructed and these communities may serve as good entities for observing the entrainment preceding a seizure. This is due, in part, because they are supposed to be less correlated during interictal periods and then entrain as evolving to ictal state. Several methods of identifying communities in network were introduced in Porter's work in 2009.

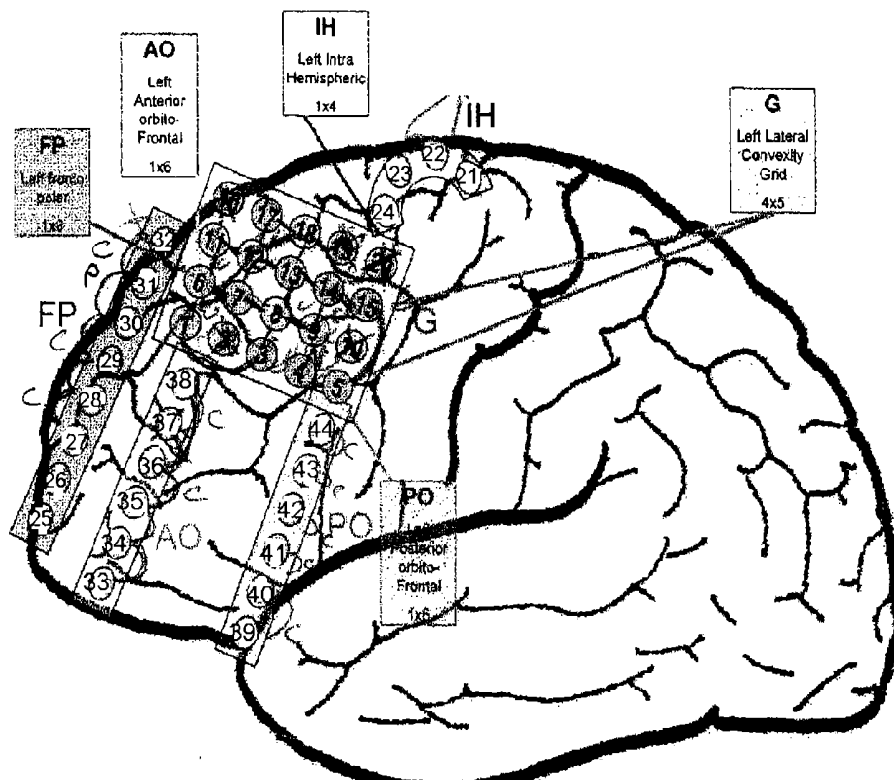


Figure 5-1. Electrode placement of the neocortical epilepsy patient. There were totally 44 electrodes placed on the left frontal cortex of the subject.

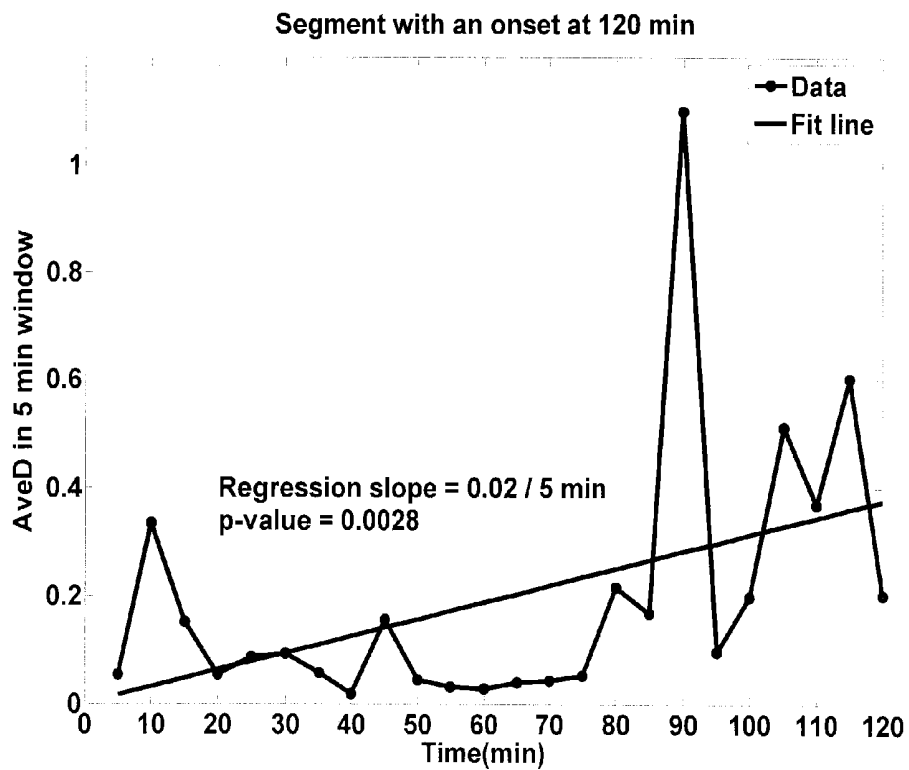


Figure 5-2. *AveD* of the segment with a seizure onset at the 120 minute. The blue line denotes the trajectory of the connectivity states for every five minutes. Least square linear regression was implemented and the result is indicated as the red line.

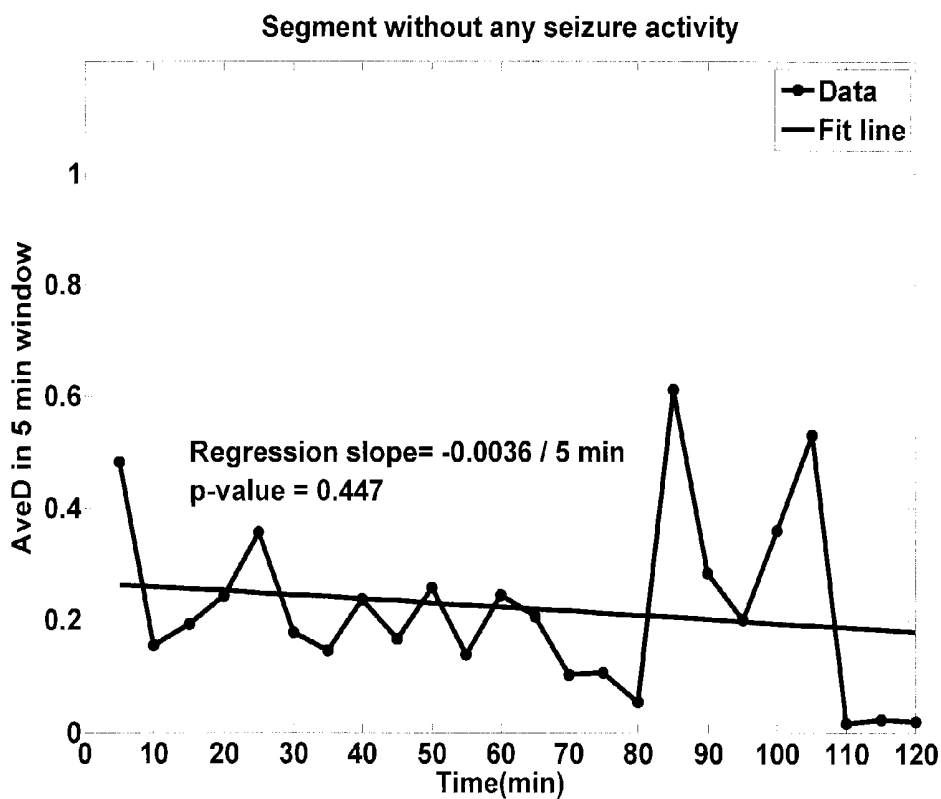


Figure 5-3. *AveD* of the segment without any seizure activity. The blue line denotes the trajectory of the connectivity states for every five minutes. Least square linear regression was implemented and the result is indicated as the red line.

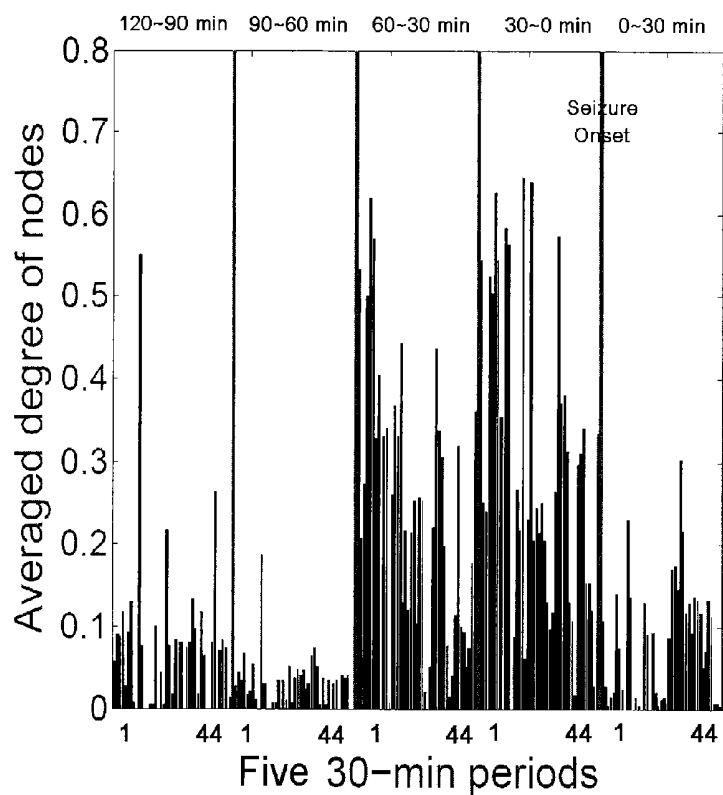


Figure 5-4. Averaged degree over 300 calculation windows of nodes in the network. It includes five periods: 120~90 min before; 90~60 min before; 60~30 min before; 30~0 min (seizure onset) before; 0~30 min after seizure onset. Red lines separate different periods. In each period, all the 44 nodes (electrodes) in the network were plotted in bars. The height of each bar denotes the averaged degree of the corresponding node.

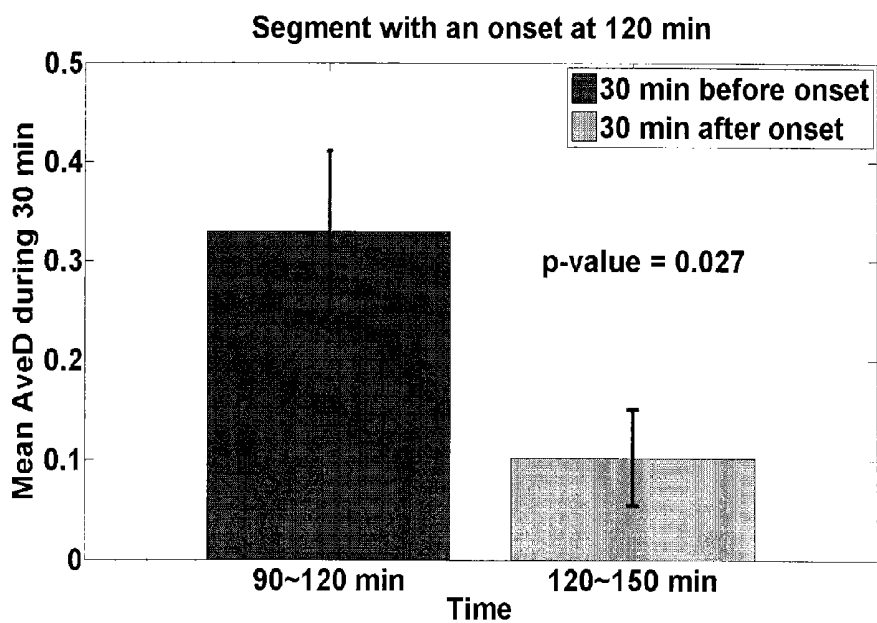


Figure 5-5. The average of *AveD* over 30 minutes before and after a seizure onset. The error bars indicate the standard error of the mean. The  $p$ -value is 0.027 ( $<0.05$ ) if it is assumed that the values of *AveD* should be the same within 30 minutes before and after the seizure onset.

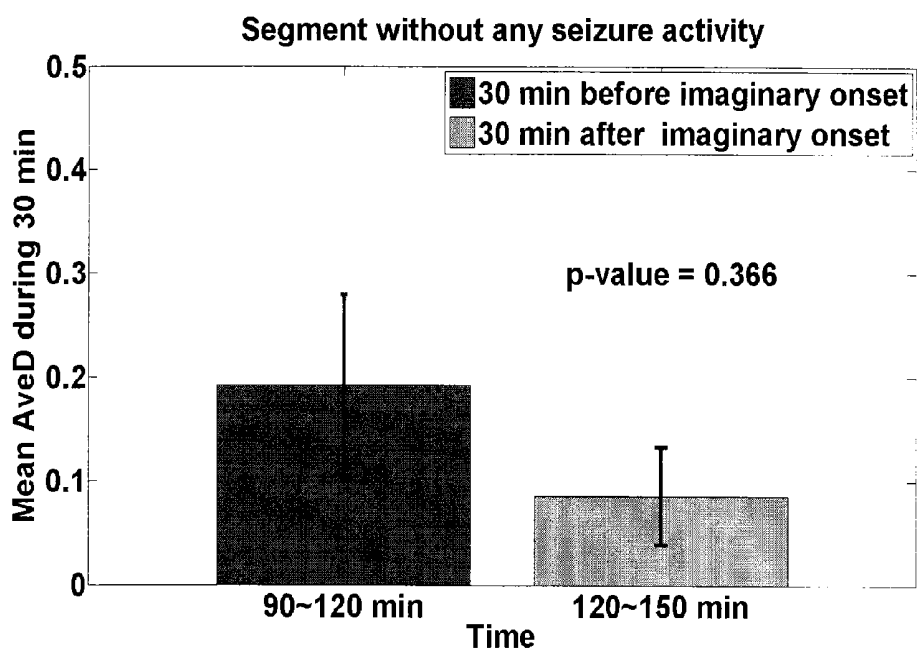


Figure 5-6. The average of *AveD* over 30 minutes before and after an imaginary seizure onset that is located at 120-minute point. The error bars indicate the standard error of the mean. The  $p$ -value is 0.366 ( $>0.05$ ) if it is assumed that the values of *AveD* should be the same within 30 minutes

## Chapter 6

## Conclusion

**[0187]** My work investigated several time series features applied to several applications relating to epileptic EEG signals. The first part of my research focused on a possible scheme for seizure prediction. While there have been numerous studies that show promising results in anticipating seizure onsets using intracranial EEG, transferring these successes to seizure prediction based on scalp EEG is still a challenging task. Many studies so far have investigated the seizure prediction problem only under very well-controlled conditions. Developing a robust scheme for seizure prediction outside the laboratory environment requires a variety of signal processing techniques. The first part of my research explored the performance of a single feature-based algorithm on long-term continuous scalp EEG. The focus here was on evaluating an automated seizure prediction algorithm that issues seizure warnings by monitoring the convergence of signal regularity among EEG channels in continuous long-term scalp EEG recordings. For each trial, the algorithm was optimized with a training dataset and its performance was evaluated using a separate test dataset. In the test dataset, the algorithm achieved an average sensitivity of 65% (i.e., ~2 out of every 3 seizures) with an average false positive rate of 0.24 per hour (~1 per 4 hours). The algorithm performance in the test dataset was nearly the same as that in the training dataset. This implies that the algorithm generated a stable performance in epileptic patients. Statistically, the overall sensitivity achieved by the test algorithm was better than a random warning scheme ( $p$ -value=0.0145). While these results are encouraging, the performance of the algorithm may not yet be sufficient for some clinical applications. For example, the performance would be of limited utility for inpatient monitoring applications, such as the EMU setting, due to the high false positive rate. However, the performance may be useful for driving seizure control devices, such as the vagus nerve stimulator. Furthermore, in this type of application, fine tuning the prediction algorithm to optimize performance for each individual patient could yield even better performance. Although the performance was not yet sufficient for its usage in a clinical environment, the results demonstrated the supremacy of the algorithm compared to a random scheme. This implied that the method found some events preceding the onsets of seizures. Further analysis needs to follow to be more specific about the positive findings in this study.

**[0188]** It is also informative to investigate the common characteristics of these negative results. For instance, the false-positives may result mostly from a certain type of event and could be muted if the triggering event is found. This could bring down the false-positive rate and possibly further increase the sensitivity of the algorithm when the parameters are chosen to be more sensitive and the false-positive rate is well suppressed to an acceptable level. Incorporating engineering techniques could help the prediction scheme become more applicable in reality. For a complex system such as the brain, it may be too ambitious to hope that only one dynamic feature or method would be sufficient to accomplish effective seizure prediction. Aggregating the advantages from several time series dynamic features can possibly join the benefit of each feature. Until now, most studies have compared one kind of method to another, such as linear vs. nonlinear and univariate vs. bivariate features. These results demonstrated that the bivariate features outperformed univariate features. Nonlinear

features have been popular since 1999 but progress since then has not been substantial. Until recently, linear methods such as the AR model or coherence have still been used and have generated satisfactory results in many EEG research fields including seizure prediction. Different features explain the same signal from different perspectives and should be clearly correlated to the raw signal so that one can better utilize a feature at the proper time for a suitable purpose. Besides signal features, additional engineering methods could benefit the prediction scheme in the preparation and post-feature stages. In the preparation stage, filtering, inverse source locating, and network analysis could help extract more seizure-relevant information from the EEG signals before the dynamic features are applied to the signals. During the post-feature stages, a decision to issue a warning or an index denoting the susceptibility of having a seizure should be output. A decider should be designed to consider situational information about the different features from the patient and integrate them in an optimal way. Optimization skills could be involved to assist in the decision process. Additionally, a prediction scheme with an updating threshold or a learning classifier would be more adaptive to the possibly changing background of EEG activities if one considers applying the prediction scheme in an ambulant environment. There are still many aspects that can be improved and deserve greater analysis or hypothesis testing in seizure prediction. The understanding of applicable features on the raw data and the integration of information are fundamental to accomplish this challenging task.

**[0189]** In my initial study, the focus was on the temporal transition from the interictal to ictal states of a group of epileptic patients. Following this, the possible differences of interictal network features between psychologically and physiologically epileptic patient groups was investigated. Graph theoretical analysis was applied to reveal the functional network structure of CPS and PNES patients when they were in the awake and relaxed interictal state. The results showed the existence of a small-world network configuration in both patient groups. Furthermore, the delta-band minimum path length was significantly smaller in the CPS patient group. This implied that the low frequency global integration was more efficient in CPS than in PNES patients. Both groups had the same small-world network indexes and clustering coefficients. These results implied that the brain either somehow maintained the structure of a small-world network or the original small-world network was attack-tolerant so that the pathological influence of epileptic discharges did not bring down the small-world configuration. The results above viewed the connection in a comprehensive scope over the whole brain. However, if the pathological effect was only locally misleading, the large-scale analysis could fail to track down the difference. To take a closer look at the connection strength of several specific pairs, the frequency power information was retrieved and compared the inter-hemispheric asymmetry for both groups. The difference of power asymmetry was revealed in all frequency bands on most of the frontal pairs. The results showed that CPS patients had more power discrepancies between contralateral pairs than PNES patients. These differences were not significant for those pairs around the rear part of the brain which may result from the epoch selection criterion. The awake and relaxed state EEG segments were selected based on the dominant alpha-band oscillations appearing around the occipital channels. This selection criterion forced the presence of high alpha power in

all segments and may have reduced the power of the statistical test. Some EEG studies in other fields also focus on power asymmetry only for the frontal region. Future research for this study could involve applying a classifier to distinguish if a subject is a CPS or PNES patient by analyzing only a short period of the awake and relaxed state EEG. This would greatly decrease the recording time and resources of an EMU. Due to the requirement that a CPS patient should receive anti-epileptic treatment, the classifier should be designed to preclude misdiagnosing a CPS patient as a PNES patient, but could be permitted to incorrectly identify a few PNES patients as CPS patients. The results of this study also suggest that future hypotheses may need to include more sensitive scales for detecting these important distinctions. For the big scale network analysis, these differences were not obvious or significant. However, a more precise comparison of specific pairs disclosed more locally detailed information and showed the expected difference as hypothesized.

Therefore, at least the following is claimed:

1. A method for cerebral diagnosis, comprising:
  - obtaining a plurality of electroencephalogram (EEG) signals from a plurality of sensors positioned about a scalp of a subject;
  - conditioning data from the plurality of EEG signals to remove artifacts;
  - generating a cerebral network model based at least in part upon the conditioned EEG signal data;
  - determining network features based upon the cerebral network model; and
  - determining a cerebral condition of the subject based at least in part upon the network features.
2. The method of claim 1, further comprising determining EEG signal features from the conditioned EEG signal data, wherein the cerebral condition is based at least in part upon the EEG signal features and the network features.
3. The method of claim 2, wherein the cerebral network model is generated based at least in part upon the determined EEG signal features.
4. The method of claim 1, wherein the removed artifacts include eye movement artifacts and muscle movement artifacts.
5. The method of claim 1, wherein the removed artifacts include sensor related artifacts.
6. The method of claim 1, wherein generating the cerebral network model comprises:
  - generating a weighted graph based upon EEG signal features determined from the conditioned EEG signal data; and
  - converting the weighted graph to a binary graph based upon a predefined threshold.
7. The method of claim 1, wherein determine network features comprises determining global network characteristics.
8. The method of claim 1, wherein determine network features comprises identifying hubs of the cerebral network model.

9. The method of claim 1, wherein determining the cerebral condition of the subject comprises determining a location of an abnormal condition.

10. The method of claim 1, wherein determining the cerebral condition of the subject comprises determining a severity of an abnormal condition.

11. A method for cerebral diagnosis, comprising:
 

- positioning a plurality of electroencephalogram (EEG) sensors about a scalp of a subject;

determining a recording condition for each of the plurality of EEG sensors based upon predefined sensor criteria; in response to an unacceptable recording condition for at least one of the plurality of EEG sensors based upon the predefined sensor criteria, providing an indication of the EEG sensor corresponding to the unacceptable recording condition and provide procedures to correct the unacceptable recording condition.

12. The method of claim 11, further comprising in response to acceptable recording conditions for the plurality of EEG sensors based upon the predefined sensor criteria, obtaining a plurality of EEG signals from the plurality of EEG sensors.

13. The method of claim 12, further comprising amplification and filtering of the obtained plurality of EEG signals.

14. The method of claim 12, further comprising sampling the obtained plurality of EEG signals to obtain digital EEG data.

15. The method of claim 14, wherein the digital EEG data is stored in memory.

16. A system for cerebral diagnosis, comprising:
 

- an electroencephalogram (EEG) recording module configured to acquire signals from a plurality of sensors positioned about a scalp of a subject;

a signal conditioning module configured to condition EEG signal data from the plurality of EEG signals;

a signal analysis module configured to determine EEG signal features and cerebral network features based at least in part upon the conditioned EEG signal data; and a condition classification module configured to determine a cerebral condition of the subject based at least in part upon the determined features.

17. The system of claim 16, further comprising an electrode application module configured to verify a recording condition of each of the plurality of sensors based upon predefined sensor criteria.

18. The system of claim 16, wherein the signal conditioning module is configured to remove artifacts associated with movement of the subject from the EEG signal data.

19. The system of claim 16, wherein the signal analysis module is configured to generate generating a cerebral network model based at least in part upon the conditioned EEG signal data.

20. The system of claim 16, wherein the condition classification module is configured to identify location and severity of an abnormal condition.

\* \* \* \* \*

专利名称(译)	用于脑功能分析的方法和系统		
公开(公告)号	<a href="#">US20150088024A1</a>	公开(公告)日	2015-03-26
申请号	US14/386643	申请日	2013-03-06
[标]申请(专利权)人(译)	佛罗里达大学研究基金会有限公司		
申请(专利权)人(译)	佛罗里达州研究基金会, Inc.的.大学.		
当前申请(专利权)人(译)	佛罗里达州研究基金会, Inc.的.大学.		
[标]发明人	SACKELLARES JAMES CHRIS BEARDEN SCOTT T PARDALOS PANAGOTE M CHIEN JUI HONG		
发明人	SACKELLARES, JAMES CHRIS BEARDEN, SCOTT T. PARDALOS, PANAGOTE M. CHIEN, JUI-HONG		
IPC分类号	A61B5/00 A61B5/04 A61B5/0478		
CPC分类号	A61B5/7214 A61B5/0478 A61B5/7475 A61B5/4094 A61B5/742 A61B5/04012 A61B5/0476 A61B5/721 A61B5/7221 A61B5/725 A61B5/7257 G06K9/00523 G06K9/00536		
优先权	61/612647 2012-03-19 US		
外部链接	<a href="#">Espacenet</a> <a href="#">USPTO</a>		

#### 摘要(译)

提供了用于脑诊断的各种方法和系统。在一个示例中,方法包括从位于受试者上的传感器获得EEG信号;调节来自所述EEG信号的数据以去除伪像;至少部分地基于所述条件数据生成脑网络模型;基于所述脑网络模型确定网络特征;以及至少部分地基于所述网络特征来确定所述对象的脑状况。在另一示例中,一种方法包括确定所定位的EEG传感器的记录条件并提供EEG传感器的不可接受的记录条件的指示。在另一示例中,一种系统包括:EEG记录模块,用于获取信号;信号调节模块,用于调节信号数据;信号分析模块,用于确定信号特征和脑网络特征;以及条件分类模块,用于确定所述对象的脑状况。

Various methods and systems are provided for cerebral diagnosis. In one example, among others, a method includes obtaining EEG signals from sensors positioned on a subject; conditioning data from the EEG signals to remove artifacts; generating a cerebral network model based at least in part upon the conditioned data; determining network features based upon the cerebral network model; and determining a cerebral condition of the subject based at least in part upon the network features. In another example, a method includes determining a recording condition of a positioned EEG sensor and providing an indication of an unacceptable recording condition of the EEG sensor. In another example, a system includes an EEG recording module to acquire signals; a signal conditioning module to condition signal data; a signal analysis module to determine signal features and cerebral network features; and a condition classification module to determine a cerebral condition of the subject.